

# RADIATION CORRECTIONS TO PROMPT PHOTON PRODUCTION IN COMPTON SCATTERING OF QUARK-GLUON $qg \rightarrow q\gamma$ AND ANNIHILATION OF QUARK- ANTINUARL PAIR $q\bar{q} \rightarrow g\gamma$ PROCESSES

*ALIZADA MOHSUN RASIM*

*Doctoral student of the Department of Theoretical Physics  
Baku State University*

Baku State University  
Department of Theoretical Physics  
Z.Khalilov 23, Az-1148 Baku, Azerbaijan  
E-mail : mohsun.alizade@gmail.com

## I. INTRODUCTION

Photons are one of the main products of high-energy proton-proton collisions. Depending on the mechanism of their formation, photons are usually divided into two main categories: prompt and thermal photons [1,2].

Photons generated in proton-proton (prompt photons) collisions with energies in the range from  $1.5 \text{ GeV}$  to several  $\text{GeV}$  carry information about the formation of the quark-gluon phase and about the distribution of partons in nucleons [3,4] as they are produced hard scattering of incoming partons, such as Compton scattering  $qg \rightarrow q\gamma$ , annihilation  $q\bar{q} \rightarrow g\gamma$ , as well as bremsstrahlung of quarks undergoing hard scattering. These processes are described by perturbative QCD (pQCD) in leading order (LO) and next-to-leading order (NLO), which dominate at LHC energies.

Prompt photons interact only electromagnetically, and therefore their mean free path is usually much greater than the transverse dimension of the region of hot matter formed in any nuclear collision.

As a result, high-energy photons produced within the plasma usually pass through the surrounding matter without interaction, transmitting information directly from where they originated to the detector.

Deep inelastic Compton scattering is a potentially useful source of information about the structure of hadrons at short distances. We present here the results for several types of corrections to the main Compton subprocess. It is shown that the contributions of subprocesses, including the functions of photon distribution and fragmentation, are small in the region of high  $p_T$  in the approximation of the highest logarithm.

The study of the processes of scattering of hadrons with large transverse momenta is a potentially rich source of information on the short-range structure of hadrons. However, many types of parton subprocesses contribute to such reactions, and the resulting complex superposition makes it difficult to draw unambiguous conclusions from the data. The situation improves somewhat if both photons and hadrons participate in reactions with high  $p_T$ . Both for photoproduction with high  $p_T$  and for the production of prompt photons with high  $p_T$ , the number of parton subprocesses decreases at each order of perturbation theory compared to the purely hadronic case.

After the initial study of deep inelastic Compton scattering using the parton model, it became clear that QCD is an excellent candidate for the theory of strong interactions.

Compton scattering dominates in these processes, while the contribution of other processes to the total differential cross section does not exceed 20%. energy at the center of mass  $10 \text{ GeV}/c^2$  [5-7].

The instantaneous production of photons plays an important role in determining the gluon distribution of the proton and testing perturbative QCD. Compared to jet production, studies of perturbative QCD for instantaneous photon production have two advantages:

1. In the lowest order, there are only four diagrams of the production of instantaneous photons, Compton and annihilation subprocesses, each with one QCD vertex.
2. The energy and direction of photon production can be measured more accurately than for a jet. In the latter case, there are problems of jet definition ambiguity and poorer energy resolution of the hadron detector.

The study of hadronic scattering processes with large transverse momentum is a potentially rich source of information related to the short-term structure of hadrons. However, such repetitions receive input from many different types of parton subprocesses, and the resulting complex superposition makes it difficult to draw unambiguous conclusions from the data.

We have previously studied the differential cross sections for the production of prompt photons in the processes of Compton scattering of quark-gluon  $qg \rightarrow q\gamma$  and annihilation of quark-antiquark pairs  $q\bar{q} \rightarrow g\gamma$ .

The purpose of this study is to determine the contributions of corrections to the main Compton scattering and annihilation of a quark-antiquark pair, to determine the dependence of the differential correction cross sections on the energy of colliding protons, on the transverse momentum  $p_T$ , the cosine of the scattering angle and photon rapidity, and on  $x_T$ , to study the effect of polarization on the differential cross section corrections.

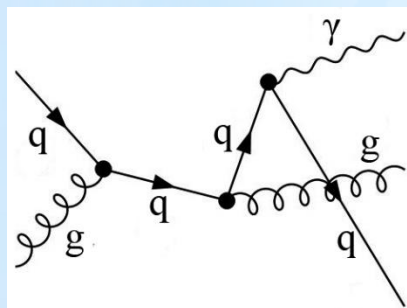
The following subprocesses are considered for Compton scattering:

1.  $qg \rightarrow qg\gamma$ , 2.  $qg \rightarrow g\gamma\gamma$ , 3.  $q\gamma \rightarrow qg\gamma$ , 4.  $g\gamma \rightarrow q\bar{q}\gamma$ , 5.  $q\gamma \rightarrow qg$ , 6.  $g\gamma \rightarrow q\bar{q}$ ,  
and 7.  $q\gamma \rightarrow q\gamma$

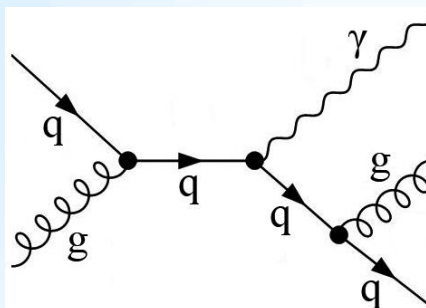
for annihilation of a quark-antiquark pair: 1.  $q\bar{q} \rightarrow gg\gamma$ , 2.  $q\bar{q} \rightarrow q\bar{q}\gamma$ , 3.  $q\bar{q} \rightarrow g\gamma\gamma$ ,  
and 4.  $q\bar{q} \rightarrow \gamma\gamma$

## II.1 Radiation corrections to the Compton quark-gluon scattering subprocess $qg \rightarrow qg\gamma$

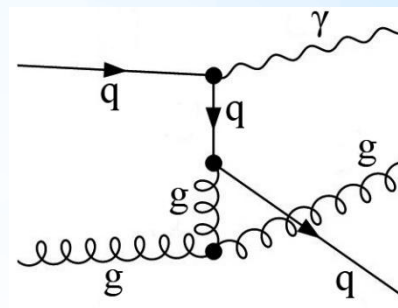
The Feynman diagrams, taking into account the radiation corrections of QCD to the Compton quark-gluon scattering  $qg \rightarrow qg\gamma$  are shown in fig.1.



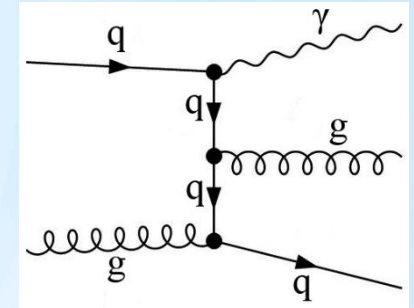
*a*



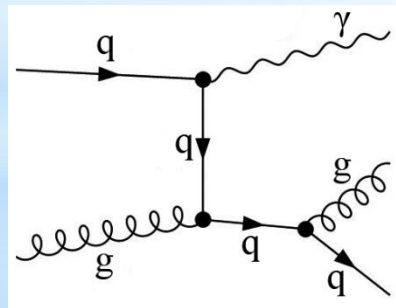
*b*



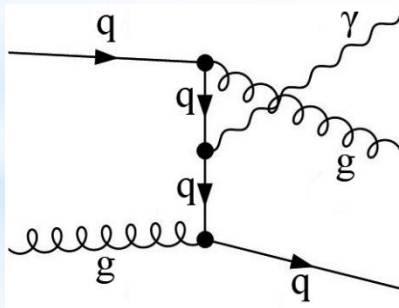
*c*



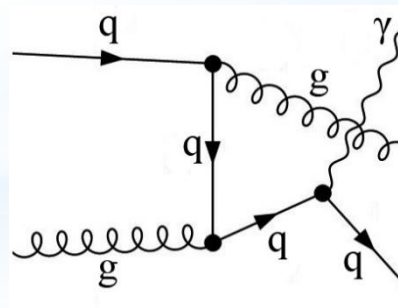
*d*



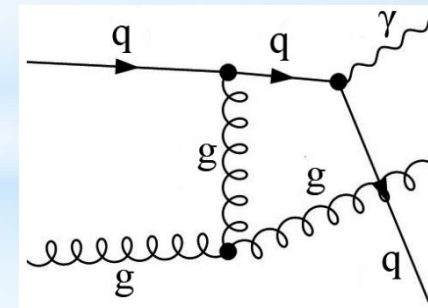
*e*



*f*



*g*



*h*

Fig.1 Feynman diagrams of subprocess  $qg \rightarrow qg\gamma$

The matrix elements for subprocess  $qg \rightarrow qg\gamma$  are as follows:

$$\begin{aligned}
M_1 &= -\frac{ee_q g_s^2 \bar{U}(p_2) \hat{\varepsilon}^*(k_2) (\hat{k}_2 + \hat{p}_2 + m_q) \hat{\varepsilon}^*(k_3) (\hat{k}_2 + \hat{k}_3 + \hat{p}_2 + m_q) \hat{\varepsilon}(k_1) U(p_1) T_{Col6Coll}^{Glu2} T_{Col5Col6}^{Glu4}}{9((-k_2 - p_2)^2 - m_q^2)((-k_2 - k_3 - p_2)^2 - m_q^2)} \\
M_2 &= -\frac{ee_q g_s^2 \bar{U}(p_2) \hat{\varepsilon}^*(k_3) (\hat{k}_3 + \hat{p}_2 + m_q) \hat{\varepsilon}^*(k_2) (\hat{k}_2 + \hat{k}_3 + \hat{p}_2 + m_q) \hat{\varepsilon}(k_1) U(p_1) T_{Col6Coll}^{Glu2} T_{Col5Col6}^{Glu4}}{9((-k_3 - p_2)^2 - m_q^2)((-k_2 - k_3 - p_2)^2 - m_q^2)} \\
M_3 &= \frac{iee_q g_s^2 f^{Glu2Glu4Glu6} (2(k_3 \cdot \varepsilon(k_1)) - k_1 \cdot \varepsilon(k_1)) T_{Col5Coll}^{Glu6} \bar{U}(p_2) \hat{\varepsilon}^*(k_3) (-\hat{k}_1 + \hat{k}_3 + \hat{p}_2 + m_q) \hat{\varepsilon}^*(k_2) U(p_1)}{9(k_1 - k_3)^2 ((k_1 - k_3 - p_2)^2 - m_q^2)} + \\
&\quad + \frac{iee_q g_s^2 f^{Glu2Glu4Glu6} (2(k_1 \cdot \varepsilon^*(k_3)) - k_3 \cdot \varepsilon^*(k_3)) T_{Col5Coll}^{Glu6} \bar{U}(p_2) \hat{\varepsilon}(k_1) (-\hat{k}_1 + \hat{k}_3 + \hat{p}_2 + m_q) \hat{\varepsilon}^*(k_2) U(p_1)}{9(k_1 - k_3)^2 ((k_1 - k_3 - p_2)^2 - m_q^2)} + \\
&\quad + \frac{iee_q g_s^2 f^{Glu2Glu4Glu6} (\varepsilon(k_1) \cdot \varepsilon^*(k_3)) T_{Col5Coll}^{Glu6} \bar{U}(p_2) (-\hat{k}_1 - \hat{k}_3) (-\hat{k}_1 + \hat{k}_3 + \hat{p}_2 + m_q) \hat{\varepsilon}^*(k_2) U(p_1)}{9(k_1 - k_3)^2 ((k_1 - k_3 - p_2)^2 - m_q^2)} \\
M_4 &= -\frac{ee_q g_s^2 \bar{U}(p_2) \hat{\varepsilon}(k_1) (\hat{p}_2 - \hat{k}_1 + m) \hat{\varepsilon}^*(k_3) (-\hat{k}_1 + \hat{k}_3 + \hat{p}_2 + m_q) \hat{\varepsilon}^*(k_2) U(p_1) T_{Col5Col6}^{Glu2} T_{Col6Coll}^{Glu4}}{9((k_1 - p_2)^2 - m_q^2)((k_1 - k_3 - p_2)^2 - m_q^2)} \\
M_5 &= -\frac{ee_q g_s^2 \bar{U}(p_2) \hat{\varepsilon}^*(k_3) (\hat{k}_3 + \hat{p}_2 + m_q) \hat{\varepsilon}(k_1) (-\hat{k}_1 + \hat{k}_3 + \hat{p}_2 + m_q) \hat{\varepsilon}^*(k_2) U(p_1) T_{Col6Coll}^{Glu2} T_{Col5Col6}^{Glu4}}{9((-k_3 - p_2)^2 - m_q^2)((k_1 - k_3 - p_2)^2 - m_q^2)}
\end{aligned} \tag{1}$$

$$M_6 = -\frac{ee_q g_s^2 \bar{U}(p_2) \hat{\varepsilon}(k_1) (\hat{p}_2 - \hat{k}_1 + m_q) \hat{\varepsilon}^*(k_2) (-\hat{k}_1 + \hat{k}_2 + \hat{p}_2 + m_q) \hat{\varepsilon}^*(k_3) U(p_1) T_{Col5Col6}^{Glu2} T_{Col6Col1}^{Glu4}}{9((k_1 - p_2)^2 - m_q^2)((k_1 - k_2 - p_2)^2 - m_q^2)}$$

$$M_7 = -\frac{ee_q g_s^2 \bar{U}(p_2) \hat{\varepsilon}^*(k_2) (\hat{k}_2 + \hat{p}_2 + m_q) \hat{\varepsilon}(k_1) (-\hat{k}_1 + \hat{k}_2 + \hat{p}_2 + m_q) \hat{\varepsilon}^*(k_3) U(p_1) T_{Col5Col6}^{Glu2} T_{Col6Col1}^{Glu4}}{9((-k_2 - p_2)^2 - m_q^2)((k_1 - k_2 - p_2)^2 - m_q^2)}$$

$$M_8 = \frac{iee_q g_s^2 f^{Glu2Glu4Glu6} (2(k_3 \cdot \varepsilon(k_1)) - k_1 \cdot \varepsilon(k_1)) T_{Col5Col1}^{Glu6} \bar{U}(p_2) \hat{\varepsilon}^*(k_2) (\hat{k}_2 + \hat{p}_2 + m_q) \hat{\varepsilon}^*(k_3) U(p_1)}{9(k_3 - k_1)^2 ((-k_2 - p_2)^2 - m_q^2)} +$$

$$+ \frac{iee_q g_s^2 f^{Glu2Glu4Glu6} (2(k_1 \cdot \varepsilon^*(k_3)) - k_3 \cdot \varepsilon^*(k_3)) T_{Col5Col1}^{Glu6} \bar{U}(p_2) \hat{\varepsilon}^*(k_2) (\hat{k}_2 + \hat{p}_2 + m_q) \hat{\varepsilon}(k_1) U(p_1)}{9(k_3 - k_1)^2 ((-k_2 - p_2)^2 - m_q^2)} +$$

$$+ \frac{iee_q g_s^2 f^{Glu2Glu4Glu6} (\varepsilon(k_1) \cdot \varepsilon^*(k_3)) T_{Col5Col1}^{Glu6} \bar{U}(p_2) \hat{\varepsilon}^*(k_2) (\hat{k}_2 + \hat{p}_2 + m_q) (-\hat{k}_1 - \hat{k}_3) U(p_1)}{9(k_3 - k_1)^2 ((-k_2 - p_2)^2 - m_q^2)}$$

where  $p_1$ ,  $k_2$ - 4-momenta of initial particles quark, gluon,  $p_2$ ,  $k_1$ ,  $k_3$ - 4-momenta of final particles quark, photon and gluon.

Mandelstam invariants for a subprocess  $qg \rightarrow qg\gamma$  have the following form:

$$s = (k_2 + p_1)^2 = (p_2 + k_3 + k_1)^2 \quad t = (k_2 - k_1)^2 = (p_2 + k_3 - p_1)^2$$

$$u = (p_1 - k_1)^2 = (p_2 + k_3 - k_2)^2 \quad q_1 = (k_2 - p_2)^2 = (k_3 + k_1 - p_1)^2 \quad q_2 = (p_1 - k_3)^2 = (p_2 + k_1 - k_2)^2 \quad (2)$$

$$s_1 = (p_2 + k_3)^2 = (k_2 + p_1 - k_1)^2 \quad t_1 = (k_2 - k_3)^2 = (p_2 + k_1 - p_1)^2 \quad u_1 = (p_1 - p_2)^2 = (k_3 + k_1 - k_2)^2$$

$$q_3 = (k_1 + p_2)^2 = (k_2 + p_1 - k_3)^2$$

$$q_4 = (k_1 + k_3)^2 = (k_2 + p_1 - p_2)^2$$

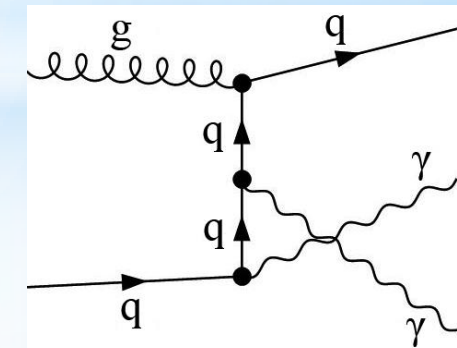
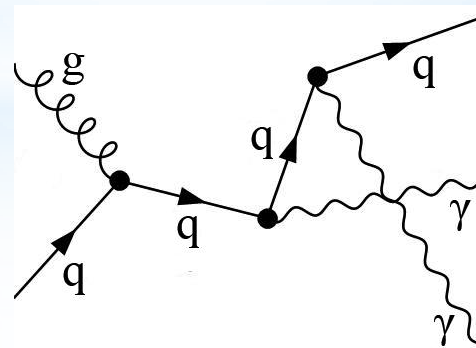
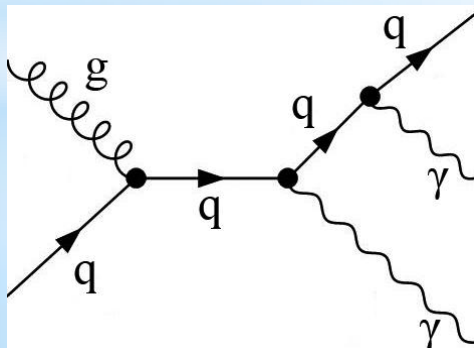
$$t = -p_T \sqrt{s} e^{-y} \quad u = -p_T \sqrt{s} e^y \quad q_1 = \left( m_q^2 - s \sqrt{p_T + m_q^2} \right) e^{-y} \quad q_2 = \left( m_q^2 - s \sqrt{p_T + m_q^2} \right) e^{-y}$$

Differential cross section of the transition process  $2 \rightarrow 3$  is defined as:

$$\frac{d\sigma}{dt} = \frac{s_1}{16\pi^2 s^4} |\bar{M}|^2 \quad (3)$$

## II.2 Radiation corrections to the Compton quark-gluon scattering subprocess of $qg \rightarrow q\gamma\gamma$

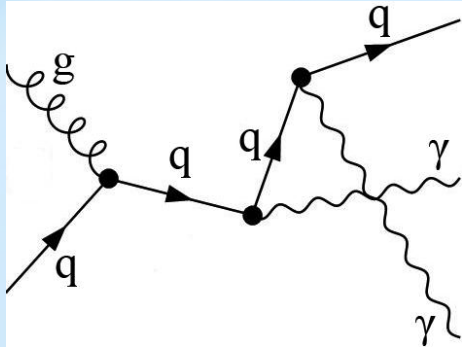
Feynman diagrams with allowance for radiation corrections to the Compton scattering subprocess  $qg \rightarrow q\gamma\gamma$  shown in fig.2 .



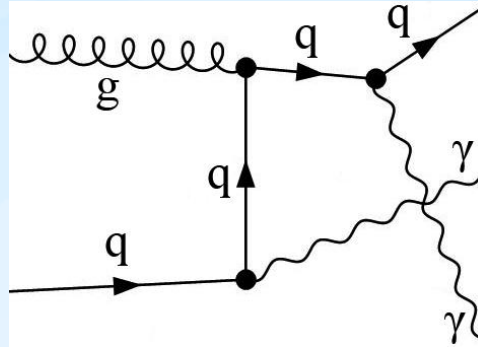
*a*

*b*

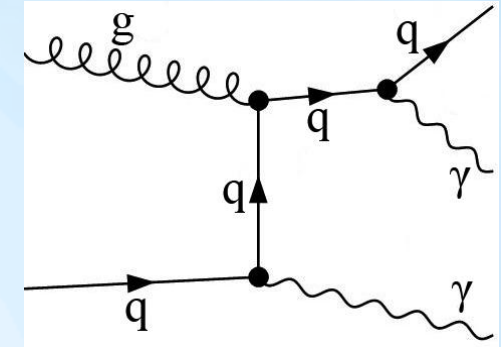
*c*



*d*



*e*



*f*

Fig.2 Feynman diagrams of subprocess  $qg \rightarrow q\gamma\gamma$

The matrix elements of subprocess  $qg \rightarrow q\gamma\gamma$  are as follows:

$$\begin{aligned}
 M_1 &= -\frac{2e^2 e_q g_s T_{Col3Col2}^{Glu1} \bar{U}(p_2) \hat{\epsilon}^*(k_1)(\hat{k}_1 + \hat{p}_2 + m_q) \hat{\epsilon}^*(k_3)(\hat{k}_1 + \hat{k}_3 + \hat{p}_2 + m_q) \hat{\epsilon}(k_2) U(p_1)}{3((-k_1 - p_2)^2 - m_q^2)((-k_1 - k_3 - p_2)^2 - m_q^2)} \\
 M_2 &= -\frac{2e^2 e_q g_s T_{Col3Col2}^{Glu1} \bar{U}(p_2) \hat{\epsilon}^*(k_3)(\hat{k}_3 + \hat{p}_2 + m_q) \hat{\epsilon}^*(k_1)(\hat{k}_1 + \hat{k}_3 + \hat{p}_2 + m_q) \hat{\epsilon}(k_2) U(p_1)}{3((-k_3 - p_2)^2 - m_q^2)((-k_1 - k_3 - p_2)^2 - m_q^2)} \\
 M_3 &= -\frac{2e^2 e_q g_s T_{Col3Col2}^{Glu1} \bar{U}(p_2) \hat{\epsilon}^*(k_2)(-\hat{k}_1 - \hat{k}_3 + \hat{p}_1 + m_q) \hat{\epsilon}^*(k_3)(\hat{p}_1 - \hat{k}_1 + m_q) \hat{\epsilon}(k_1) U(p_1)}{3((k_1 - p_1)^2 - m_q^2)((k_1 + k_3 - p_1)^2 - m_q^2)} \\
 M_4 &= -\frac{2e^2 e_q g_s T_{Col3Col2}^{Glu1} \bar{U}(p_2) \hat{\epsilon}^*(k_2)(-\hat{k}_1 - \hat{k}_3 + \hat{p}_1 + m_q) \hat{\epsilon}^*(k_1)(\hat{p}_1 - \hat{k}_3 + m_q) \hat{\epsilon}(k_3) U(p_1)}{3((k_3 - p_1)^2 - m_q^2)((k_1 + k_3 - p_1)^2 - m_q^2)}
 \end{aligned} \tag{4}$$

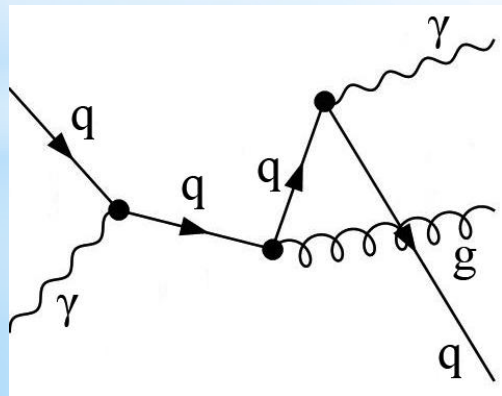
$$M_5 = -\frac{2e^2 e_q g_s T_{Col3Col2}^{Glu1} \bar{U}(p_2) \hat{\epsilon}^*(k_3) (\hat{k}_3 + \hat{p}_2 + m_q) \hat{\epsilon}^*(k_2) (\hat{p}_1 - \hat{k}_1 + m_q) \hat{\epsilon}(k_1) U(p_1)}{3((k_1 - p_1)^2 - m_q^2)((-k_3 - p_2)^2 - m_q^2)}$$

$$M_6 = -\frac{2e^2 e_q g_s T_{Col3Col2}^{Glu1} \bar{U}(p_2) \hat{\epsilon}^*(k_1) (\hat{k}_1 + \hat{p}_2 + m_q) \hat{\epsilon}^*(k_2) (\hat{p}_1 - \hat{k}_3 + m_q) \hat{\epsilon}(k_3) U(p_1)}{3((-k_1 - p_2)^2 - m_q^2)((k_3 - p_1)^2 - m_q^2)}$$

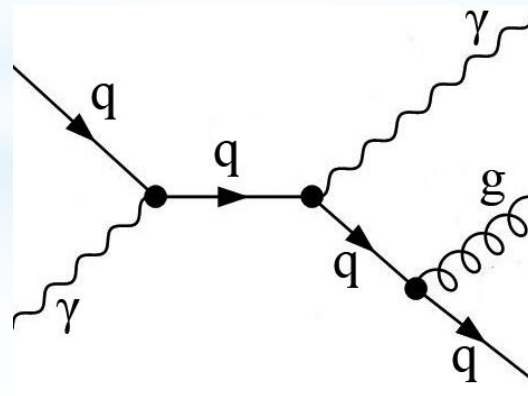
The Mandelshtam invariants are chosen as shown in (2), and the differential cross section is calculated as in (3).

### II.3 Radiation corrections to the Compton quark-gluon scattering subprocess $q\gamma \rightarrow qg\gamma$

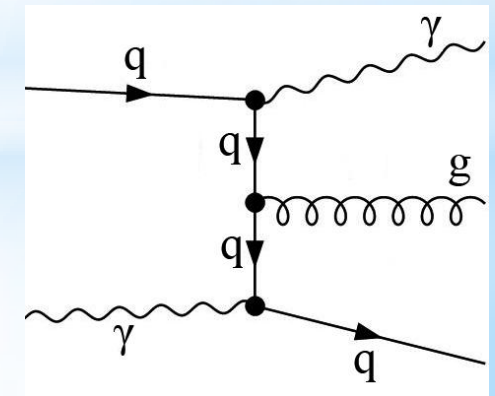
The Feynman diagrams of a subprocess  $q\gamma \rightarrow qg\gamma$  are as follows:



*a*



*b*



*c*

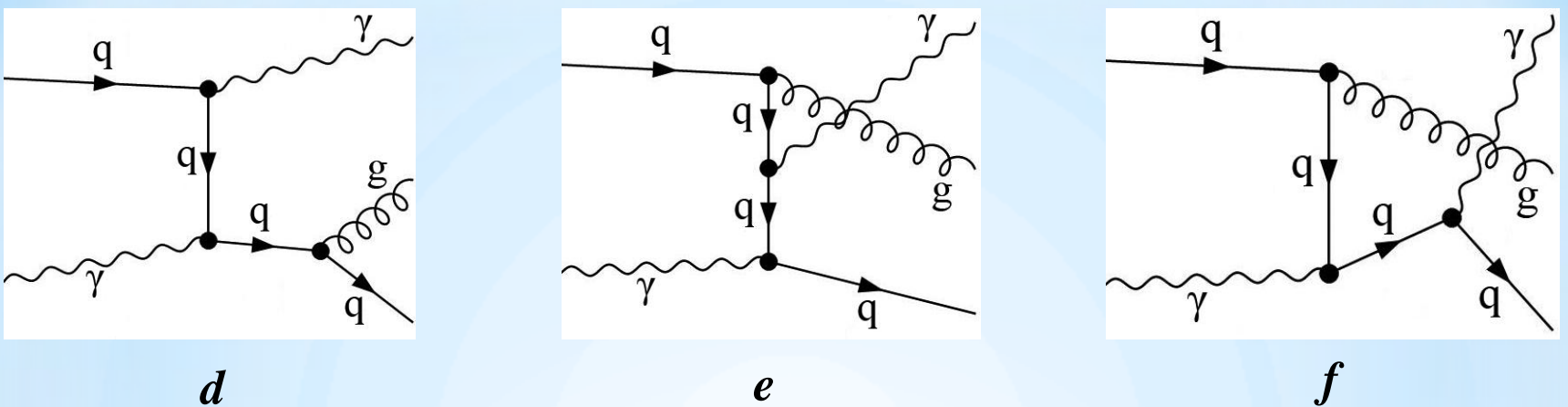


Fig.3 Feynman diagrams of subprocess  $q\gamma \rightarrow qg\gamma$

The matrix elements of subprocess  $q\gamma \rightarrow qg\gamma$  are as follows:

$$M_1 = \frac{-2e^2 e_q g_s T_{Col4Coll}^{Glu4} \bar{U}(p_2) \hat{\epsilon}^*(k_1)(\hat{k}_1 + \hat{p}_2 + m_q) \hat{\epsilon}^*(k_3)(\hat{k}_1 + \hat{k}_3 + \hat{p}_2 + m_q) \hat{\epsilon}(k_2) U(p_1)}{3((-k_1 - p_2)^2 - m_q^2)((-k_1 - k_3 - p_2)^2 - m_q^2)}$$

$$M_2 = \frac{-2e^2 e_q g_s T_{Col4Coll}^{Glu4} \bar{U}(p_2) \hat{\epsilon}^*(k_3)(\hat{k}_3 + \hat{p}_2 + m_q) \hat{\epsilon}^*(k_1)(\hat{k}_1 + \hat{k}_3 + \hat{p}_2 + m_q) \hat{\epsilon}(k_2) U(p_1)}{3((-k_3 - p_2)^2 - m_q^2)((-k_1 - k_3 - p_2)^2 - m_q^2)}$$

$$M_3 = \frac{-2e^2 e_q g_s T_{Col4Coll}^{Glu4} \bar{U}(p_2) \hat{\epsilon}(k_2)(\hat{p}_2 - \hat{k}_2 + m_q) \hat{\epsilon}^*(k_3)(-\hat{k}_2 + \hat{k}_3 + \hat{p}_2 + m_q) \hat{\epsilon}^*(k_1) U(p_1)}{3((k_2 - p_2)^2 - m_q^2)((k_2 - k_3 - p_2)^2 - m_q^2)}$$

$$M_4 = \frac{-2e^2 e_q g_s T_{Col4Coll}^{Glu4} \bar{U}(p_2) \hat{\epsilon}^*(k_3)(\hat{k}_3 + \hat{p}_2 + m_q) \hat{\epsilon}(k_2)(-\hat{k}_2 + \hat{k}_3 + \hat{p}_2 + m_q) \hat{\epsilon}^*(k_1) U(p_1)}{3((-k_3 - p_2)^2 - m_q^2)((k_2 - k_3 - p_2)^2 - m_q^2)}$$

$$M_5 = \frac{-2e^2 e_q g_s T_{Col4Coll}^{Glu4} \bar{U}(p_2) \hat{\epsilon}(k_2) (\hat{p}_2 - \hat{k}_2 + m_q) \hat{\epsilon}^*(k_1) (\hat{k}_1 - \hat{k}_2 + \hat{p}_2 + m_q) \hat{\epsilon}^*(k_3) U(p_1)}{3((k_2 - p_2)^2 - m_q^2)((-k_1 + k_2 - p_2)^2 - m_q^2)}$$

$$M_6 = \frac{-2e^2 e_q g_s T_{Col4Coll}^{Glu4} \bar{U}(p_2) \hat{\epsilon}^*(k_1) (\hat{k}_1 + \hat{p}_2 + m_q) \hat{\epsilon}(k_2) (\hat{k}_1 - \hat{k}_2 + \hat{p}_2 + m_q) \hat{\epsilon}^*(k_3) U(p_1)}{3((-k_1 - p_2)^2 - m_q^2)((-k_1 + k_2 - p_2)^2 - m_q^2)}$$

The Mandelstam invariants for the subprocess  $q\gamma \rightarrow qg\gamma$  are chosen as follows:

$$\hat{s} = (p_1 + k_2)^2 = (k_1 + k_3 + p_2)^2 \quad \hat{t} = (p_1 - k_1)^2 = (k_2 + k_3 - p_2)^2$$

$$\hat{u} = (k_2 - k_1)^2 = (p_2 + k_3 - p_1)^2 \quad \hat{q}_1 = (p_1 - k_3)^2 = (k_3 + p_2 - k_1)^2 \quad \hat{q}_2 = (k_2 - p_2)^2 = (k_1 + k_3 - p_1)^2$$

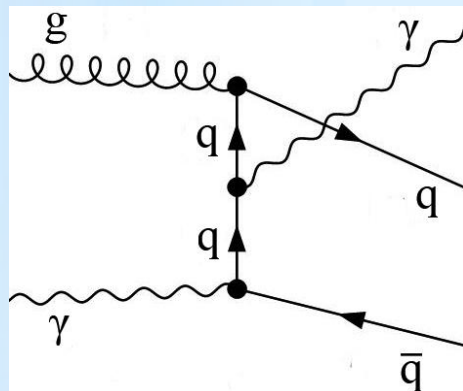
$$\hat{s}_1 = (k_3 + p_2)^2 = (p_1 + k_1 - k_3)^2 \quad \hat{t}_1 = (p_1 - p_2)^2 = (k_2 + k_3 - p_2)^2 \quad \hat{u}_1 = (k_2 - k_3)^2 = (k_2 + p_2 - p_1)^2$$

$$\hat{q}_3 = (k_1 + k_3)^2 = (p_1 + p_2 - k_2)^2 \quad \hat{q}_4 = (k_1 + p_2)^2 = (p_1 + k_3 - k_2)^2$$

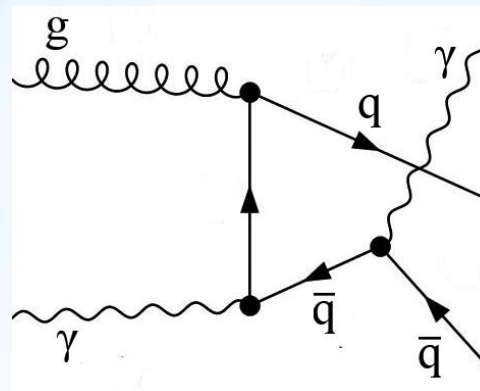
The differential cross section of the subprocess  $q\gamma \rightarrow qg\gamma$  is calculated as in (3).

## II.4 Radiation corrections to the Compton quark-gluon scattering subprocess $g\gamma \rightarrow q\bar{q}\gamma$

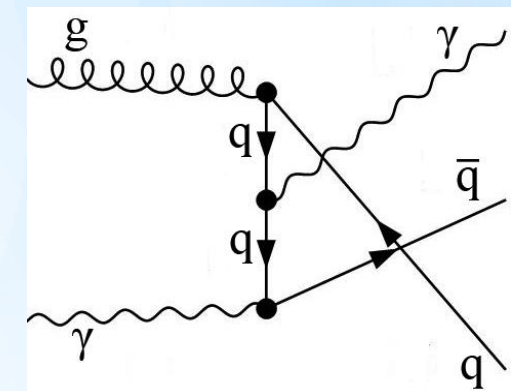
Feynman diagrams of subprocess  $g\gamma \rightarrow q\bar{q}\gamma$  look like this:



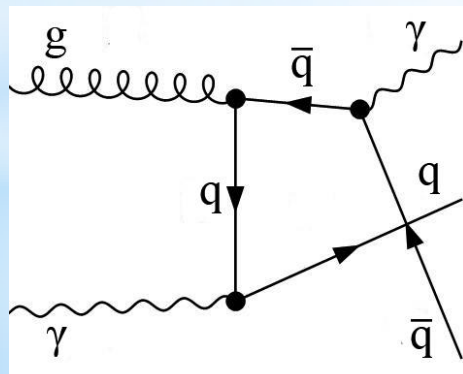
*a*



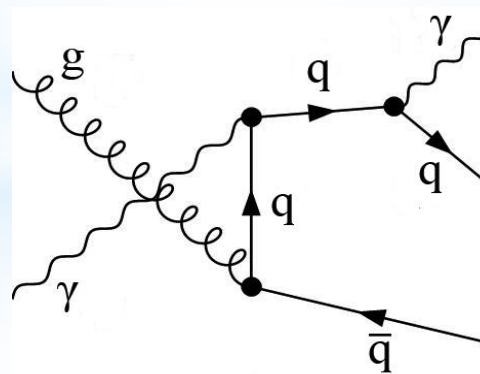
*b*



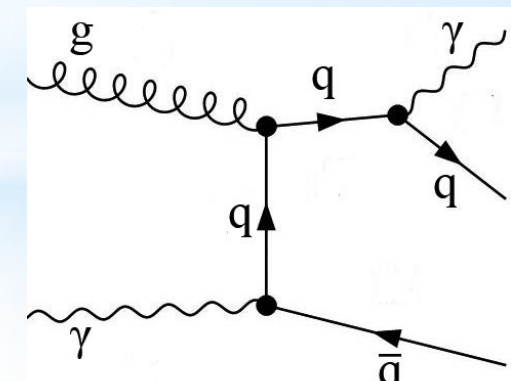
*c*



*d*



*e*



*f*

Fig.4 Feynman diagrams of subprocess  $g\gamma \rightarrow q\bar{q}\gamma$

The matrix elements of aubprocess  $g\gamma \rightarrow q\bar{q}\gamma$  are as follows:

$$M_1 = \frac{2e^2 e_q g_s T_{Col4Col5}^{Glu1} \bar{v}(p_1) \hat{\epsilon}(k_3)(-\hat{k}_1 + \hat{k}_2 - \hat{p}_2 + m_q) \hat{\epsilon}(k_1)(\hat{k}_2 - \hat{p}_2 + m_q) \hat{\epsilon}(k_2) v(p_2)}{3((p_2 - k_2)^2 - m_q^2)((k_1 - k_2 + p_2)^2 - m_q^2)}$$

$$M_2 = \frac{2e^2 e_q g_s T_{Col4Col5}^{Glu1} \bar{v}(p_1) \hat{\epsilon}(k_3)(-\hat{k}_1 + \hat{k}_2 - \hat{p}_2 + m_q) \hat{\epsilon}(k_2)(-\hat{k}_1 - \hat{p}_2 + m_q) \hat{\epsilon}(k_1) v(p_2)}{3((k_1 + p_2)^2 - m_q^2)((k_1 - k_2 + p_2)^2 - m_q^2)}$$

$$M_3 = \frac{2e^2 e_q g_s T_{Col4Col5}^{Glu1} \bar{v}(p_1) \hat{\epsilon}(k_2)(\hat{p}_1 - \hat{k}_2 + m_q) \hat{\epsilon}(k_1)(\hat{k}_1 - \hat{k}_2 + \hat{p}_1 + m_q) \hat{\epsilon}(k_3) v(p_2)}{3((k_2 - p_1)^2 - m_q^2)((-k_1 + k_2 - p_1)^2 - m_q^2)}$$

$$M_4 = \frac{2e^2 e_q g_s T_{Col4Col5}^{Glu1} \bar{v}(p_1) \hat{\epsilon}(k_2)(\hat{p}_1 - \hat{k}_2 + m_q) \hat{\epsilon}(k_3)(-\hat{k}_1 - \hat{p}_2 + m_q) \hat{\epsilon}(k_1) v(p_2)}{3((k_1 + p_2)^2 - m_q^2)((k_2 - p_1)^2 - m_q^2)}$$

$$M_5 = \frac{2e^2 e_q g_s T_{Col4Col5}^{Glu1} \bar{v}(p_1) \hat{\epsilon}(k_1)(\hat{k}_1 + \hat{p}_1 + m_q) \hat{\epsilon}(k_2)(\hat{k}_1 - \hat{k}_2 + \hat{p}_1 + m_q) \hat{\epsilon}(k_3) v(p_2)}{3((-k_1 - p_1)^2 - m_q^2)((-k_1 + k_2 - p_1)^2 - m_q^2)}$$

$$M_6 = \frac{2e^2 e_q g_s T_{Col4Col5}^{Glu1} \bar{v}(p_1) \hat{\epsilon}(k_1) (\hat{k}_1 + \hat{p}_1 + m_q) \hat{\epsilon}(k_3) (\hat{k}_2 - \hat{p}_2 + m_q) \hat{\epsilon}(k_2) v(p_2)}{3((-k_1 - p_1)^2 - m_q^2)(-p_2 - k_2)^2 - m_q^2)}$$

The Mandelstam invariants for subprocess  $g\gamma \rightarrow q\bar{q}\gamma$  are as follows:

$$\hat{s} = (k_3 + k_2)^2 = (p_1 + k_1 + p_2)^2 \quad \hat{t} = (k_3 - k_1)^2 = (p_1 + p_2 - k_2)^2$$

$$\hat{u} = (k_2 - k_1)^2 = (p_1 + p_2 - k_3)^2 \quad \hat{q}_1 = (k_3 - p_1)^2 = (k_1 + p_2 - k_2)^2 \quad \hat{q}_2 = (k_2 - p_2)^2 = (p_1 + k_1 - k_3)^2$$

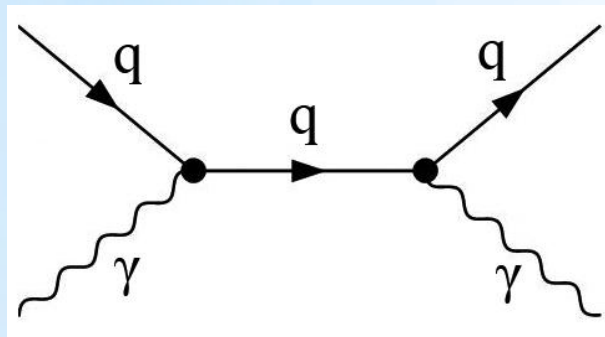
$$\hat{s}_1 = (p_1 + p_2)^2 = (k_3 + k_2 - k_1)^2 \quad \hat{t}_1 = (k_3 - p_2)^2 = (p_1 + k_1 - k_2)^2 \quad \hat{u}_1 = (k_2 - p_1)^2 = (k_1 + p_2 - k_3)^2$$

$$\hat{q}_3 = (k_1 + p_1)^2 = (k_3 + k_2 - p_2)^2 \quad \hat{q}_4 = (p_2 + k_1)^2 = (k_3 + k_2 - p_1)^2$$

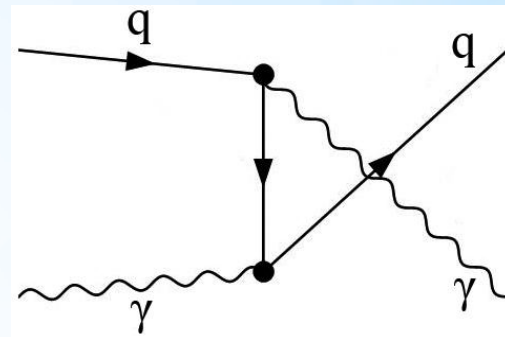
The differential cross section of the subprocess  $g\gamma \rightarrow q\bar{q}\gamma$  is calculated as in (3).

## II.5 Radiation corrections to the Compton quark-gluon scattering subprocess $q\gamma \rightarrow q\gamma$

Feynman diagrams of the Compton scattering subprocess  $q\gamma \rightarrow q\gamma$  shown in fig.5.



*a*



*b*

Fig.5 Feynman diagrams of subprocess  $q\gamma \rightarrow q\gamma$

The matrix elements of subprocess  $q\gamma \rightarrow q\gamma$  are as follows:

$$M_1 = -\frac{2e^2 e_q \delta_{CollCol3} \bar{U}(p_2) \hat{\varepsilon}^*(k_1) (\hat{k}_1 + \hat{p}_2 + m_q) \hat{\varepsilon}(k_2) U(p_1)}{3((-k_1 - p_2)^2 - m_q^2)}$$

$$M_2 = -\frac{2e^2 e_q \delta_{CollColl} \bar{U}(p_2) \hat{\epsilon}(k_2) (\hat{p}_2 - \hat{k}_2 + m_q) \hat{\epsilon}^*(k_1) U(p_1)}{3((k_2 - p_2)^2 - m_q^2)}$$

The Mandelstam invariants for the subprocess  $q\gamma \rightarrow q\gamma$  are chosen as follows:

$$\hat{s} = (k_2 + p_1)^2 \quad , \quad \hat{t} = (k_2 - k_1)^2 \quad , \quad \hat{u} = (p_1 - k_1)^2$$

The square of the modulus of the matrix element, averaged over the spin of the initial particles, has the following expression:

$$|\bar{M}|^2 = -\frac{8e^2 e_q^2 (\hat{s}^2 + \hat{u}^2)}{27 \hat{s} \hat{u}}$$

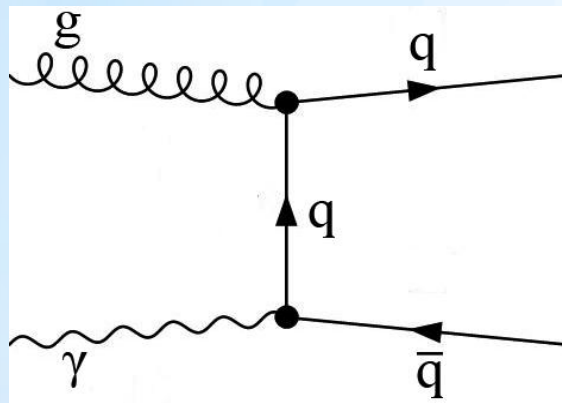
The differential cross section of a subprocess  $q\gamma \rightarrow q\gamma$  has the following form:

$$\frac{d\sigma}{dt} = -\frac{e^4 e_q^2 (\hat{s}^2 + \hat{u}^2)}{54\pi \hat{s}^3 \hat{u}}$$

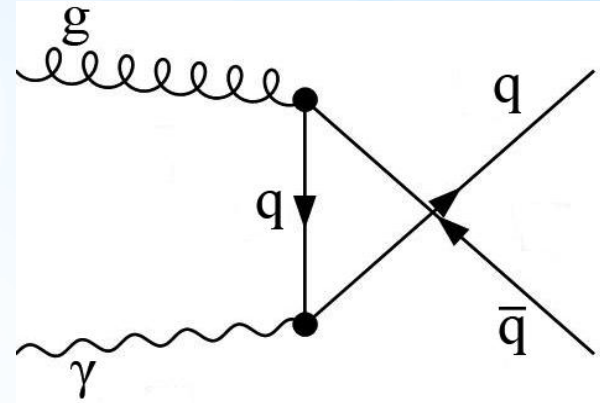
Such a contribution is suppressed due to the smallness of the fine structure constant, i.e., it acts as an electrodynamic correction.

## II.6 Radiation corrections to the Compton quark-gluon scattering subprocess $g\gamma \rightarrow q\bar{q}$

Feynman diagrams of the subprocess  $g\gamma \rightarrow q\bar{q}$  are shown in fig.6.



*a*



*b*

Fig.6 Feynman diagrams of subprocess  $g\gamma \rightarrow q\bar{q}$

The matrix elements of a subprocess  $g\gamma \rightarrow q\bar{q}$  are as follows:

$$M_1 = \frac{ee_q g_s T_{Col3Col4}^{Glu1} \bar{v}(p_1) \hat{e}(k_1) (\hat{k}_2 - \hat{p}_2 + m_q) \hat{e}(k_2) U(p_2)}{(p_2 - k_2)^2 - m_q^2}$$

$$M_2 = \frac{ee_q g_s T_{Col3Col4}^{Glu1} \bar{v}(p_1) \hat{\epsilon}(k_2) (\hat{p}_1 - \hat{k}_2 + m_q) \hat{\epsilon}(k_1) U(p_2)}{(k_2 - p_1)^2 - m_q^2}$$

The Mandelstam invariants for a subprocess  $g\gamma \rightarrow q\bar{q}$  are as follows:

$$\begin{aligned}\hat{s} &= (k_1 + k_2)^2 = (p_1 + p_2)^2 & \hat{u} &= (k_1 - p_1)^2 = (k_2 - p_2)^2 \\ \hat{t} &= (k_1 - p_2)^2 = (k_2 - p_1)^2\end{aligned}$$

Matrix element square:

$$|\bar{M}|^2 = \frac{8e^2 e_q^2 g_s^2 (\hat{t}^2 + \hat{u}^2)}{9\hat{t}\hat{u}}$$

## II.7 Radiation corrections to the Compton quark-gluon scattering subprocess $q\gamma \rightarrow qg$

Feynman diagrams of the subprocess  $q\gamma \rightarrow qg$  are shown in fig.7.

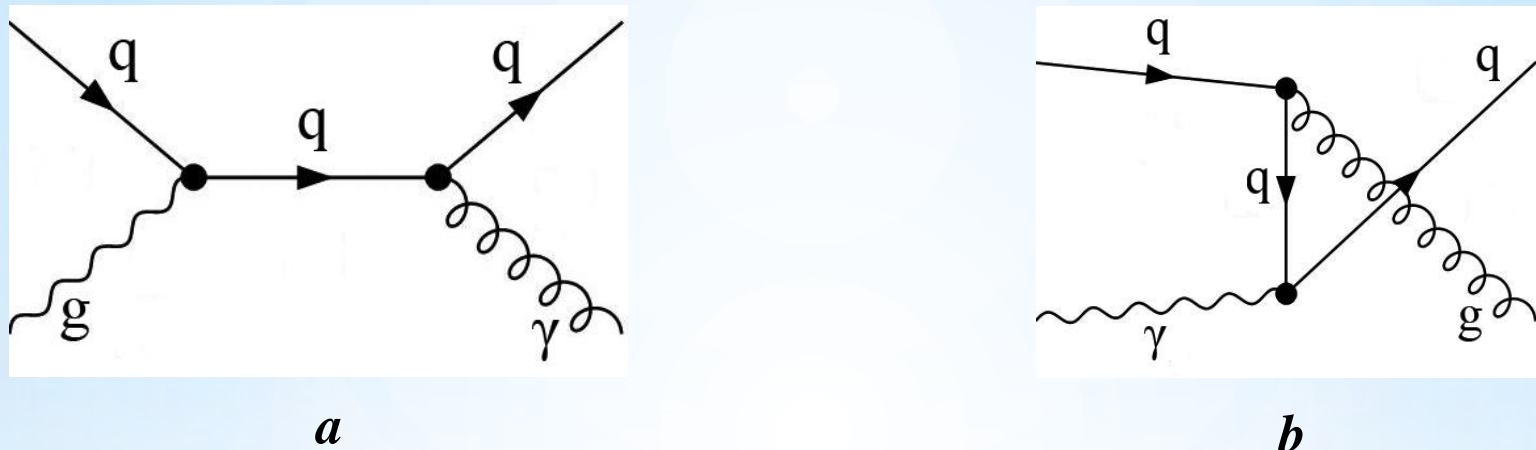


Fig.7 Feynman diagrams of subprocess  $q\gamma \rightarrow qg$

The matrix elements of subprocess  $q\gamma \rightarrow qg$  are as follows:

$$M_1 = -\frac{ee_q g_s T_{Col3Coll}^{Glu4} \bar{U}(p_2) \hat{\epsilon}^*(k_2)(\hat{k}_2 + \hat{p}_2 + m_q) \hat{\epsilon}(k_1) U(p_2)}{\left((-k_2 - p_2)^2 - m_q^2\right)}$$

$$M_2 = -\frac{ee_q g_s T_{Col3Coll}^{Glu4} \bar{U}(p_2) \hat{\epsilon}(k_1) (\hat{p}_2 - \hat{k}_1 + m_q) \hat{\epsilon}^*(k_2) U(p_1)}{((k_1 - p_2)^2 - m_q^2)}$$

The Mandelstam invariants for subprocess  $q\gamma \rightarrow qg$  are as follows:

$$\hat{s} = (k_1 + p_1)^2 = (k_2 + p_2)^2 \quad \hat{u} = (p_1 - k_2)^2 = (p_2 - k_1)^2$$

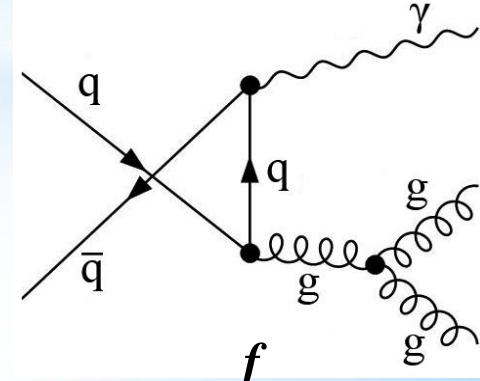
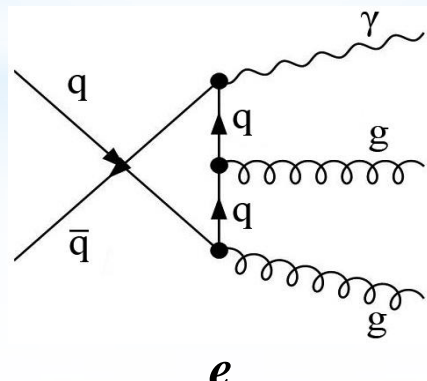
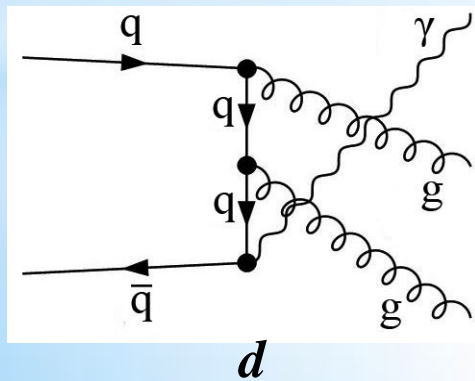
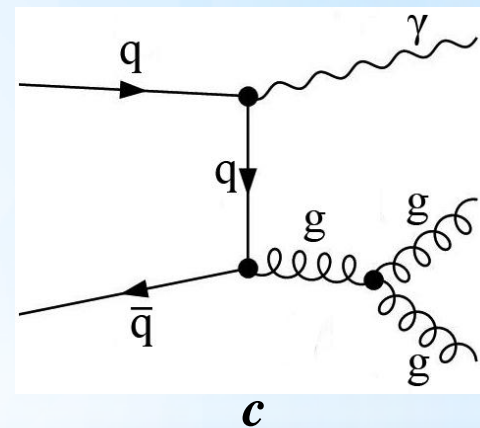
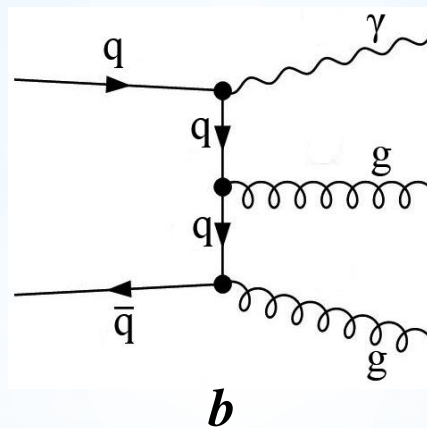
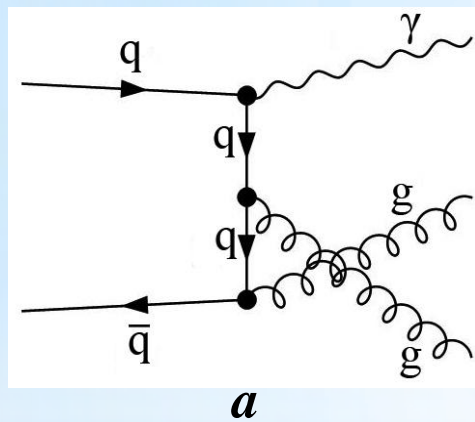
$$\hat{t} = (k_1 - k_2)^2 = (p_1 - p_2)^2$$

Matrix element square:

$$|\bar{M}|^2 = -\frac{8e^2 e_q^2 g_s^2 (\hat{s}^2 + \hat{u}^2)}{9\hat{s}\hat{u}}$$

### III.1 Radiation corrections to the annihilation of quark-antiquark pair subprocess $q\bar{q} \rightarrow g g \gamma$

Feynman diagrams with allowance for radiation corrections for the annihilation of quark-antiquark pair subprocess  $q\bar{q} \rightarrow g g \gamma$  shown in fig.8



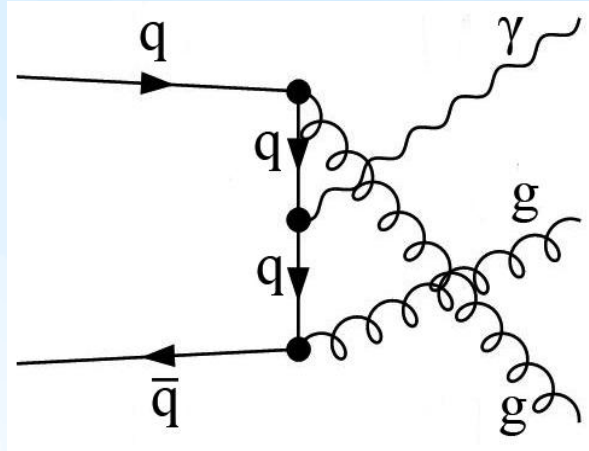
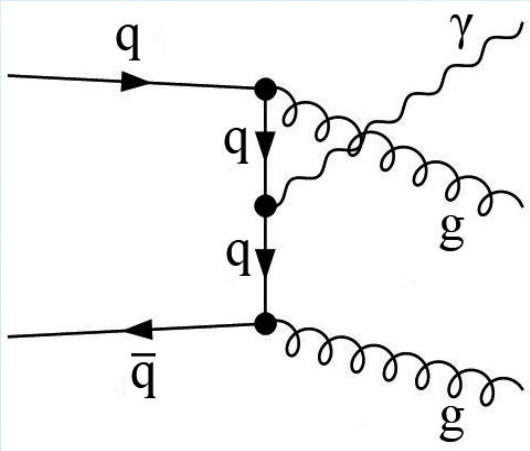


Fig.8 Feynman diagrams of subprocess  $q\bar{q} \rightarrow gg\gamma$

The matrix elements for subprocess  $q\bar{q} \rightarrow gg\gamma$  are:

$$M_1 = -\frac{ee_q g_s^2 T_{Col2Col6}^{Glu4} T_{Col6Col1}^{Glu5} \bar{U}(p_2) \hat{\epsilon}^*(k_2)(\hat{k}_2 - \hat{p}_2 + m_q) \hat{\epsilon}^*(k_3)(\hat{k}_2 + \hat{k}_3 - \hat{p}_2 + m_q) \hat{\epsilon}^*(k_1) U(p_1)}{9((p_2 - k_2)^2 - m_q^2)((-k_2 - k_3 + p_2)^2 - m_q^2)}$$

$$M_2 = -\frac{ee_q g_s^2 T_{Col6Col1}^{Glu4} T_{Col2Col6}^{Glu5} \bar{U}(p_2) \hat{\epsilon}^*(k_3)(\hat{k}_3 - \hat{p}_2 + m_q) \hat{\epsilon}^*(k_2)(\hat{k}_2 + \hat{k}_3 - \hat{p}_2 + m_q) \hat{\epsilon}^*(k_1) U(p_1)}{9((p_2 - k_3)^2 - m_q^2)((-k_2 - k_3 + p_2)^2 - m_q^2)}$$

$$M_3 = \frac{iee_q g_s^2 f^{Glu4Glu5Glu6} (k_2 \cdot \varepsilon^*(k_2) + 2(k_3 \cdot \varepsilon^*(k_2))) T_{Col2Coll}^{Glu6} \bar{U}(p_2) \hat{\varepsilon}^*(k_3) (\hat{k}_2 + \hat{k}_3 - \hat{p}_2 + m_q) \hat{\varepsilon}^*(k_1) U(p_1)}{9(k_2 + k_3)^2 ((-k_2 - k_3 + p_2)^2 - m_q^2)} +$$

$$+ \frac{iee_q g_s^2 f^{Glu4Glu5Glu6} (-2(k_2 \cdot \varepsilon^*(k_3)) - (k_3 \cdot \varepsilon^*(k_3))) T_{Col2Coll}^{Glu6} \bar{U}(p_2) \hat{\varepsilon}^*(k_2) (\hat{k}_2 + \hat{k}_3 - \hat{p}_2 + m_q) \hat{\varepsilon}^*(k_1) U(p_1)}{9(k_2 + k_3)^2 ((-k_2 - k_3 + p_2)^2 - m_q^2)} +$$

$$+ \frac{iee_q g_s^2 f^{Glu4Glu5Glu6} (\varepsilon^*(k_2) \cdot \varepsilon^*(k_3)) T_{Col2Coll}^{Glu6} \bar{U}(p_2) (\hat{k}_2 - \hat{k}_3) (\hat{k}_2 + \hat{k}_3 - \hat{p}_2 + m_q) \hat{\varepsilon}^*(k_1) U(p_1)}{9(k_2 + k_3)^2 ((-k_2 - k_3 + p_2)^2 - m_q^2)}$$

$$M_4 = - \frac{ee_q g_s^2 T_{Col6Coll}^{Glu4} T_{Col2Col6}^{Glu5} \bar{U}(p_2) \hat{\varepsilon}^*(k_1) (\hat{k}_1 - \hat{p}_2 + m_q) \hat{\varepsilon}^*(k_3) (\hat{k}_1 + \hat{k}_3 - \hat{p}_2 + m_q) \hat{\varepsilon}^*(k_2) U(p_1)}{9((p_2 - k_1)^2 - m_q^2)((-k_1 - k_3 + p_2)^2 - m_q^2)}$$

$$M_5 = - \frac{ee_q g_s^2 T_{Col2Col6}^{Glu4} T_{Col6Coll}^{Glu5} \bar{U}(p_2) \hat{\varepsilon}^*(k_1) (\hat{k}_1 - \hat{p}_2 + m_q) \hat{\varepsilon}^*(k_2) (\hat{k}_1 + \hat{k}_2 - \hat{p}_2 + m_q) \hat{\varepsilon}^*(k_3) U(p_1)}{9((p_2 - k_1)^2 - m_q^2)((-k_1 - k_2 + p_2)^2 - m_q^2)}$$

$$M_6 = \frac{iee_q g_s^2 f^{Glu4Glu5Glu6} (k_2 \cdot \varepsilon^*(k_2) + 2(k_3 \cdot \varepsilon^*(k_2))) T_{Col2Coll}^{Glu6} \bar{U}(p_2) \hat{\varepsilon}^*(k_1) (\hat{k}_1 - \hat{p}_2 + m_q) \hat{\varepsilon}^*(k_3) U(p_1)}{9(k_2 + k_3)^2 ((\hat{p}_2 - \hat{k}_1)^2 - m_q^2)} +$$

$$+ \frac{iee_q g_s^2 f^{Glu4Glu5Glu6} (-2(k_2 \cdot \varepsilon^*(k_3)) - (k_3 \cdot \varepsilon^*(k_3))) T_{Col2Coll}^{Glu6} \bar{U}(p_2) \hat{\varepsilon}^*(k_1) (\hat{k}_1 - \hat{p}_2 + m_q) \hat{\varepsilon}^*(k_2) U(p_1)}{9(k_2 + k_3)^2 ((\hat{p}_2 - \hat{k}_1)^2 - m_q^2)} +$$

$$+ \frac{iee_q g_s^2 f^{Glu4Glu5Glu6} (\varepsilon^*(k_2) \cdot \varepsilon^*(k_3)) T_{Col2Coll}^{Glu6} \bar{U}(p_2) \hat{\varepsilon}^*(k_1) (\hat{k}_1 - \hat{p}_2 + m_q) (\hat{k}_2 - \hat{k}_3) U(p_1)}{9(k_2 + k_3)^2 \left( (\hat{p}_2 - \hat{k}_1)^2 - m_q^2 \right)}$$

$$M_7 = - \frac{ee_q g_s^2 T_{Col6Coll}^{Glu4} T_{Col2Col6}^{Glu5} \bar{U}(p_2) \hat{\varepsilon}^*(k_3) (\hat{k}_3 - \hat{p}_2 + m_q) \hat{\varepsilon}^*(k_1) (\hat{k}_1 + \hat{k}_3 - \hat{p}_2 + m_q) \hat{\varepsilon}^*(k_2) U(p_1)}{9((p_2 - k_3)^2 - m_q^2)((-k_1 - k_3 + p_2)^2 - m_q^2)}$$

$$M_8 = - \frac{ee_q g_s^2 T_{Col2Col6}^{Glu4} T_{Col6Coll}^{Glu5} \bar{U}(p_2) \hat{\varepsilon}^*(k_2) (\hat{k}_2 - \hat{p}_2 + m_q) \hat{\varepsilon}^*(k_1) (\hat{k}_1 + \hat{k}_2 - \hat{p}_2 + m_q) \hat{\varepsilon}^*(k_3) U(p_1)}{9((p_2 - k_2)^2 - m_q^2)((-k_1 - k_2 + p_2)^2 - m_q^2)}$$

where  $p_1, p_2$  - 4-momenta of initial particles quark, antiquark,  $k_1, k_2, k_3$  - 4-momenta of final particles photon and two gluons.

The Mandelstam invariants for subprocess  $q\bar{q} \rightarrow gg\gamma$  have the following form:  $s = (p_1 + p_2)^2 = (k_1 + k_2 + k_3)^2$      $t = (p_1 - k_3)^2 = (k_2 + k_1 - p_2)^2$

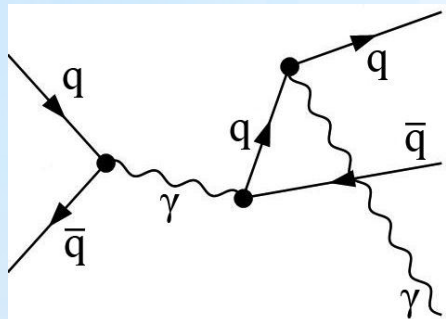
$$q_1 = (p_1 - k_1)^2 = (k_3 + k_2 - p_2)^2 \quad q_2 = (p_2 - k_2)^2 = (k_3 + k_1 - p_1)^2 \quad u = (p_2 - k_3)^2 = (k_2 + k_1 - p_1)^2$$

$$s_1 = (k_2 + k_1)^2 = (p_1 + p_2 - k_3)^2 \quad t_1 = (p_1 - k_2)^2 = (k_3 + k_1 - p_2)^2 \quad u_1 = (p_2 - k_1)^2 = (k_3 + k_{21} - p_1)^2$$

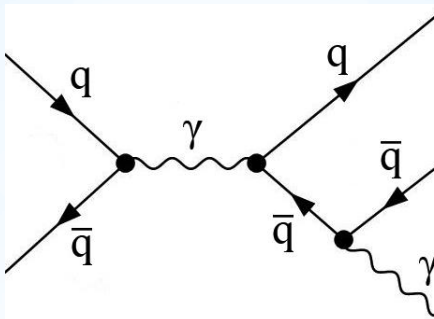
$$q_3 = (k_1 + k_3)^2 = (p_1 + p_2 - k_2)^2 \quad q_4 = (k_2 + k_3)^2 = (p_1 + p_2 - k_1)^2$$

### III.2 Radiation corrections to the annihilation of quark-antiquark pair subprocess $q\bar{q} \rightarrow q\bar{q}\gamma$

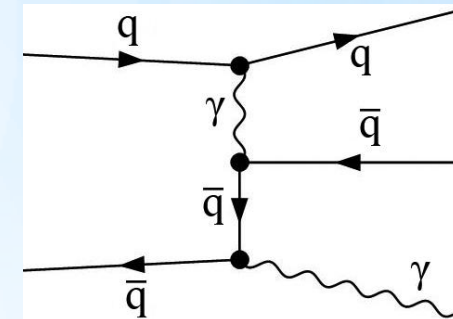
Feynman diagrams with allowance for radiation corrections for the annihilation of quark-antiquark pair subprocess  $q\bar{q} \rightarrow q\bar{q}\gamma$  with a photon propagator are shown in fig.9.



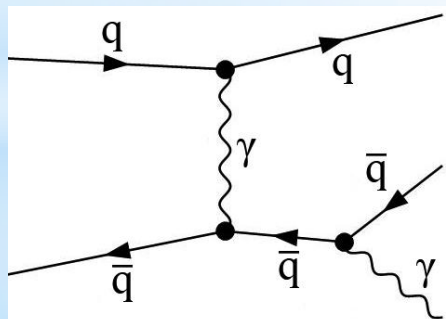
*a*



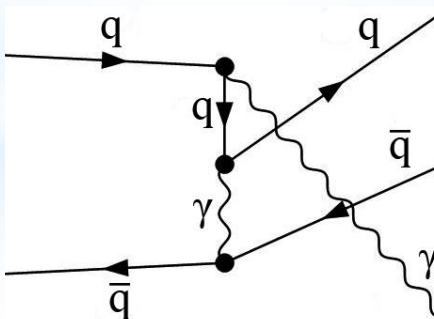
*b*



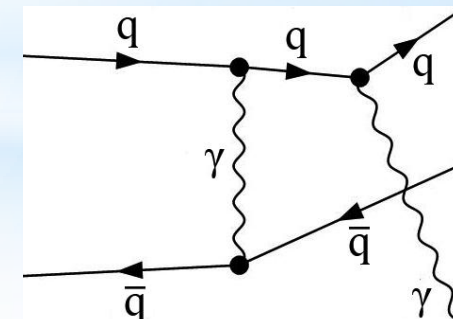
*c*



*d*



*e*



*f*

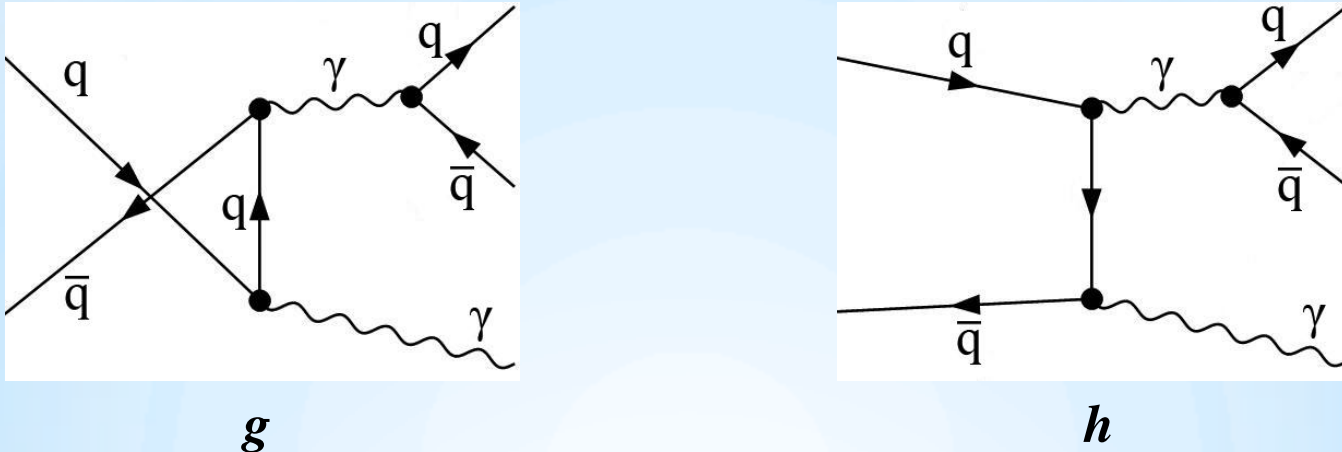


Fig.9 Feynman diagrams of subprocess  $q\bar{q} \rightarrow q\bar{q}\gamma$

Matrix elements of subprocess  $q\bar{q} \rightarrow q\bar{q}\gamma$  with a gluon in the propagator have the form:

$$M_1 = \frac{-4e^3 e_q \delta_{Col1Col2} \delta_{Col3Col4} \bar{v}(p_2) \gamma U(p_1) \bar{U}(p_3) \hat{\epsilon}^*(k_1) (\hat{k}_1 + \hat{p}_3 + m_q) v(p_4)}{81(k_1 + p_3 + p_4)^2 ((-k_1 - p_3)^2 - m_q^2)}$$

$$M_2 = \frac{-4e^3 e_q \delta_{Col1Col2} \delta_{Col3Col4} \bar{v}(p_2) \gamma U(p_1) \bar{U}(p_3) \gamma (-\hat{k}_1 - \hat{p}_4 + m_q) \hat{\epsilon}^*(k_1) v(p_4)}{81(k_1 + p_3 + p_4)^2 ((k_1 + p_4)^2 - m_q^2)}$$

$$M_3 = \frac{4e^3 e_q \delta_{Col1Col3} \delta_{Col2Col4} \bar{U}(p_3) \gamma U(p_1) \bar{v}(p_2) \hat{\epsilon}^*(k_1) (\hat{k}_1 - \hat{p}_2 + m_q) v(p_4)}{81(k_1 - p_2 + p_4)^2 ((p_2 - k_1)^2 - m_q^2)}$$

$$M_4 = \frac{4e^3 e_q \delta_{Col1Col3} \delta_{Col2Col4} \bar{U}(p_3) \gamma U(p_1) \bar{v}(p_2) \gamma (\hat{k}_1 - \hat{p}_4 + m_q) \hat{\epsilon}^*(k_1) v(p_4)}{81(k_1 - p_2 + p_4)^2 ((k_1 + p_4)^2 - m_q^2)}$$

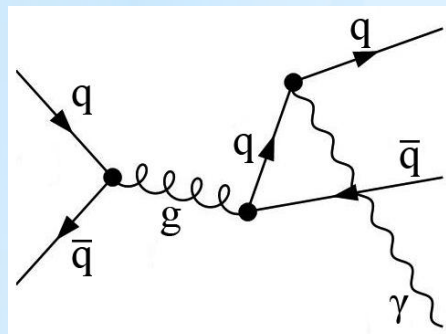
$$M_5 = \frac{4e^3 e_q \delta_{Col1Col3} \delta_{Col2Col4} \bar{v}(p_2) \gamma v(p_4) \bar{U}(p_3) \gamma (-\hat{p}_2 + \hat{p}_3 + \hat{p}_4 + m_q) \hat{\epsilon}^*(k_1) U(p_1)}{81(p_2 - p_4)^2 ((p_2 - p_3 - p_4)^2 - m_q^2)}$$

$$M_6 = \frac{4e^3 e_q \delta_{Col1Col3} \delta_{Col2Col4} \bar{v}(p_2) \gamma v(p_4) \bar{U}(p_3) \hat{\epsilon}^*(k_1) (\hat{k}_1 + \hat{p}_3 + m_q) \gamma U(p_1)}{81(p_4 - p_2)^2 ((-k_1 - p_3)^2 - m_q^2)}$$

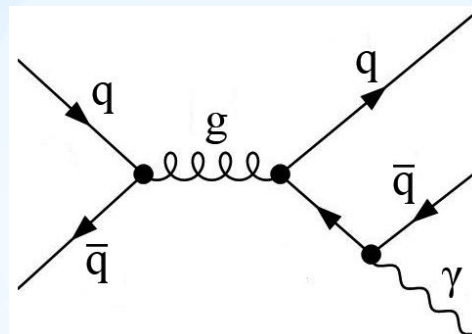
$$M_7 = \frac{-4e^3 e_q \delta_{Col1Col2} \delta_{Col3Col4} \bar{U}(p_3) \gamma v(p_4) \bar{v}(p_2) \gamma (-\hat{p}_2 + \hat{p}_3 + \hat{p}_4 + m_q) \hat{\epsilon}^*(k_1) U(p_1)}{81(p_3 + p_4)^2 ((p_2 - p_3 - p_4)^2 - m_q^2)}$$

$$M_8 = \frac{-4e^3 e_q \delta_{Col1Col2} \delta_{Col3Col4} \bar{U}(p_3) \gamma v(p_4) \bar{v}(p_2) \hat{\epsilon}^*(k_1) (\hat{k}_1 - \hat{p}_2 + m_q) \gamma U(p_1)}{81(p_3 + p_4)^2 ((p_2 - k_1)^2 - m_q^2)}$$

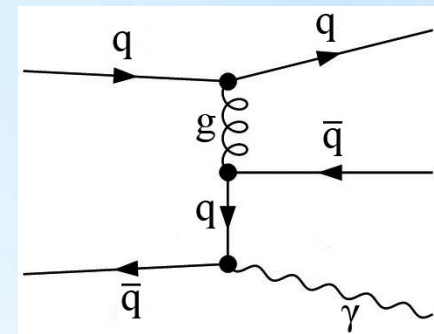
Except photon in subprocess propagator  $q\bar{q} \rightarrow q\bar{q}\gamma$  annihilation of a quark-antiquark pair maybe a gluon. Feynman diagrams of such a subprocess are shown in fig.10.



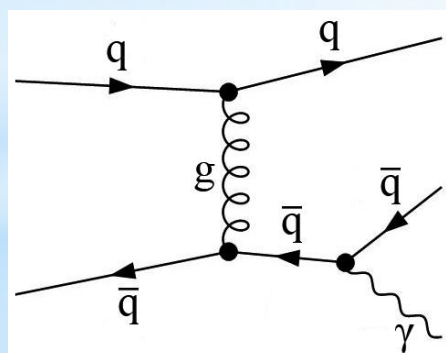
*a*



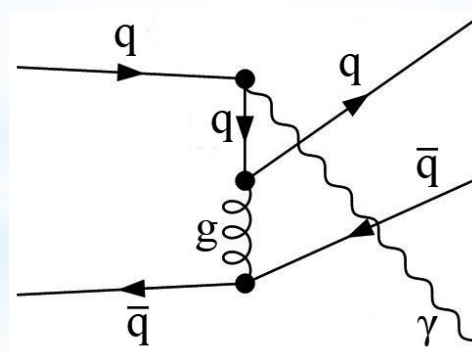
*b*



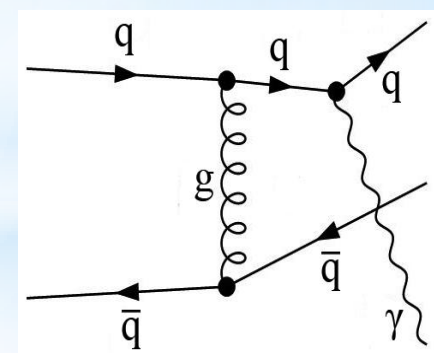
*c*



*d*



*e*



*f*

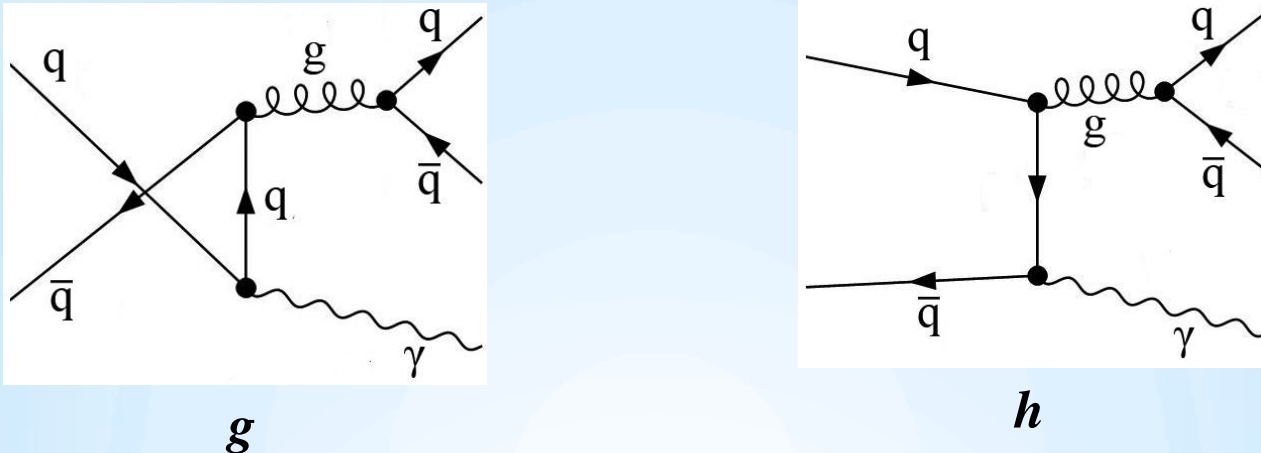


Fig.10 Feynman diagrams of subprocess  $q\bar{q} \rightarrow q\bar{q}\gamma$

Matrix elements of subprocess  $q\bar{q} \rightarrow q\bar{q}\gamma$  with a gluon in the propagator have the form:

$$M_1 = \frac{-ee_q g_s^2 T_{Col2Coll}^{Glu6} T_{Col3Col4}^{Glu6} \bar{v}(p_2) \gamma U(p_1) \bar{U}(p_3) \hat{\epsilon}^*(k_1) (\hat{k}_1 + \hat{p}_3 + m_q) v(p_4)}{9(k_1 + p_3 + p_4)^2 ((-k_1 - p_3)^2 - m_q^2)}$$

$$M_2 = \frac{-ee_q g_s^2 T_{Col2Coll}^{Glu6} T_{Col3Col4}^{Glu6} \bar{v}(p_2) \gamma U(p_1) \bar{U}(p_3) \gamma (-\hat{k}_1 - \hat{p}_4 + m_q) \hat{\epsilon}^*(k_1) v(p_4)}{9(k_1 + p_3 + p_4)^2 ((k_1 + p_4)^2 - m_q^2)}$$

$$M_3 = \frac{ee_q g_s^2 T_{Col2Coll}^{Glu6} T_{Col3Coll}^{Glu6} \bar{U}(p_3) \gamma U(p_1) \bar{v}(p_2) \hat{\epsilon}^*(k_1) (\hat{k}_1 - \hat{p}_2 + m_q) v(p_4)}{9(k_1 - p_2 + p_4)^2 ((p_2 - k_1)^2 - m_q^2)}$$

$$M_4 = \frac{ee_q g_s^2 T_{Col2Col4}^{Glu6} T_{Col3Col1}^{Glu6} \bar{U}(p_3) \gamma U(p_1) \bar{\nu}(p_2) \gamma (\hat{k}_1 - \hat{p}_4 + m_q) \hat{\epsilon}^*(k_1) \nu(p_4)}{9(k_1 - p_2 + p_4)^2 ((k_1 + p_4)^2 - m_q^2)}$$

$$M_5 = \frac{ee_q g_s^2 T_{Col2Col4}^{Glu6} T_{Col3Col1}^{Glu6} \bar{\nu}(p_2) \gamma \nu(p_4) \bar{U}(p_3) \gamma (-\hat{p}_2 + \hat{p}_3 + \hat{p}_4 + m_q) \hat{\epsilon}^*(k_1) U(p_1)}{9(p_2 - p_4)^2 ((p_2 - p_3 - p_4)^2 - m_q^2)}$$

$$M_6 = \frac{ee_q g_s^2 T_{Col2Col4}^{Glu6} T_{Col3Col1}^{Glu6} \bar{\nu}(p_2) \gamma \nu(p_4) \bar{U}(p_3) \hat{\epsilon}^*(k_1) (\hat{k}_1 + \hat{p}_3 + m_q) \gamma U(p_1)}{9(p_4 - p_2)^2 ((-k_1 - p_3)^2 - m_q^2)}$$

$$M_7 = \frac{ee_q g_s^2 T_{Col2Col1}^{Glu6} T_{Col3Col4}^{Glu6} \bar{U}(p_3) \gamma \nu(p_4) \bar{\nu}(p_2) \gamma (-\hat{p}_2 + \hat{p}_3 + \hat{p}_4 + m_q) \hat{\epsilon}^*(k_1) \gamma U(p_1)}{9(p_3 + p_4)^2 ((p_2 - p_3 - p_4)^2 - m_q^2)}$$

$$M_8 = \frac{-ee_q g_s^2 T_{Col2Col1}^{Glu6} T_{Col3Col4}^{Glu6} \bar{U}(p_3) \gamma \nu(p_4) \bar{\nu}(p_2) \hat{\epsilon}^*(k_1) (\hat{k}_1 - \hat{p}_2 + m_q) \gamma U(p_1)}{9(p_3 + p_4)^2 ((p_2 - k_1)^2 - m_q^2)}$$

Mandelstam invariants for subprocess  $q\bar{q} \rightarrow q\bar{q}\gamma$  have the following form:

$$s = (p_1 + p_2)^2 = (k_1 + p_3 + p_4)^2 \quad t = (p_1 - k_1)^2 = (p_4 + p_3 - p_2)^2$$

$$u = (p_2 - k_1)^2 = (p_4 + p_3 - p_1)^2 \quad q_1 = (p_1 - p_3)^2 = (k_1 + p_4 - p_2)^2 \quad q_2 = (p_2 - p_4)^2 = (k_1 + p_3 - p_1)^2$$

$$s_1 = (p_4 + p_3)^2 = (p_1 + p_2 - k_1)^2 \quad t_1 = (p_1 - p_4)^2 = (k_1 + p_1 - p_2)^2 \quad u_1 = (p_2 - p_1)^2 = (k_1 + p_4 - p_1)^2$$

$$q_3 = (p_3 + k_1)^2 = (p_1 + p_2 - p_1)^2 \quad q_4 = (p_4 + k_1)^2 = (p_1 + p_2 - p_3)^2$$

Differential cross section of subprocess  $q\bar{q} \rightarrow q\bar{q}\gamma$  calculated as in (3).

### III.3 Radiation corrections to the annihilation of quark-antiquark pair subprocess $q\bar{q} \rightarrow g\gamma\gamma$

Feynman diagrams with allowance for radiation corrections to the annihilation of quark-antiquark pair subprocess  $q\bar{q} \rightarrow g\gamma\gamma$  has the form shown in fig.11 .

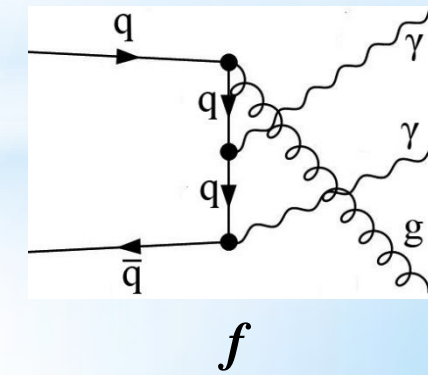
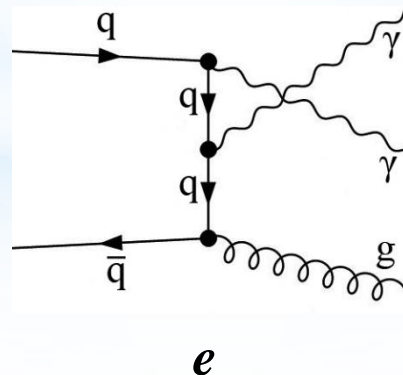
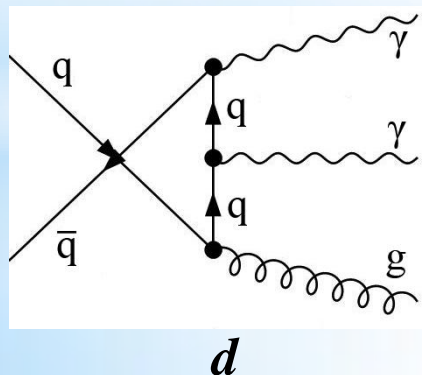
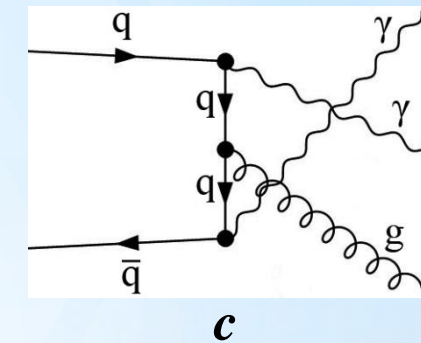
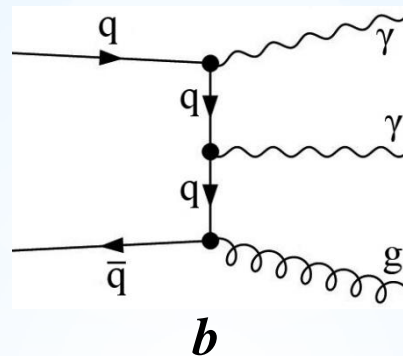
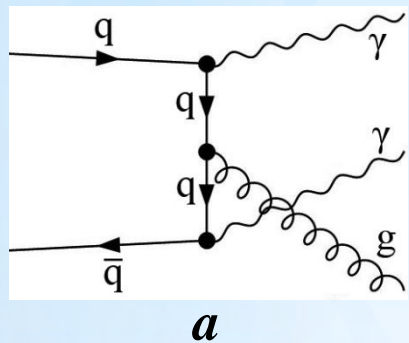


Fig.11 Feynman diagrams of subprocess  $q\bar{q} \rightarrow g\gamma\gamma$

Matrix elements of subprocess  $q\bar{q} \rightarrow g\gamma\gamma$  has the following form:

$$M_1 = -\frac{2e^2 e_q g_s T_{Col2Coll}^{Glu5} \bar{v}(p_2) \hat{\epsilon}^*(k_2) (\hat{k}_2 - \hat{p}_2 + m_q) \hat{\epsilon}^*(k_3) (\hat{k}_2 + \hat{k}_3 - \hat{p}_2 + m_q) \hat{\epsilon}^*(k_1) U(p_1)}{27((p_2 - k_2)^2 - m_q^2)((-k_2 - k_3 + p_2)^2 - m_q^2)}$$

$$M_2 = -\frac{2e^2 e_q g_s T_{Col2Coll}^{Glu5} \bar{v}(p_2) \hat{\epsilon}^*(k_3) (\hat{k}_3 - \hat{p}_2 + m_q) \hat{\epsilon}^*(k_2) (\hat{k}_2 + \hat{k}_3 - \hat{p}_2 + m_q) \hat{\epsilon}^*(k_1) U(p_1)}{27((p_2 - k_3)^2 - m_q^2)((-k_2 - k_3 + p_2)^2 - m_q^2)}$$

$$M_3 = -\frac{2e^2 e_q g_s T_{Col2Coll}^{Glu5} \bar{v}(p_2) \hat{\epsilon}^*(k_1) (\hat{k}_1 - \hat{p}_2 + m_q) \hat{\epsilon}^*(k_3) (\hat{k}_1 + \hat{k}_3 - \hat{p}_2 + m_q) \hat{\epsilon}^*(k_2) U(p_1)}{27((p_2 - k_1)^2 - m_q^2)((-k_1 - k_3 + p_2)^2 - m_q^2)}$$

$$M_4 = -\frac{2e^2 e_q g_s T_{Col2Coll}^{Glu5} \bar{v}(p_2) \hat{\epsilon}^*(k_1) (\hat{k}_1 - \hat{p}_2 + m_q) \hat{\epsilon}^*(k_2) (\hat{k}_1 + \hat{k}_2 - \hat{p}_2 + m_q) \hat{\epsilon}^*(k_3) U(p_1)}{27((p_2 - k_1)^2 - m_q^2)((-k_1 - k_2 + p_2)^2 - m_q^2)}$$

$$M_5 = -\frac{2e^2 e_q g_s T_{Col2Coll}^{Glu5} \bar{v}(p_2) \hat{\epsilon}^*(k_3) (\hat{k}_3 - \hat{p}_2 + m_q) \hat{\epsilon}^*(k_1) (\hat{k}_1 + \hat{k}_3 - \hat{p}_2 + m_q) \hat{\epsilon}^*(k_2) U(p_1)}{27((p_2 - k_3)^2 - m_q^2)((-k_1 - k_3 + p_2)^2 - m_q^2)}$$

$$M_6 = -\frac{2e^2 e_q g_s T_{Col2Coll}^{Glu5} \bar{v}(p_2) \hat{\epsilon}^*(k_2) (\hat{k}_2 - \hat{p}_2 + m_q) \hat{\epsilon}^*(k_1) (\hat{k}_1 + \hat{k}_2 - \hat{p}_2 + m_q) \hat{\epsilon}^*(k_3) U(p_1)}{27((p_2 - k_2)^2 - m_q^2)((-k_1 - k_2 + p_2)^2 - m_q^2)}$$

Mandelstam invariants for subprocess  $q\bar{q} \rightarrow g\gamma\gamma$  have the following form:

$$s = (p_1 + p_2)^2 = (k_1 + k_2 + k_3)^2 \quad t = (p_1 - k_2)^2 = (k_3 + k_1 - p_2)^2$$

$$u = (p_2 - k_2)^2 = (k_3 + k_1 - p_1)^2 \quad q_1 = (p_1 - k_1)^2 = (k_3 + k_2 - p_2)^2 \quad q_2 = (p_2 - k_3)^2 = (k_2 + k_1 - p_1)^2$$

$$s_1 = (k_1 + k_3)^2 = (p_1 + p_2 - k_2)^2 \quad t_1 = (p_1 - k_3)^2 = (k_2 + k_1 - p_2)^2 \quad u_1 = (p_2 - k_1)^2 = (k_3 + k_{21} - p_1)^2$$

$$q_3 = (k_1 + k_2)^2 = (p_1 + p_2 - k_3)^2 \quad q_4 = (k_2 + k_3)^2 = (p_1 + p_2 - k_1)^2$$

Differential cross section of subprocess  $q\bar{q} \rightarrow g\gamma\gamma$  calculated as in (3).

### III.4 Radiation corrections to the annihilation of quark-antiquark pair subprocess $q\bar{q} \rightarrow \gamma\gamma$

Feynman diagrams with radiation corrections to the annihilation quark-antiquark pair subprocess  $q\bar{q} \rightarrow \gamma\gamma$  has the form shown in fig.12 .



Fig.12 Feynman diagrams of subprocess  $q\bar{q} \rightarrow \gamma\gamma$

Matrix elements of subprocess  $q\bar{q} \rightarrow \gamma\gamma$  has the following form:

$$M_1 = -\frac{2e^2 e_q g_s \delta_{Col1Col2} \bar{v}(p_2) \hat{\epsilon}^*(k_2) (\hat{k}_2 - \hat{p}_2 + m_q) \hat{\epsilon}^*(k_1) U(p_1)}{3((p_2 - k_2)^2 - m_q^2)}$$

$$M_2 = -\frac{2e^2 e_q g_s \delta_{CollCol2} \bar{v}(p_2) \hat{\varepsilon}^*(k_1) (\hat{k}_1 - \hat{p}_2 + m_q) \hat{\varepsilon}^*(k_2) U(p_1)}{3((p_2 - k_1)^2 - m_q^2)}$$

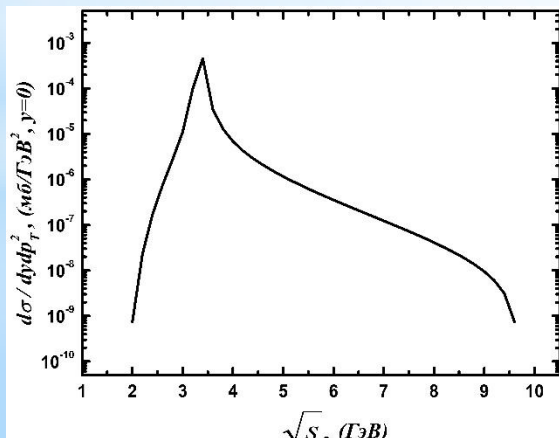
Subprocess Mandelstam invariants  $q\bar{q} \rightarrow \gamma\gamma$  has the following form:

$$\hat{s} = (p_1 + p_2)^2 \quad \hat{t} = (p_1 - k_1)^2 \quad \hat{u} = (p_2 - k_1)^2$$

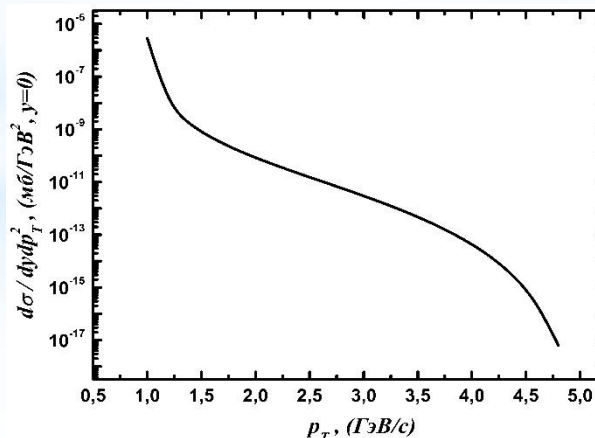
## IV. Numerical results and discussion

### IV.1 Corrections to the Compton scattering of quark-gluon

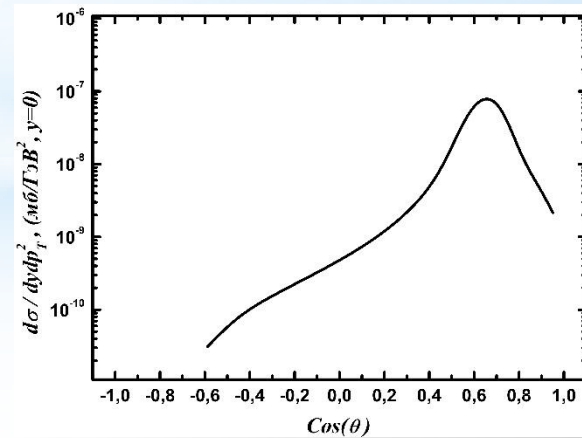
#### 1. Subprocess $qg \rightarrow qg\gamma$



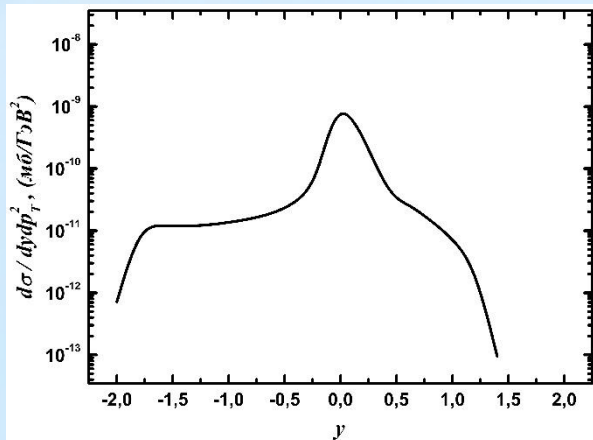
**a**



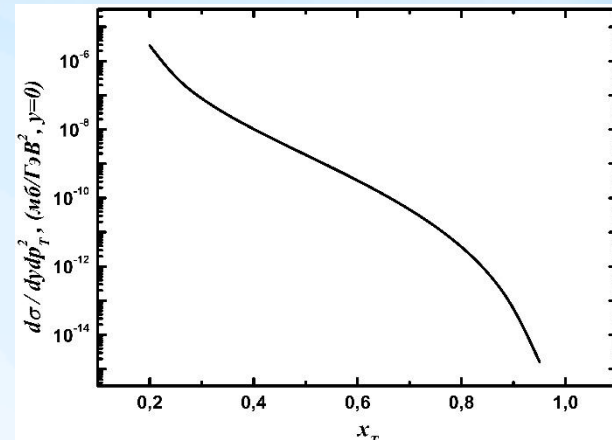
**b**



**c**



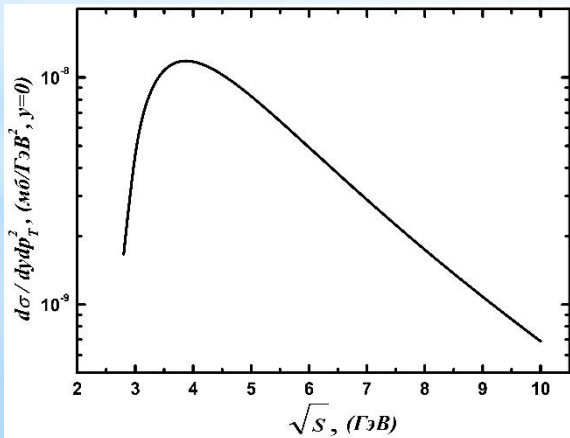
**d**



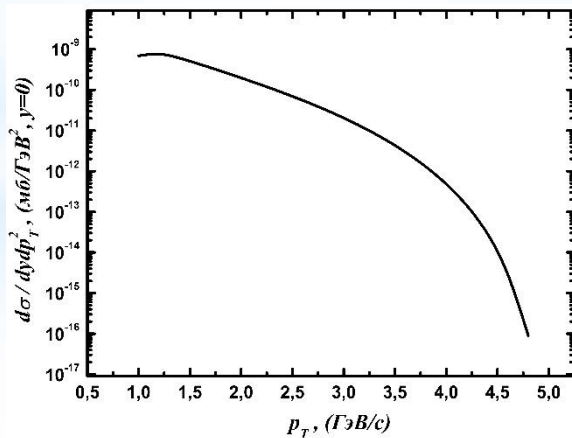
**e**

Fig.13 Dependence of the differential cross sections on a) the sum of energies of colliding particles  $\sqrt{s}$  at  $p_T = 0.9 \text{ GeV}/c$  and  $y=0$ , b) transverse momentum of photon  $p_T$  c) the cosine of the scattering angle, d) the rapidity of produced photons, e)  $x_T$  at  $\sqrt{s}=10 \text{ GeV}$  and  $y=0$

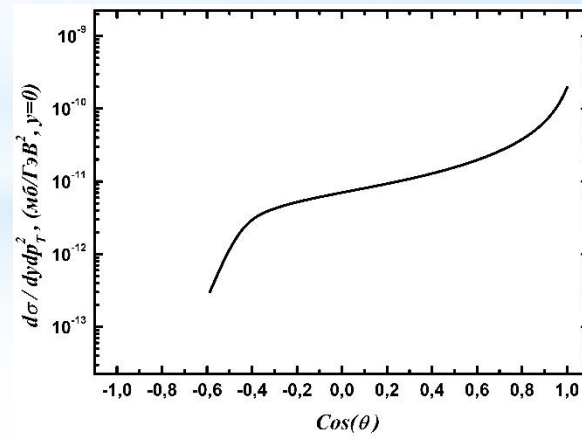
## 2. Subprocess $qg \rightarrow q\gamma\gamma$



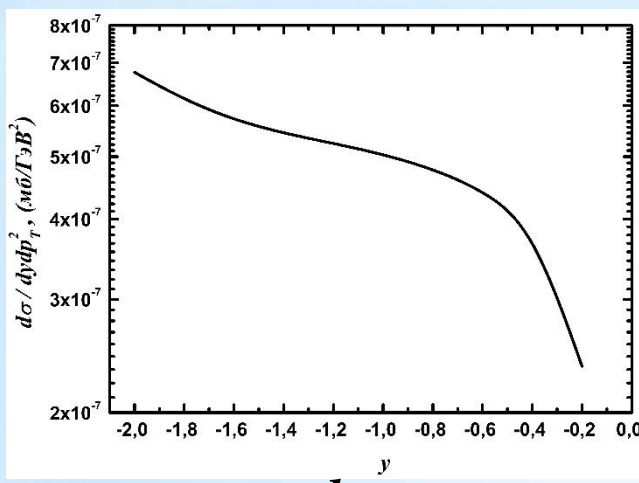
**a**



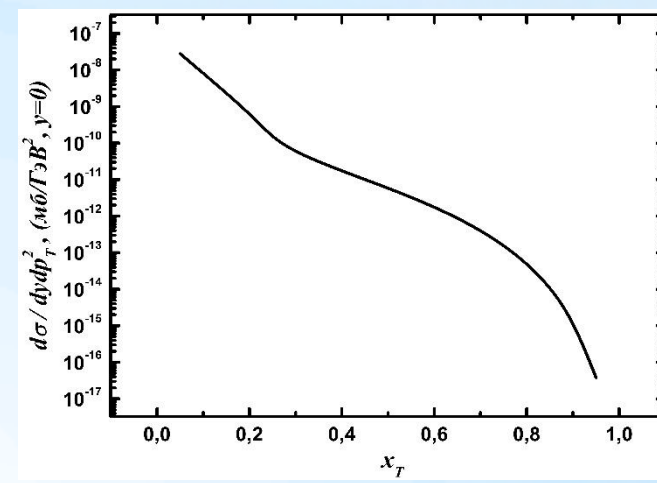
**b**



**c**



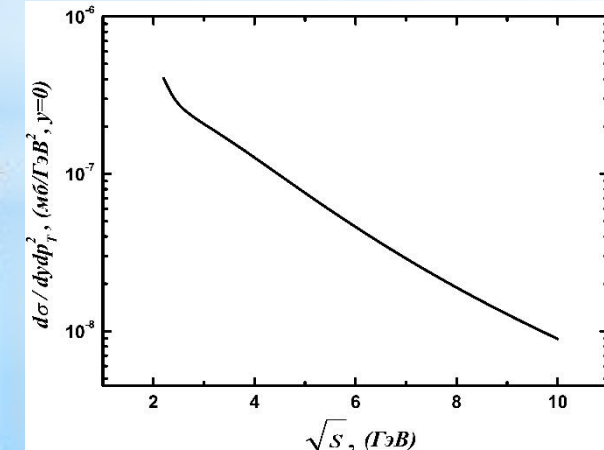
*d*



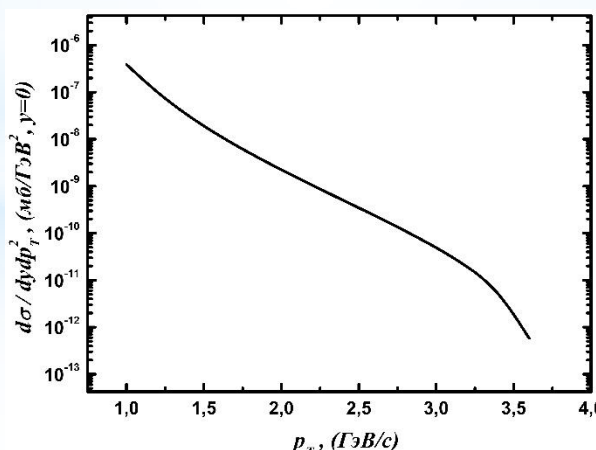
*e*

Fig.14 Dependence of the differential cross sections on a) the sum of energies of colliding particles  $\sqrt{s}$  at  $p_T = 0.9 \text{ GeV}/c$  and  $y=0$ , b) transverse momentum of photon  $p_T$  c) the cosine of the scattering angle, d) the rapidity of produced photons, e)  $x_T$  at  $\sqrt{s}=10 \text{ GeV}$  and  $y=0$

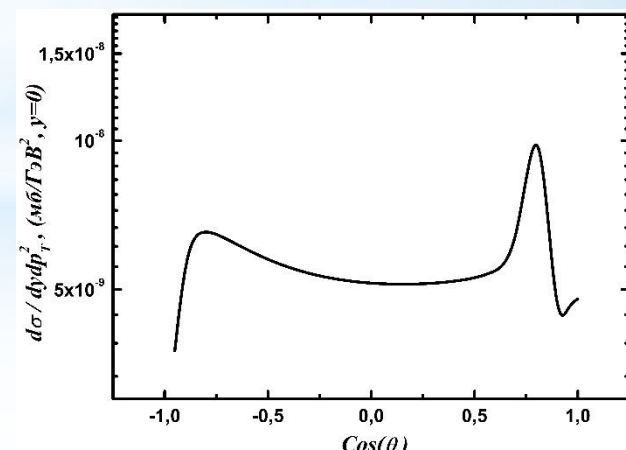
### 3. Subprocess $q\gamma \rightarrow qg\gamma$



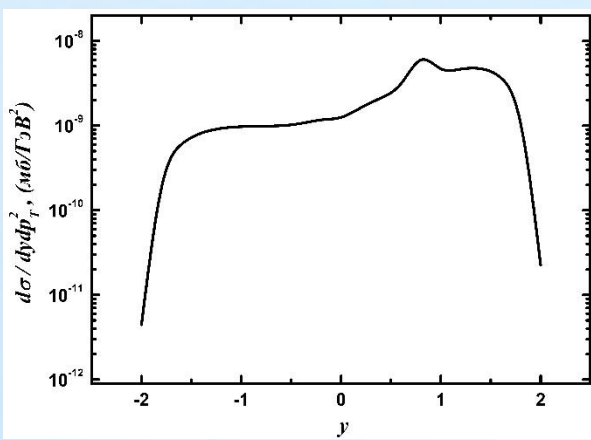
*a*



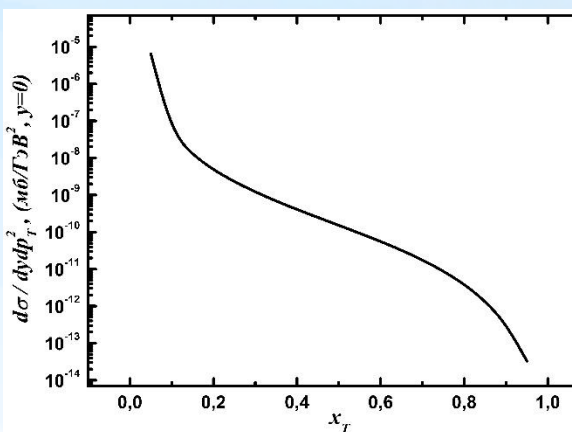
*b*



*c*



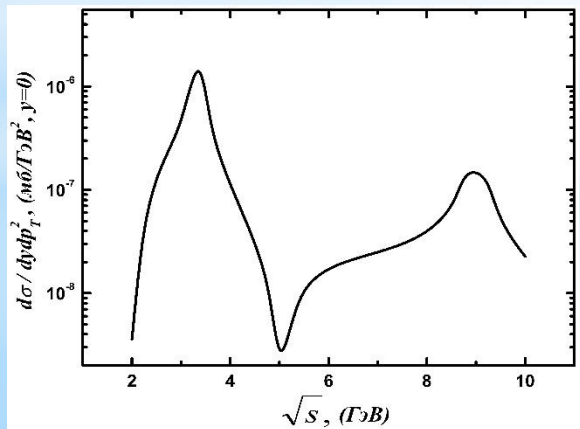
*d*



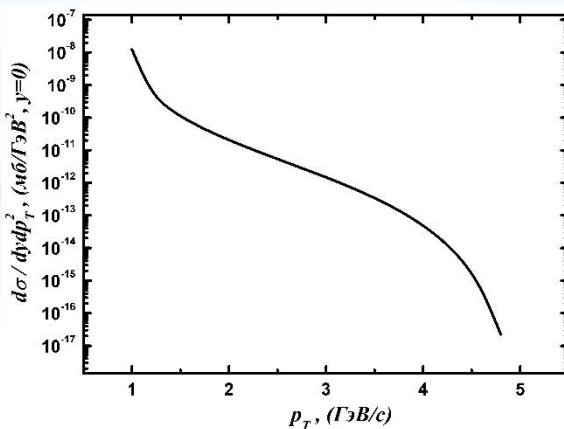
*e*

Fig.15 Dependence of the differential cross sections on a) the sum of energies of colliding particles  $\sqrt{s}$  at  $p_T=0.9 \text{ GeV}/c$  and  $y=0$  , b) transverse momentum of photon  $p_T$ , c) the cosine of the scattering angle, d) the rapidity of produced photons, e)  $x_T$  at  $\sqrt{s}=10 \text{ GeV}$  and  $y=0$

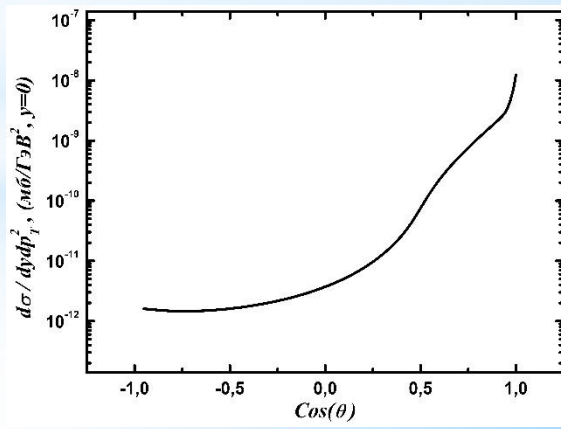
#### 4. Subprocess $g\gamma \rightarrow q\bar{q}\gamma$



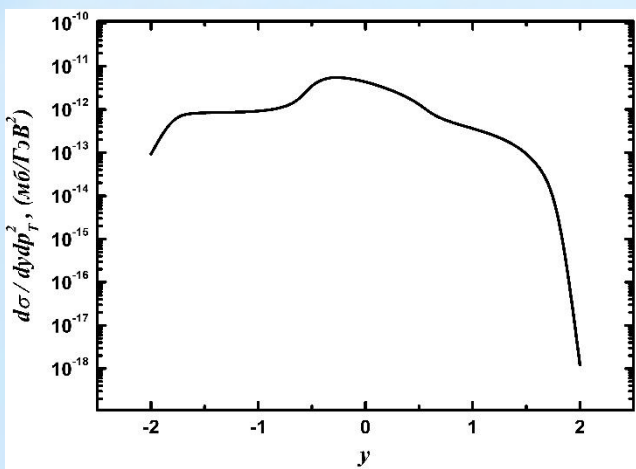
*a*



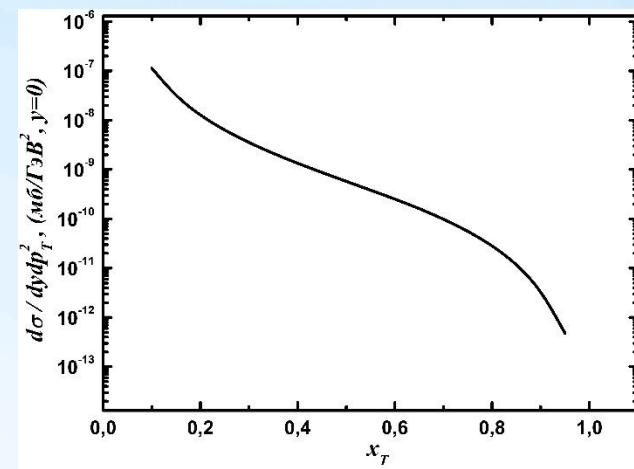
*b*



*c*



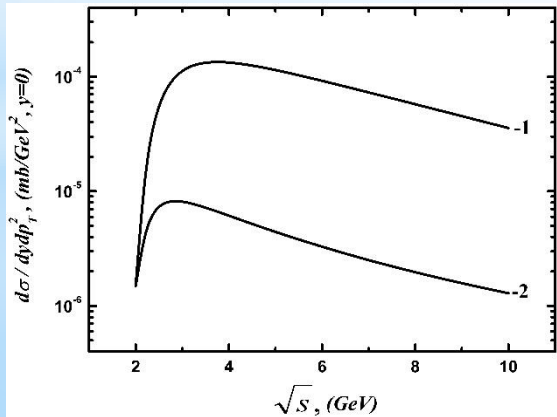
*d*



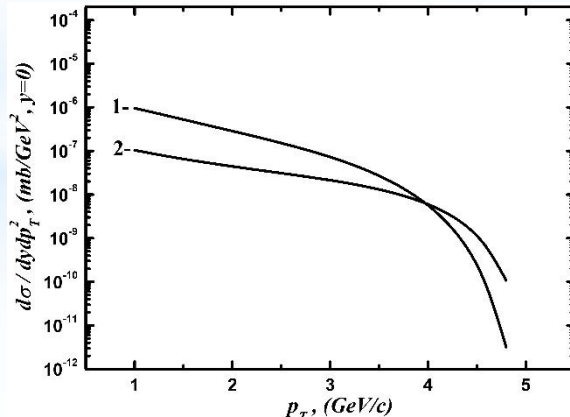
*e*

Fig.16 Dependence of the differential cross sections on a) the sum of energies of colliding particles  $\sqrt{s}$  at  $p_T=0.9 \text{ GeV}/c$  and  $y=0$ , b) transverse momentum of photon  $p_T$ , c) the cosine of the scattering angle, d) the rapidity of produced photons, e)  $x_T$  at  $\sqrt{s}=10 \text{ GeV}$  and  $y=0$

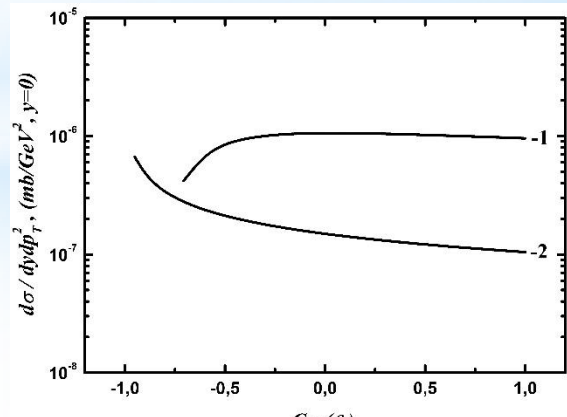
## 5. Subprocesses $q\gamma \rightarrow q\gamma$ and $qg \rightarrow q\gamma$



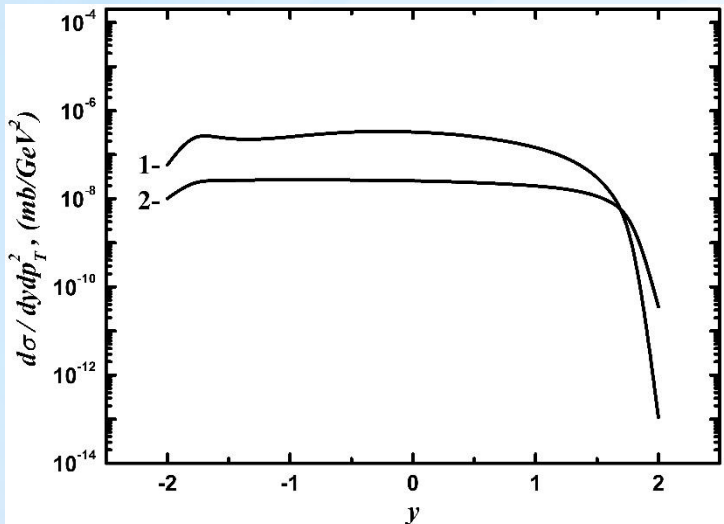
*a*



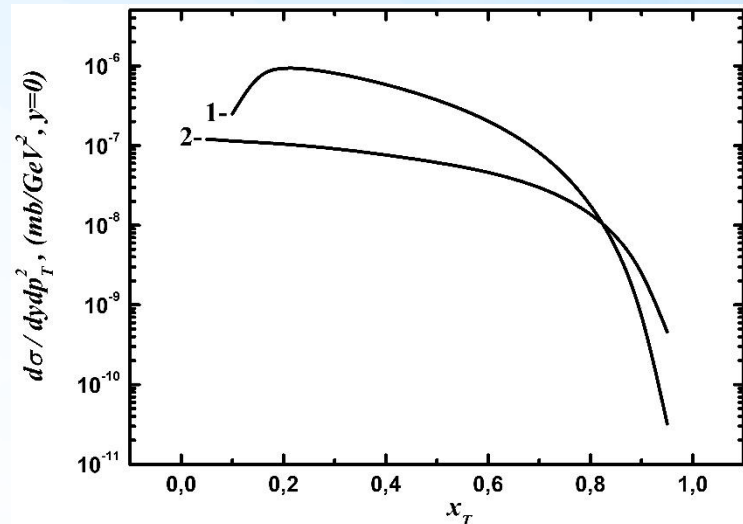
*b*



*c*

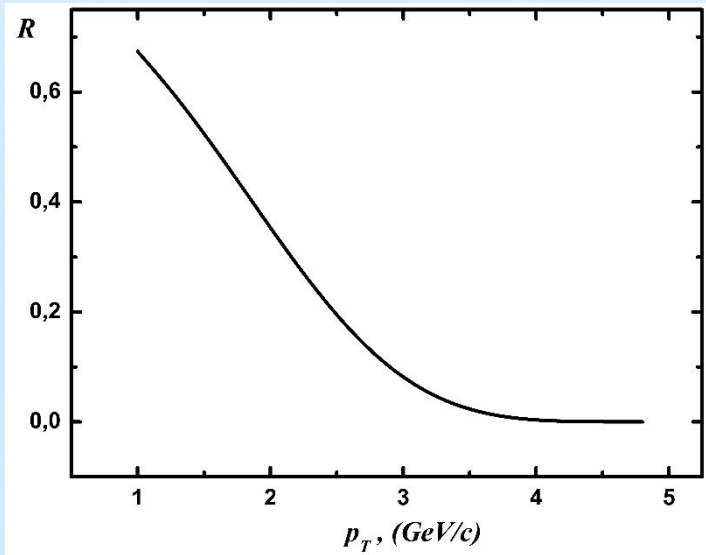


*d*

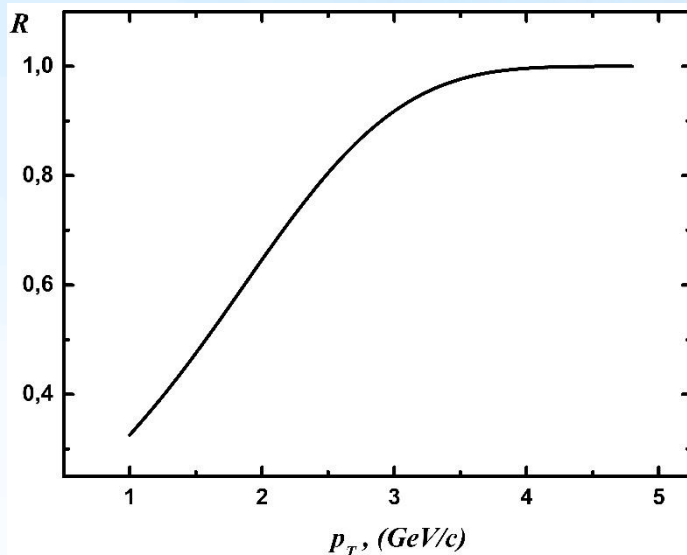


*e*

Fig.17 Dependence of the differential cross sections 1-  $qg \rightarrow q\gamma$  , 2-  $q\gamma \rightarrow q\gamma$  on a) the sum of energies of colliding particles  $\sqrt{s}$  at  $p_T = 0.9 \text{ GeV}/c$  and  $y=0$  , b) transverse momentum of photon  $p_T$ , c) the cosine of the scattering angle, d) the rapidity of produced photons, e)  $x_T$  at  $\sqrt{s} = 10 \text{ GeV}$  and  $y=0$



**a**



**b**

Fig.18 Dependence  $R = \frac{\frac{d^2\sigma(q_s\gamma \rightarrow q_s\gamma)}{dydp_T^2}}{\frac{d^2\sigma(q\gamma \rightarrow q\gamma)}{dydp_T^2}}$  (a),  $R = \frac{\frac{d^2\sigma(q_v\gamma \rightarrow q_v\gamma)}{dydp_T^2}}{\frac{d^2\sigma(q\gamma \rightarrow q\gamma)}{dydp_T^2}}$  (b) on the transverse

momentum of produced prompt photons  $p_T$  at  $\sqrt{s} = 10 \text{ GeV}$  and  $y=0$ .

At low values of  $p_T$ , the subprocess with sea quarks dominates (Fig.18(a)). As can be seen from fig.18(b), at high values of  $p_T$  the dominant subprocess is the subprocess with valence quarks in the subprocess .

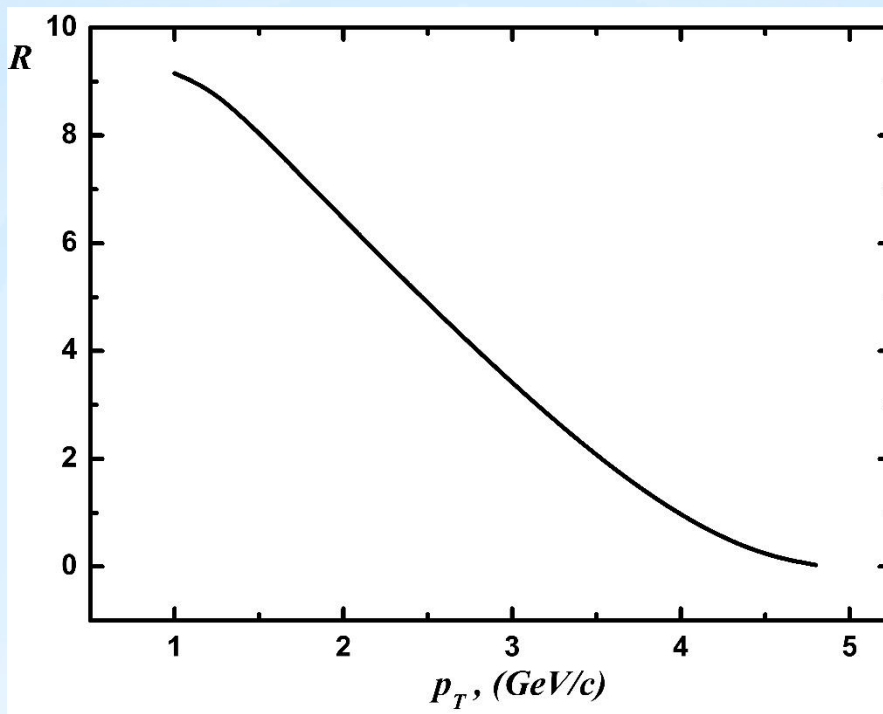


Fig.20 Dependence of the ratio of differential cross sections transverse momentum of photon  $p_T$  at  $\sqrt{s} = 10 \text{ GeV}$  and  $y=0$ .

$$R = \frac{d\sigma(qg \rightarrow q\gamma)}{d\sigma(q\gamma \rightarrow q\gamma)} \quad \text{on the}$$

As can be seen from fig.20, the real Compton scattering  $q\gamma \rightarrow q\gamma$  has a smaller differential cross section than the process of virtual Compton scattering  $qg \rightarrow q\gamma$ . This is due to the fact that, at the initial moment of collision, the distribution of photons inside the quark gluon plasma is smaller than the distribution of gluons.

## 6. Subprocess $g\gamma \rightarrow q\bar{q}$

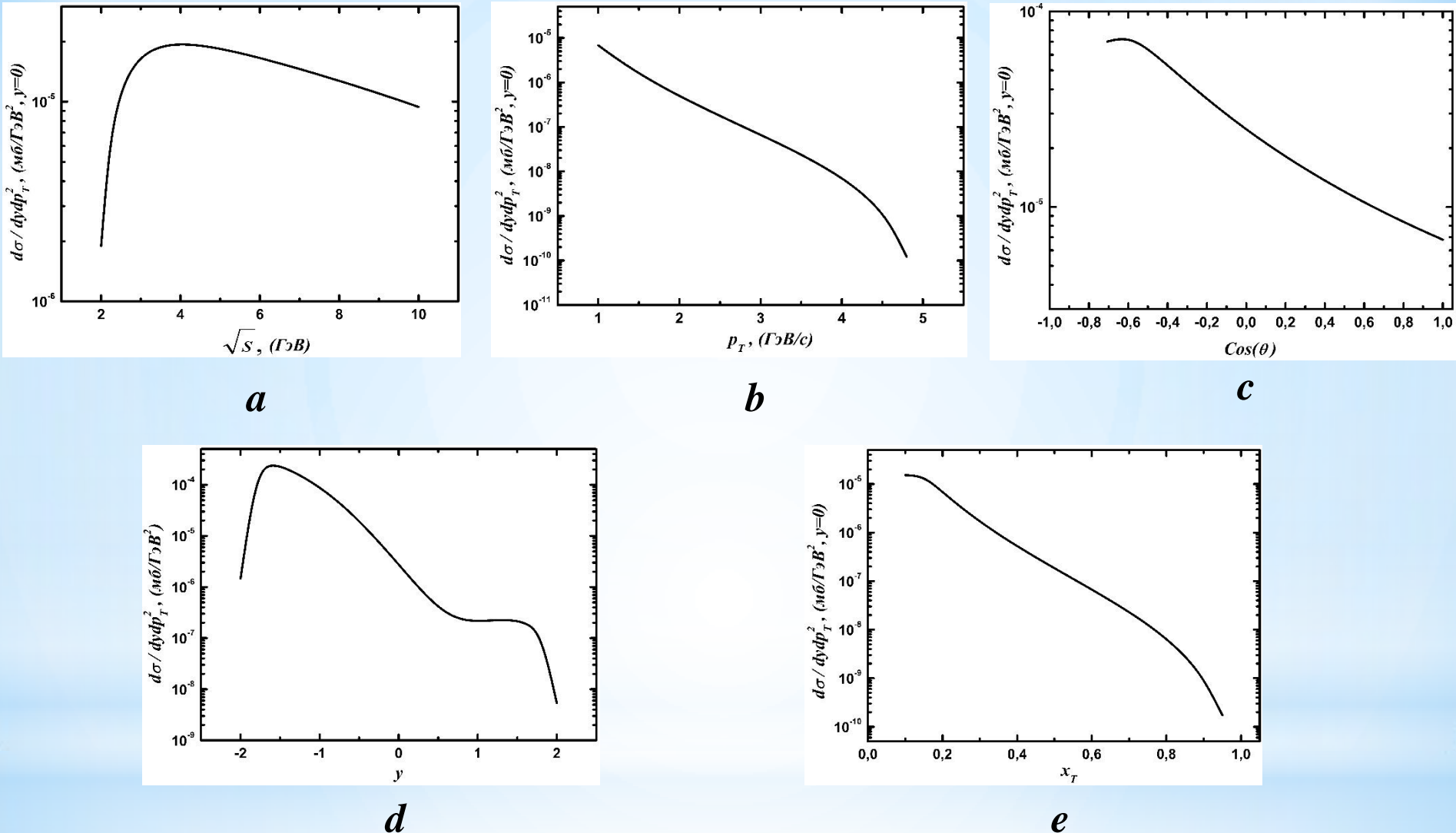


Fig.21 Dependence of the differential cross sections on a) the sum of energies of colliding particles  $\sqrt{s}$  at  $p_T=0.9 \text{ GeV}/c$  and  $y=0$ , b) transverse momentum of photon  $p_T$ , c) the cosine of the scattering angle, d) the rapidity of produced photons, e)  $x_T$  at  $\sqrt{s}=10 \text{ GeV}$  and  $y=0$

## 7. Subprocess $q\gamma \rightarrow qg$

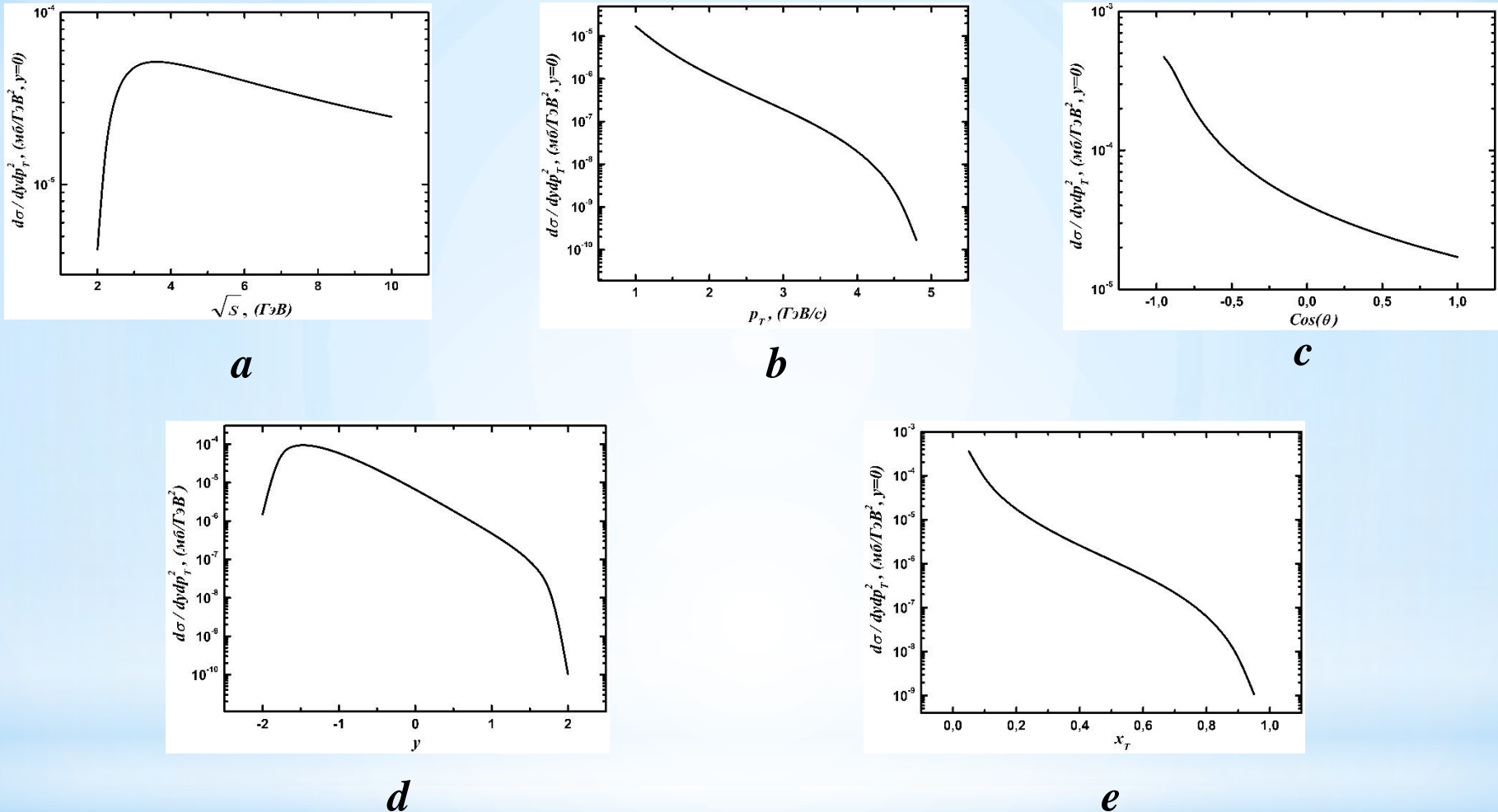
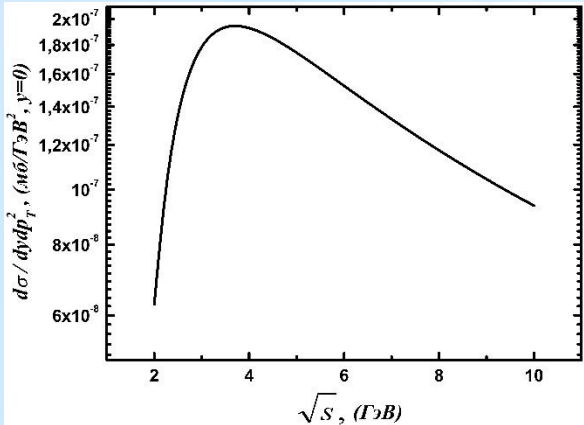


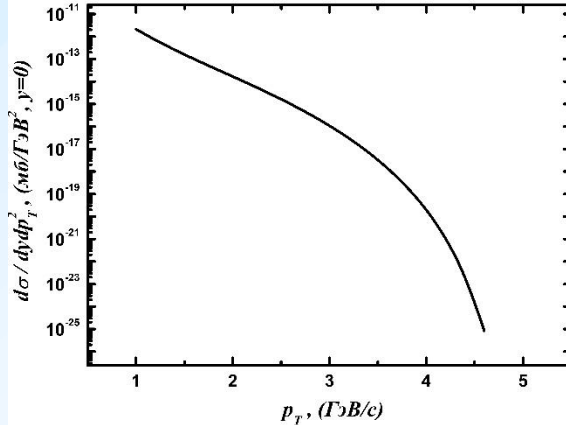
Fig.22 Dependence of the differential cross sections on a) the sum of energies of colliding particles  $\sqrt{s}$  at  $p_T=0.9$  GeV/c and  $y=0$ , b) transverse momentum of photon  $p_T$ , c) the cosine of the scattering angle, d) the rapidity of produced photons, e)  $x_T$  at  $\sqrt{s}=10$  GeV and  $y=0$

## IV.2 Corrections to the annihilation of quark-antiquark pair

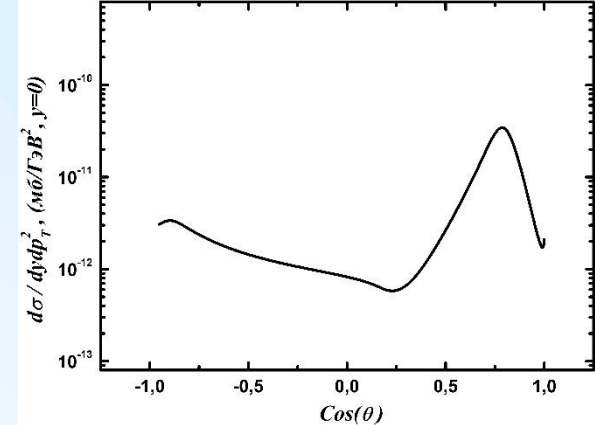
### 1.1 Subprocess $q\bar{q} \rightarrow g g \gamma$



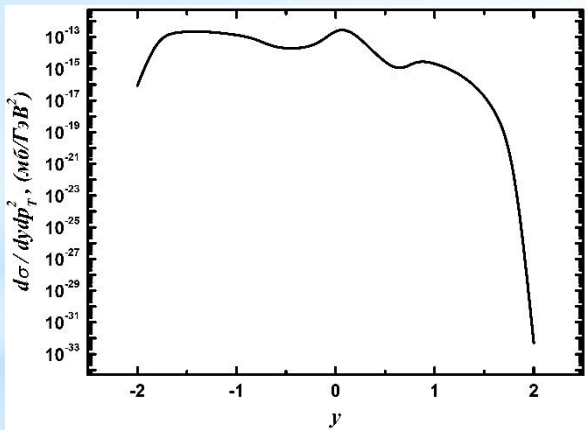
*a*



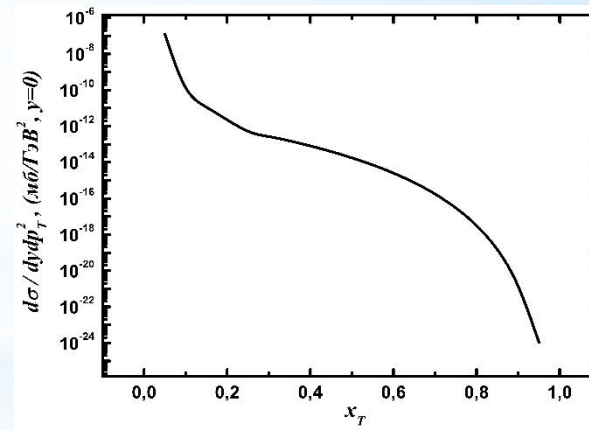
*b*



*c*



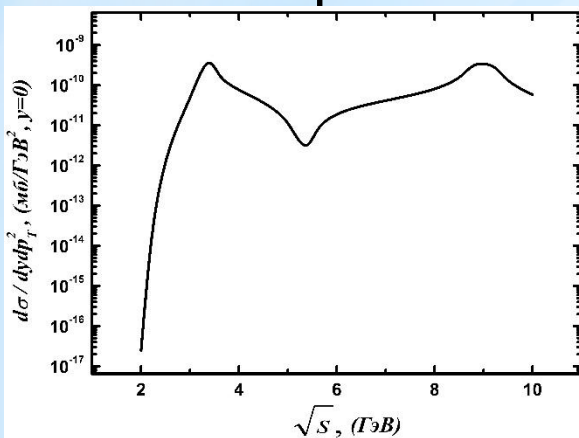
*d*



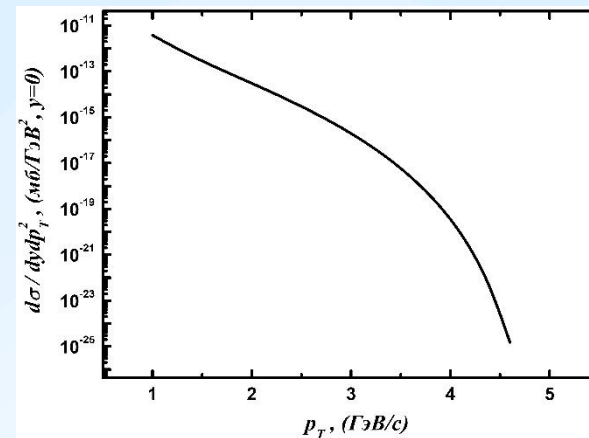
*e*

Fig.23 Dependence of the differential cross sections on a) the sum of energies of colliding particles  $\sqrt{s}$  at  $p_T=0.9$   $GeV/c$  and  $y=0$  , b) transverse momentum of photon  $p_T$ , c) the cosine of the scattering angle, d) the rapidity of produced photons, e)  $x_T$  at  $\sqrt{s}=10$   $GeV$  and  $y=0$

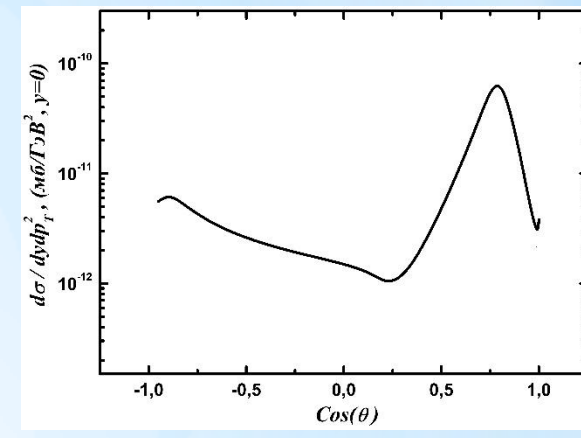
## 1.2 Subprocess $q\bar{q} \rightarrow ggg$ with taking into account the polarization of the initial particles



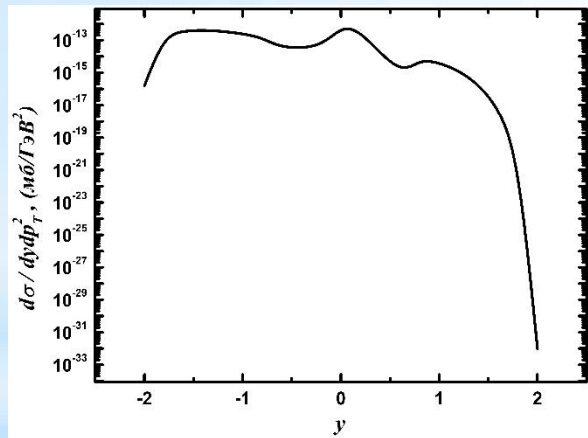
**a**



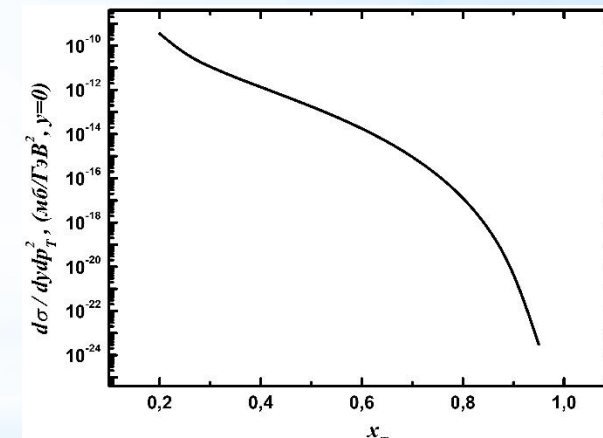
**b**



**c**



**d**



**e**

Fig.24 Dependence of the differential cross sections on a) the sum of energies of colliding particles  $\sqrt{s}$  at  $p_T = 0.9 \text{ GeV}/c$  and  $y = 0$ , b) transverse momentum of photon  $p_T$ , c) the cosine of the scattering angle, d) the rapidity of produced photons, e)  $x_T$  at  $\sqrt{s} = 10 \text{ GeV}$  and  $y = 0$

## 2.1 Subprocess $q\bar{q} \rightarrow q\bar{q}\gamma$

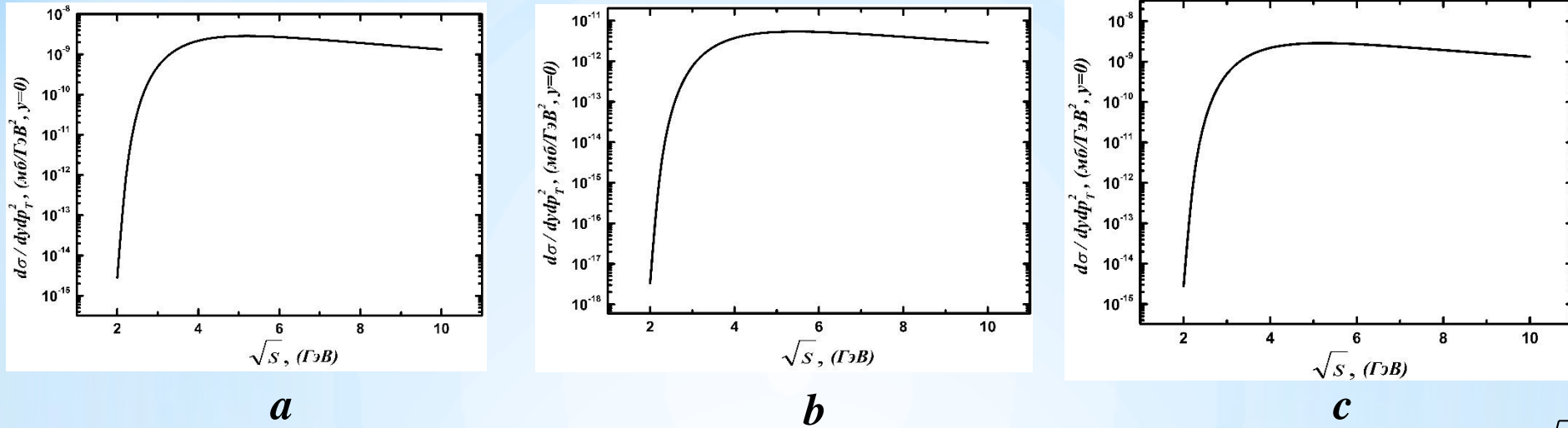


Fig.25 Dependence of the differential cross section on the sum of energy of colliding particles  $\sqrt{s}$   
 a) in the propagator  $\gamma$ , b) in the proragator  $g$ , c) the complete subprocess  $q\bar{q} \rightarrow q\bar{q}\gamma$  at  $p_T=0.9$  GeV/c and  $y=0$

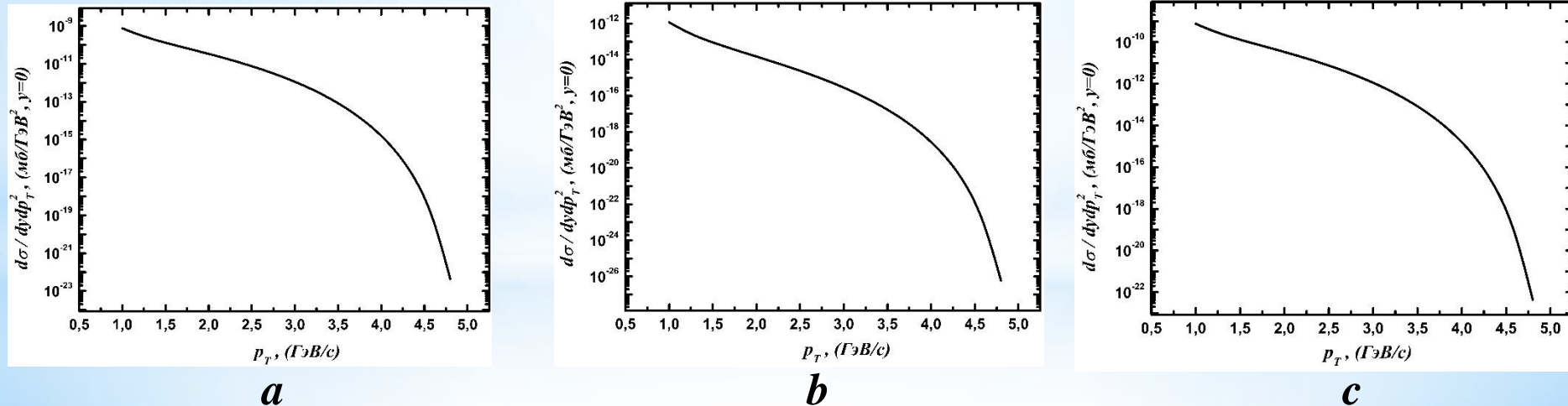
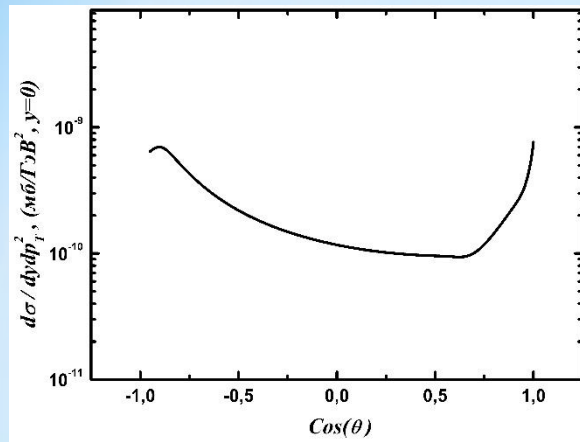
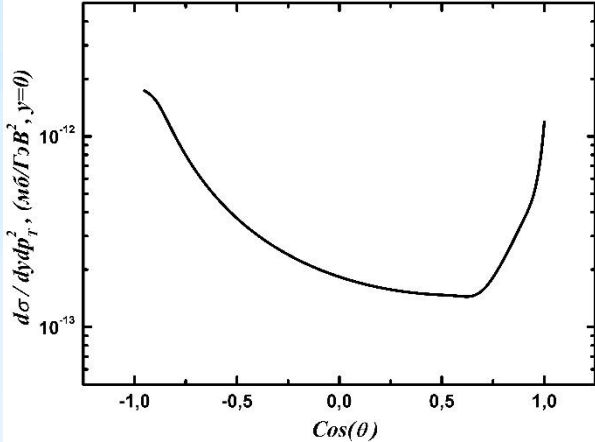


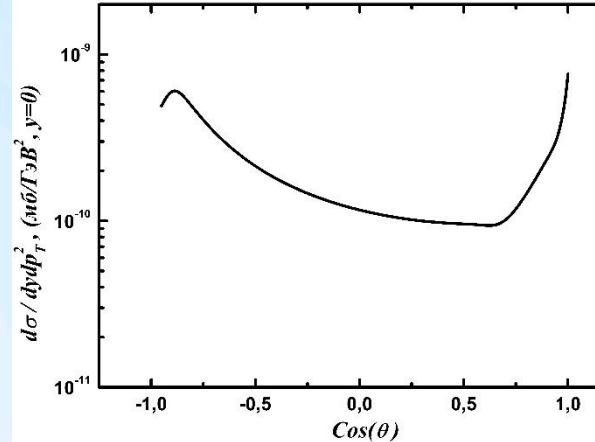
Fig.26 Dependence of the differential cross section on the transverse momentum of photon  $p_T$   
 a) in the propagator  $\gamma$ , b) in the proragator  $g$ , c) the complete subprocess at  $\sqrt{s}=10$  GeV and  $y=0$



**a**

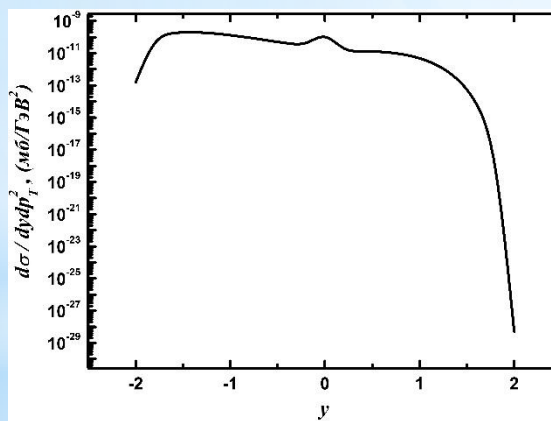


**b**

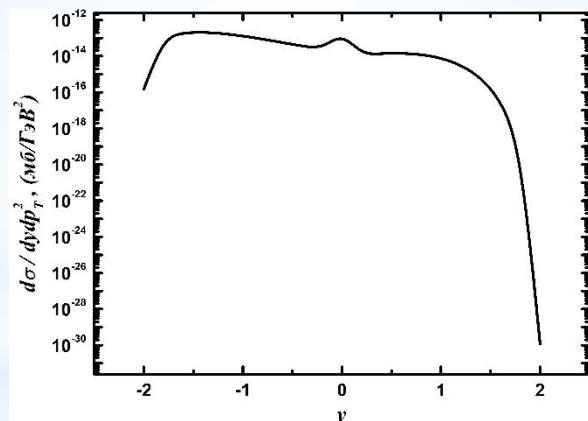


**c**

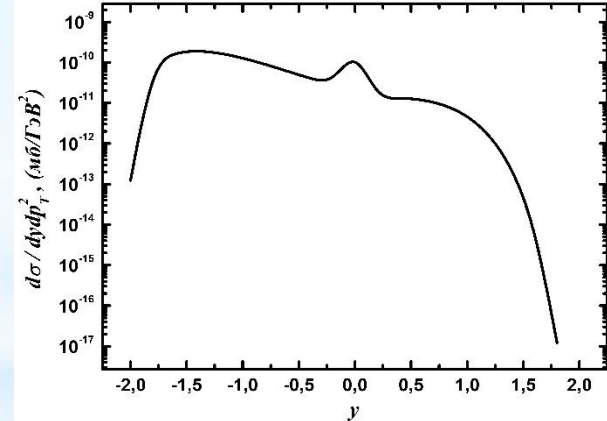
Fig.27 Dependence of the differential cross section on the cosine of the scattering angle  $\text{Cos}(\theta)$  a) in the propagator  $\gamma$ , b) in the proragator  $g$ , c) the complete subprocess at  $\sqrt{s}=10 \text{ GeV}$  and  $y=0$



**a**

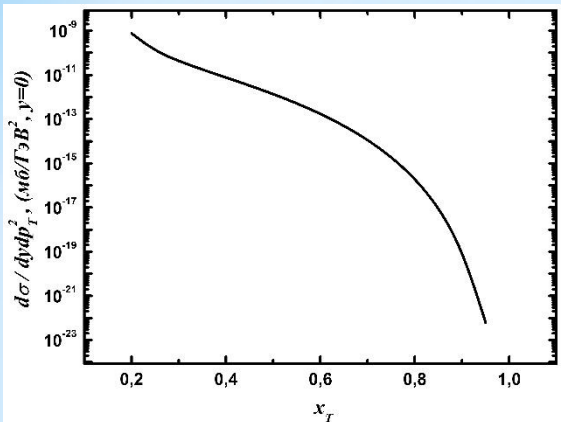


**b**

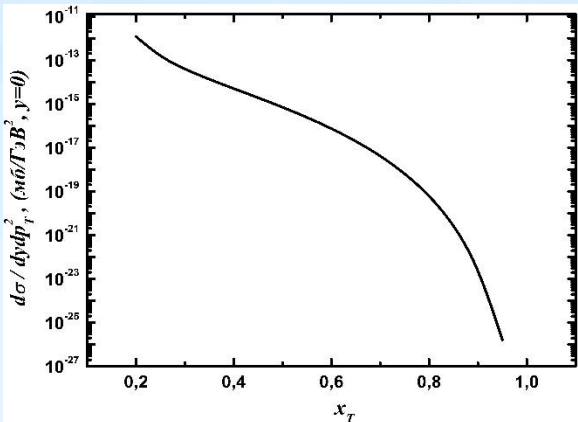


**c**

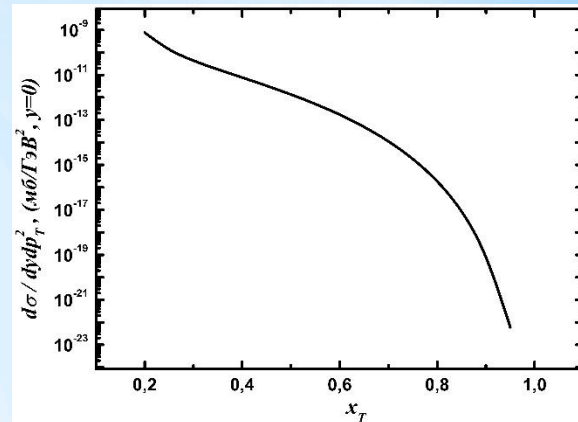
Fig.28 Dependence of the differential cross section on the  $y$  a) in the propagator  $\gamma$ , b) in the proragator  $g$ , c) the complete subprocess at  $\sqrt{s}=10 \text{ GeV}$  and  $p_T=0.9 \text{ GeV}/c$



*a*



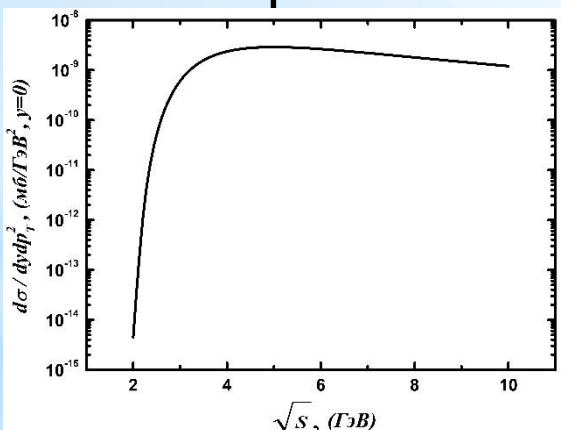
*b*



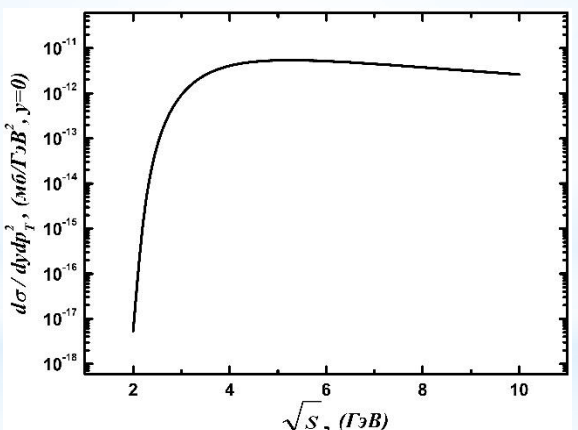
*c*

Fig.29 Dependence of the differential cross section on  $x_T$  a) in the propagator  $\gamma$ , b) in the propagator  $g$ , c) the complete subprocess

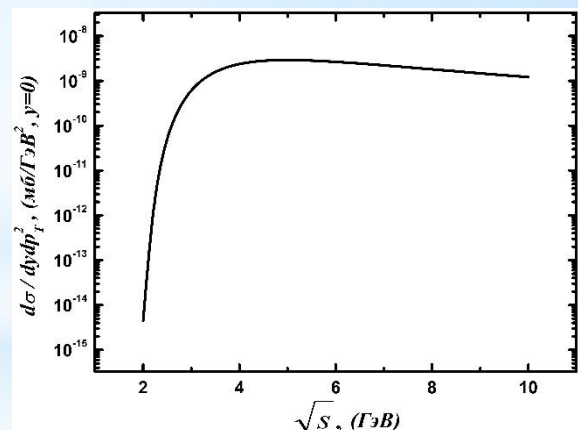
## 2.2 Subprocess $q\bar{q} \rightarrow q\bar{q}\gamma$ with taking into account the polarization of the initial particles



*a*

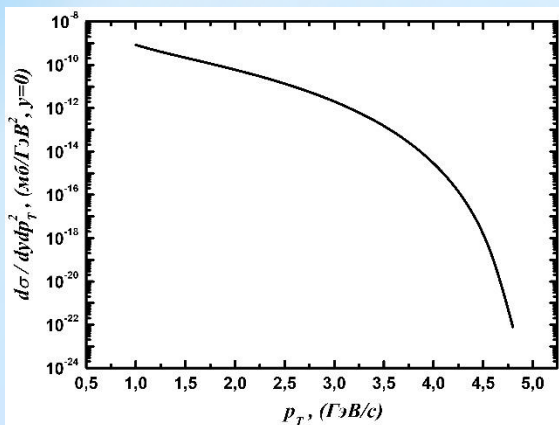


*b*

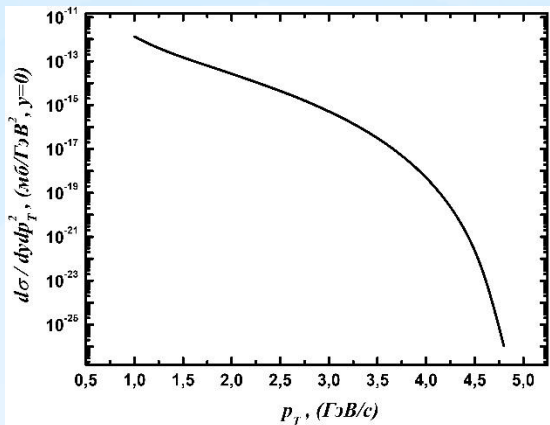


*c*

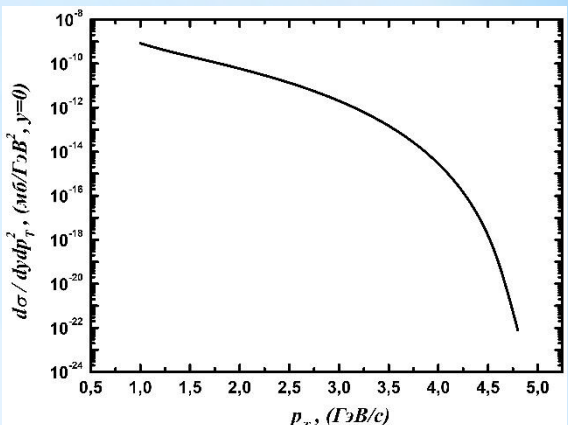
Fig.30 Dependence of the differential cross section on the sum of energy of colliding particles  $\sqrt{s}$  taking into account the polarization of the initial particles a) in the propagator  $\gamma$ , b) in the propagator  $g$ , c) the complete subprocess



**a**

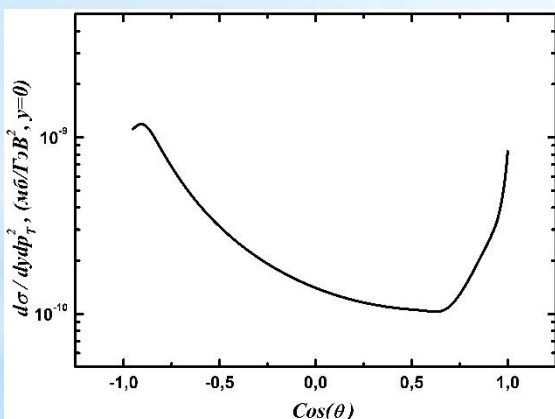


**b**

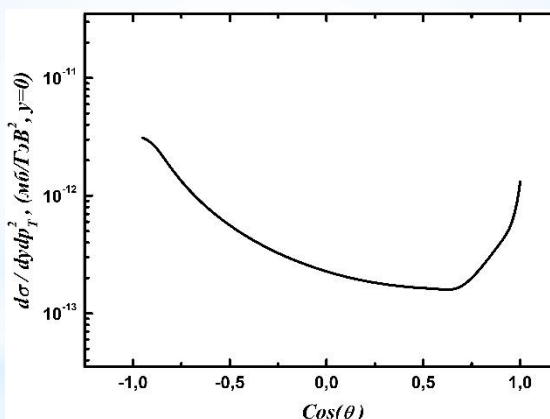


**c**

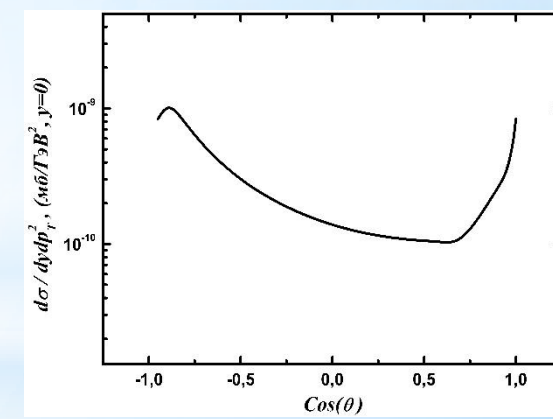
Fig.31 Dependence of the differential cross section on the transverse momentum of photon  $p_T$  taking into account the polarization of the initial particles a) in the propagator  $\gamma$ , b) in the proragator  $g$ , c) the complete subprocess



**a**

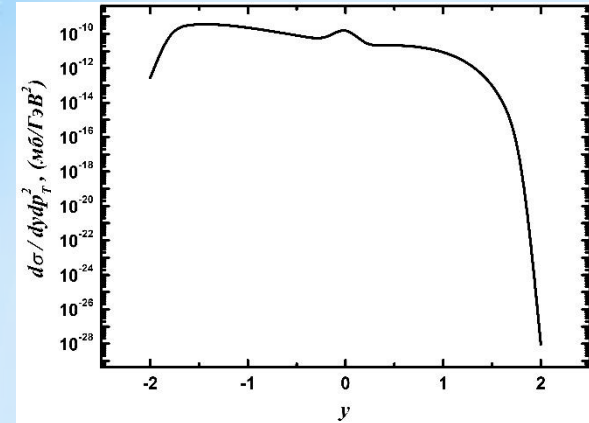


**b**

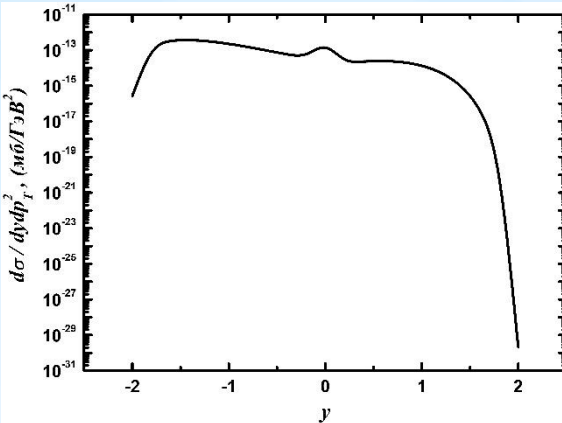


**c**

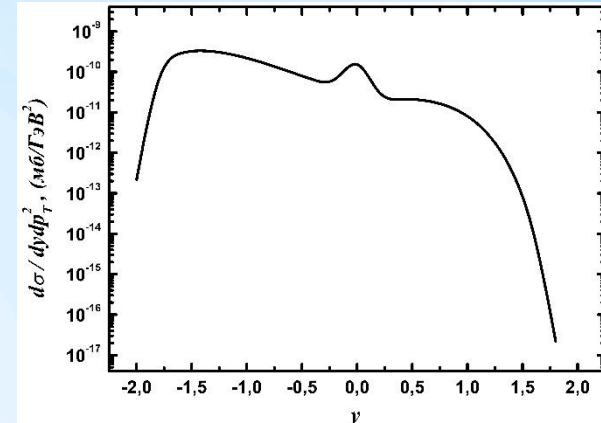
Fig.32 Dependence of the differential cross section on the cosine of the scattering angle  $Cos(\theta)$  taking into account the polarization of the initial particles a) in the propagator  $\gamma$ , b) in the proragator  $g$ , c) the complete subprocess



*a*

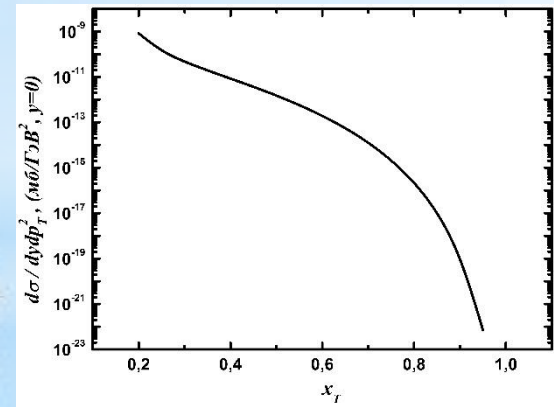


*b*

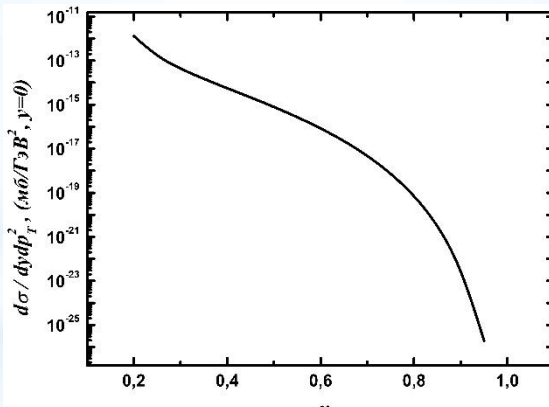


*c*

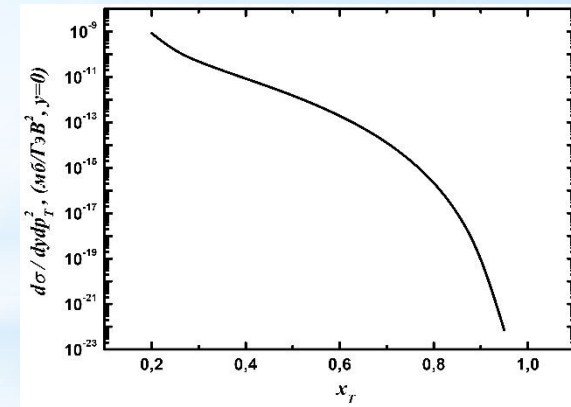
Fig.33 Dependence of the differential cross section on the rapidity of photons  $y$ , taking into account the polarization of the initial particles a) in the propagator  $\gamma$ , b) in the propagator  $g$ , c) the complete subprocess



*a*



*b*



*c*

Fig.34 Dependence of the differential cross section on  $x_T$  taking into account the polarization of the initial particles a) in the propagator  $\gamma$ , b) in the proragator  $g$ , c) the complete subprocess

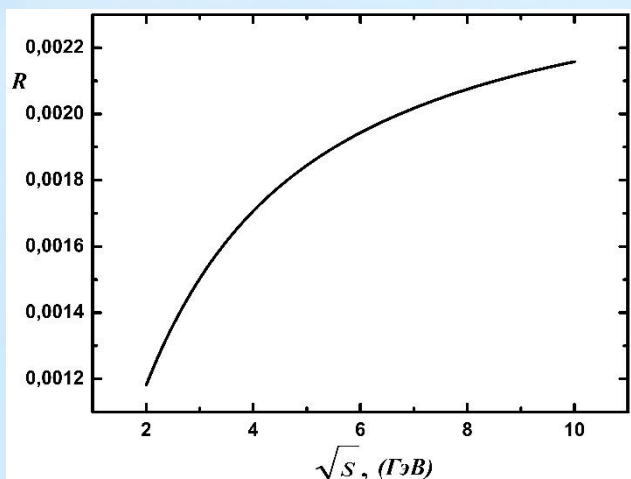


Fig.35 Dependence of the ratio of differential cross sections  $R$  (Photon/Gluon) from  $\sqrt{s}$  at  $p_T=0.9\text{GeV}/c$  and  $y=0$

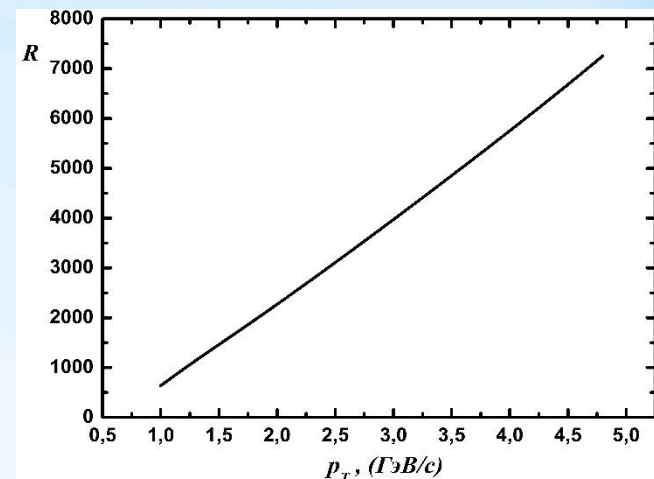


Fig.36 Dependence of the ratio of differential cross sections  $R$  on the transverse momentum of photon  $p_T$  at  $\sqrt{s}=10\text{ GeV}$  and  $y=0$

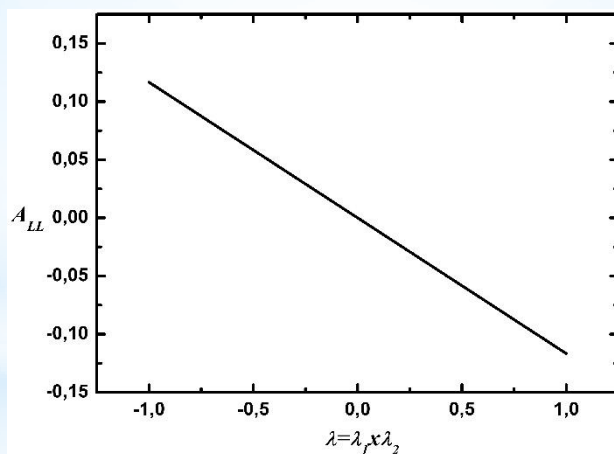
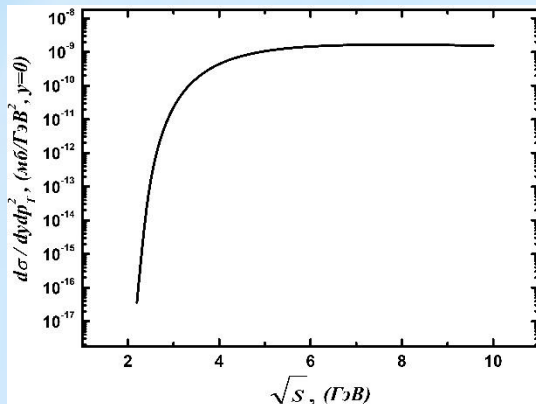
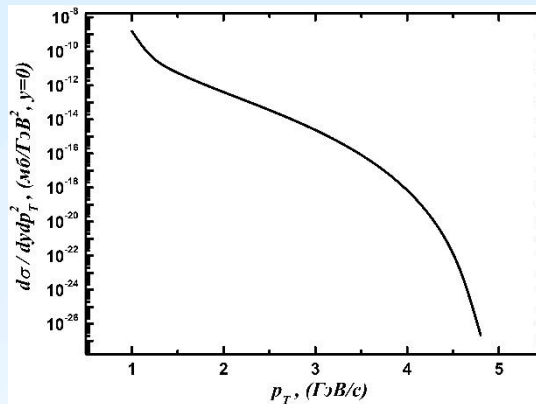


Fig.37 Dependence of the double-spin asymmetry  $A_{LL}$  on the helicity product  $\lambda_1\lambda_2$  at  $p_T=1\text{ GeV}/c$ ,  $\sqrt{s}=10\text{ GeV}$  and  $y=0$

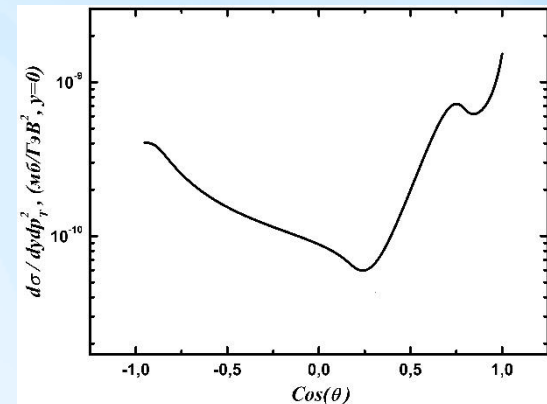
### 3.1 Subprocess $q\bar{q} \rightarrow g\gamma\gamma$



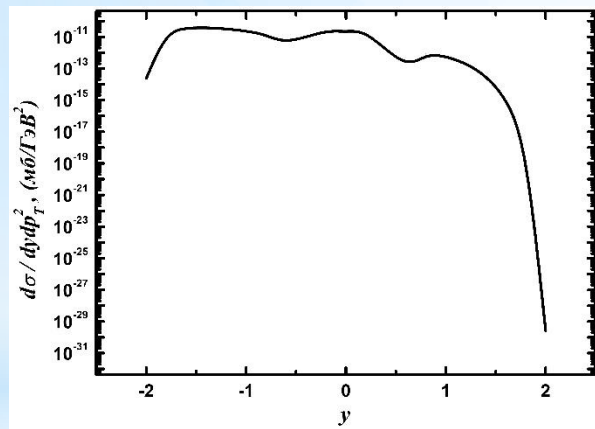
*a*



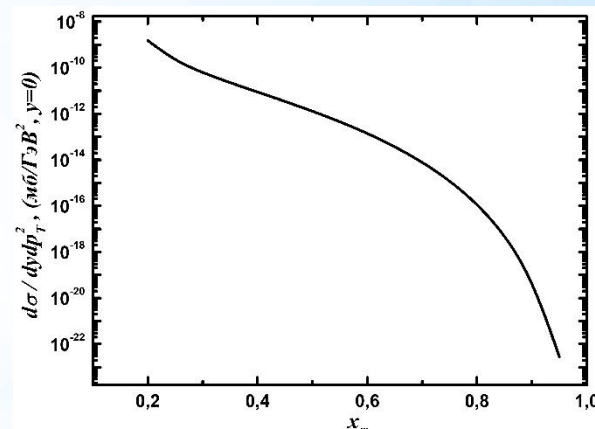
*b*



*c*



*d*



*e*

Fig.38 Dependence of the differential cross sections on a) the sum of energies of colliding particles  $\sqrt{s}$  at  $p_T = 0.9$   $GeV/c$  and  $y = 0$ , b) transverse momentum of photon  $p_T$ , c) the cosine of the scattering angle, d) the rapidity of produced photons, e)  $x_T$  at  $\sqrt{s} = 10$   $GeV$  and  $y = 0$

### 3.2 Subprocess $q\bar{q} \rightarrow g\gamma\gamma$ with taking into account the polarization of the initial particles

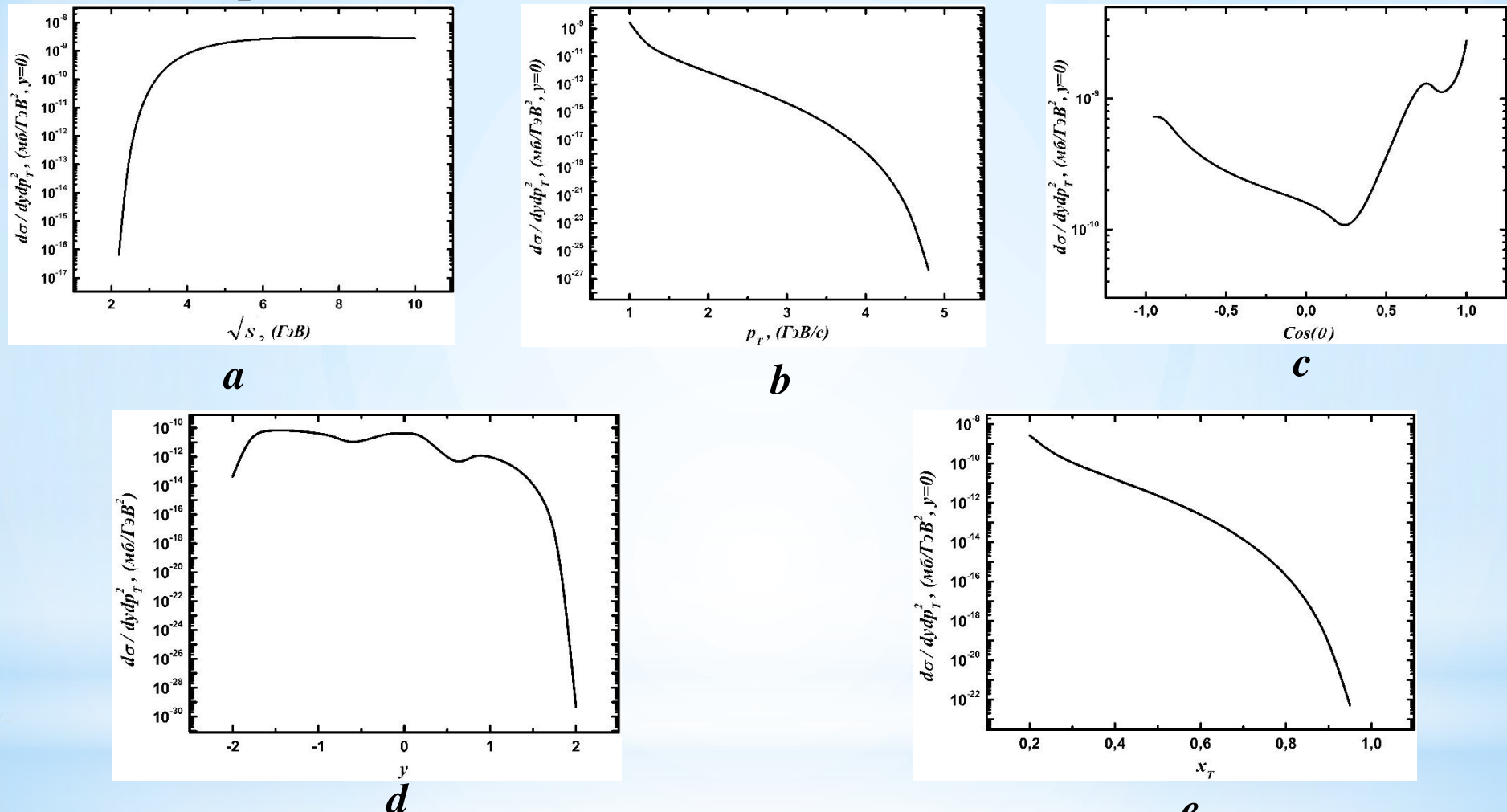
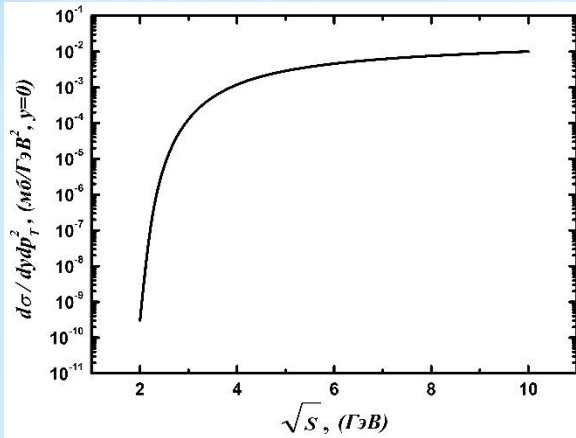


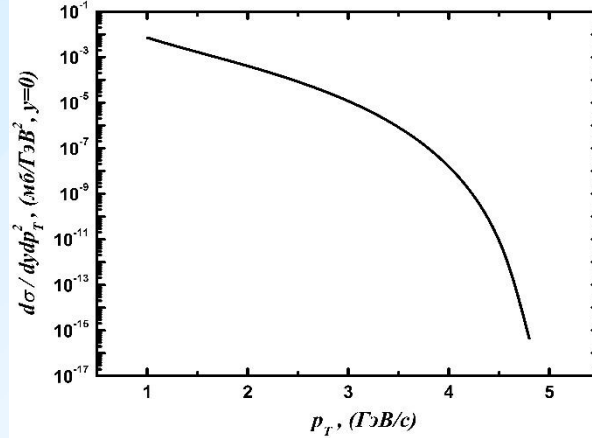
Fig.39 Dependence of the differential cross sections on a) the sum of energies of colliding particles  $\sqrt{s}$  at  $p_T = 0.9 \text{ GeV}/c$  and  $y = 0$ , b) transverse momentum of photon  $p_T$  c) the cosine of the scattering angle, d) the rapidity of produced photons, e)  $x_T$  at  $\sqrt{s} = 10 \text{ GeV}$  and  $y = 0$

## 4.1 Subprocess

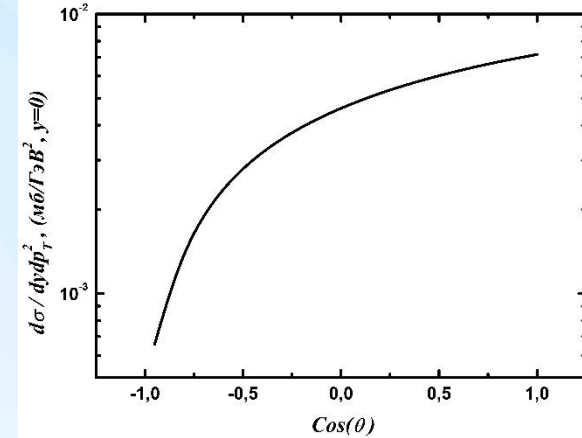
$$q\bar{q} \rightarrow \gamma\gamma$$



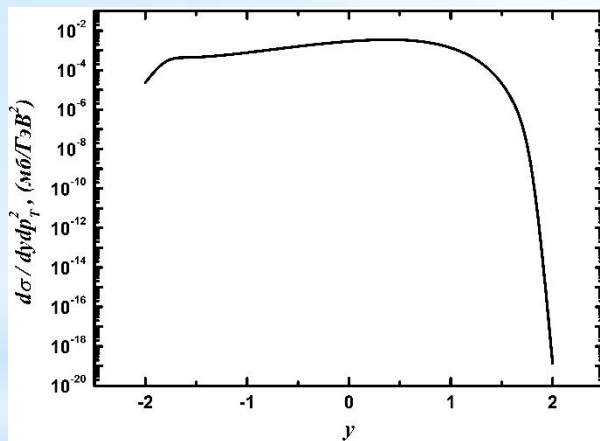
*a*



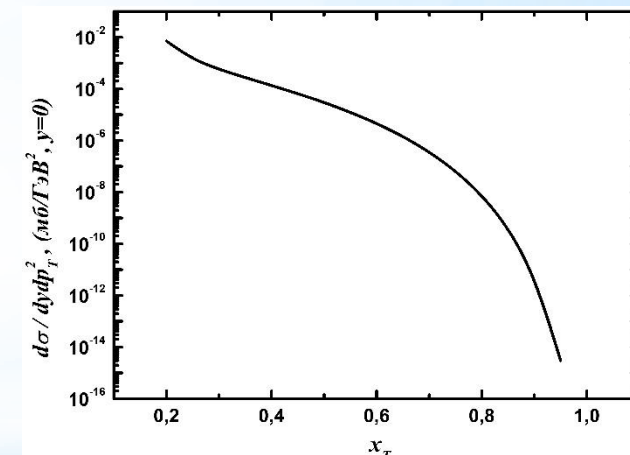
*b*



*c*



*d*



*e*

Fig.40 Dependence of the differential cross sections on a) the sum of energies of colliding particles  $\sqrt{s}$  at  $p_T = 0.9 \text{ GeV}/c$  and  $y = 0$ , b) transverse momentum of photon  $p_T$  c) the cosine of the scattering angle, d) the rapidity of produced photons, e)  $x_T$  at  $\sqrt{s} = 10 \text{ GeV}$  and  $y = 0$

## 4.2 Subprocess $q\bar{q} \rightarrow \gamma\gamma$ with taking into account the polarization of the initial particles

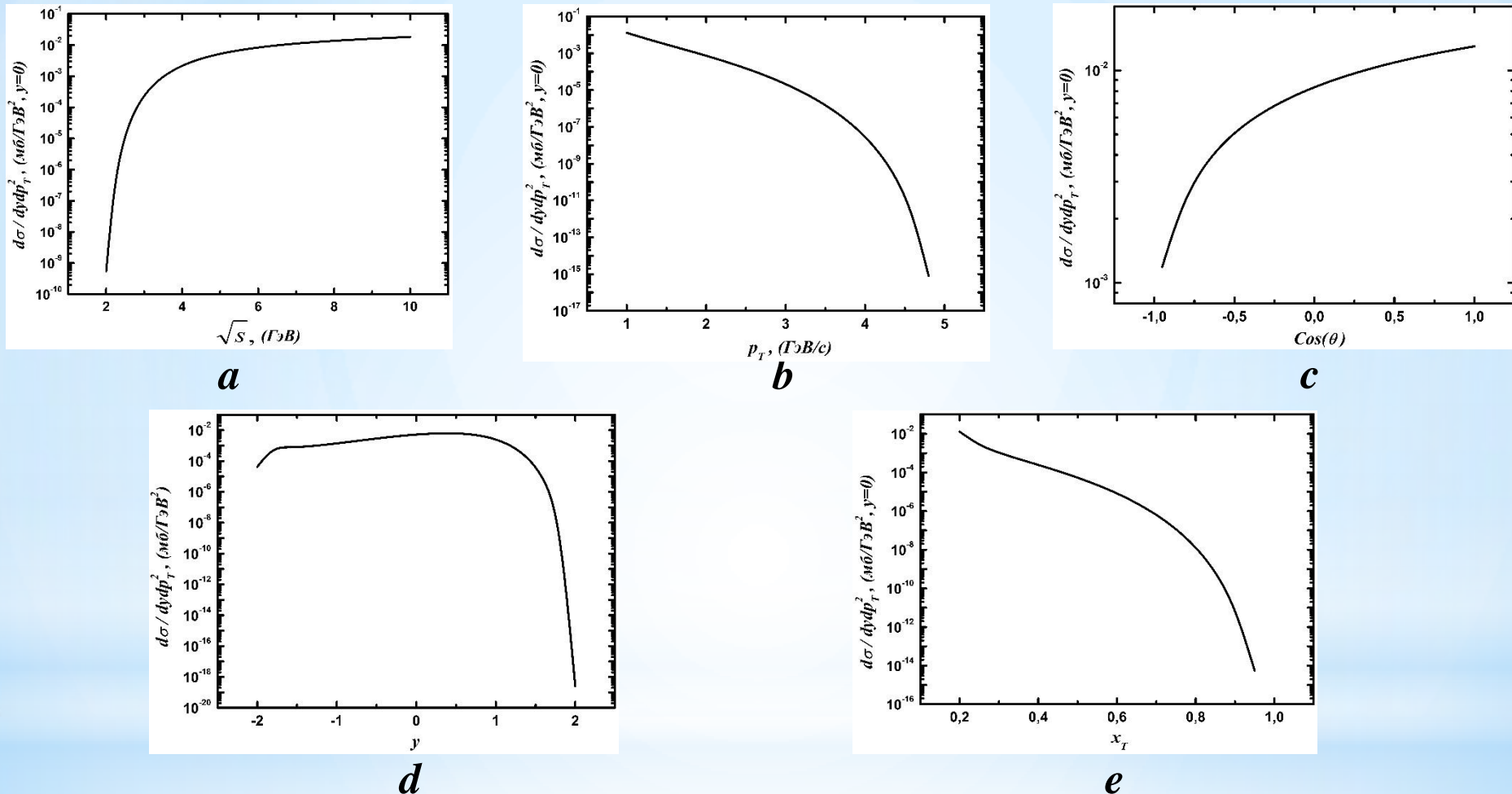


Fig.41 Dependence of the differential cross sections on a) the sum of energies of colliding particles  $\sqrt{s}$  at  $p_T=0.9 \text{ GeV}/c$  and  $y=0$ , b) transverse momentum of photon  $p_T$ , c) the cosine of the scattering angle, d) the rapidity of produced photons, e)  $x_T$  at  $\sqrt{s}=10 \text{ GeV}$  and  $y=0$

## V. Comparison of contributions of corrections to the Compton scattering of quark-gluon and annihilation of quark-antiquark pair

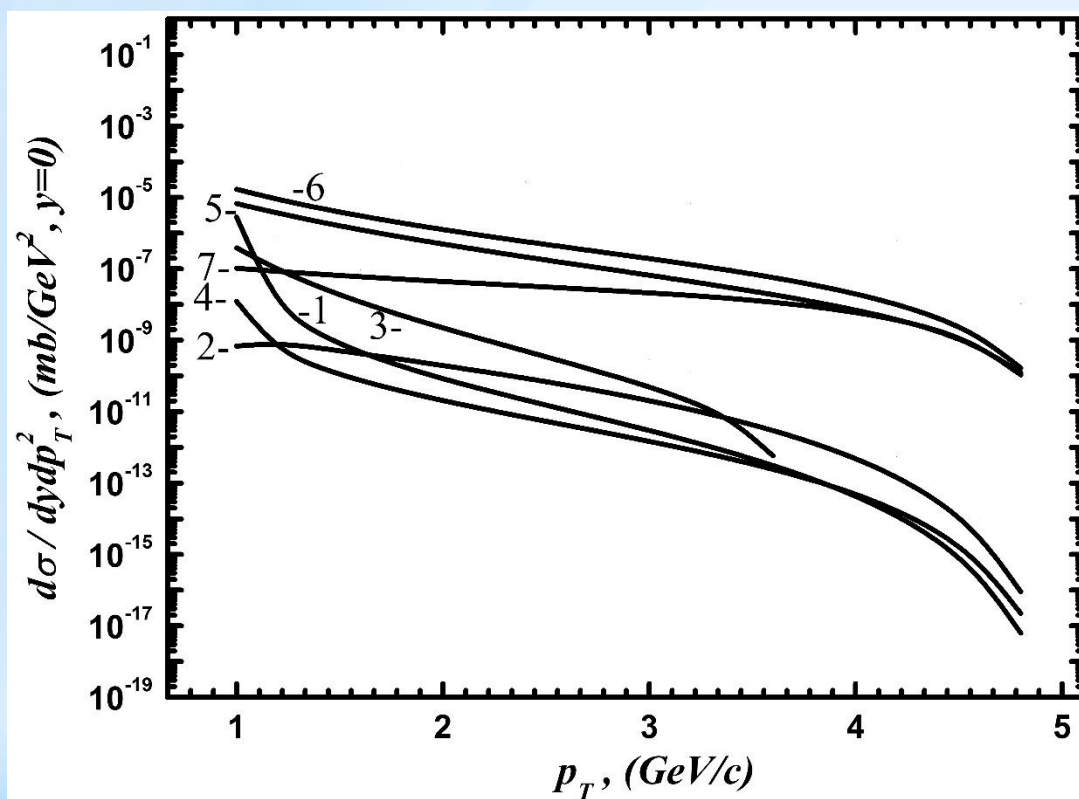


Fig.42 Comparing of the dependences of the differential cross section on the transverse momentum of photon  $p_T$  of subprocesses :

1.  $qg \rightarrow qg\gamma$  , 2.  $qg \rightarrow g\gamma\gamma$ ,
3.  $q\gamma \rightarrow qg\gamma$  , 4.  $g\gamma \rightarrow q\bar{q}\gamma$ ,
5.  $g\gamma \rightarrow q\bar{q}$  , 6.  $q\gamma \rightarrow qg$  and
7.  $q\gamma \rightarrow q\gamma$  , respectively at  $\sqrt{s} = 10 \text{ GeV}$  and  $y=0$

Figure 42 shows contribution of all the corrections to the Compton process. As can be seen from the figure, the correction of process 6 ( $q\gamma \rightarrow qg$ ) is larger and among these processes this process is dominant. Process 4 gives the minimum contribution. All contributions tend to decrease with increasing  $p_T$ . The contribution of the corrections is significant at small value of  $p_T$ .

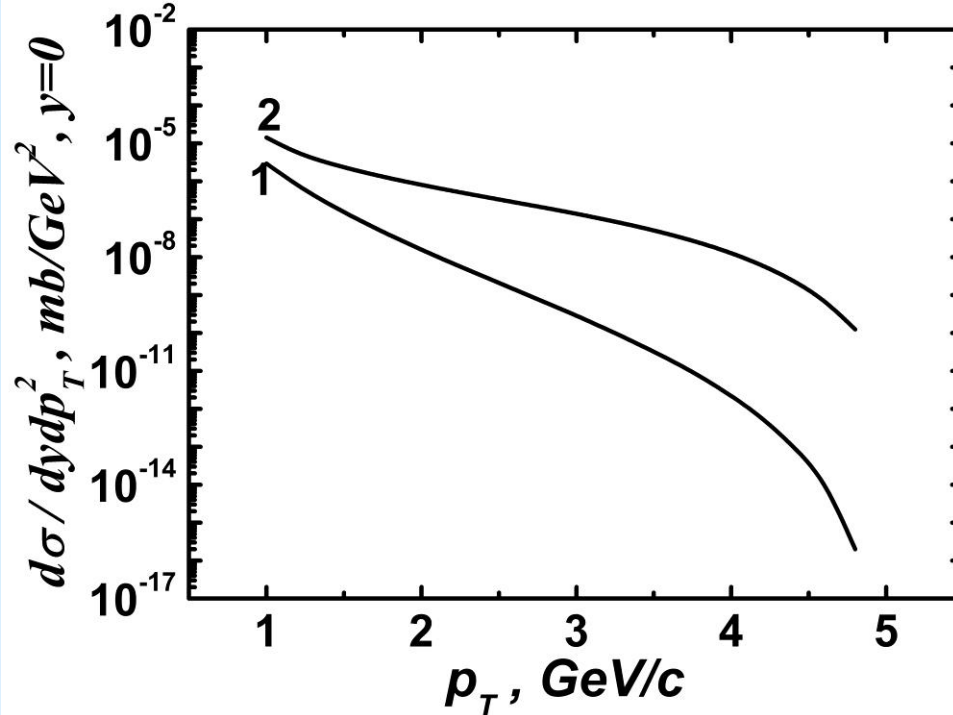


Fig.43 The dependence of differential cross section of Compton scattering quark-gluon (curve 1) and sum of all differential cross sections of corrections and Compton scattering (curve 2) on transverse momentum .

Contributions of corrections to Compton scattering is significant at big values of  $p_T$ .

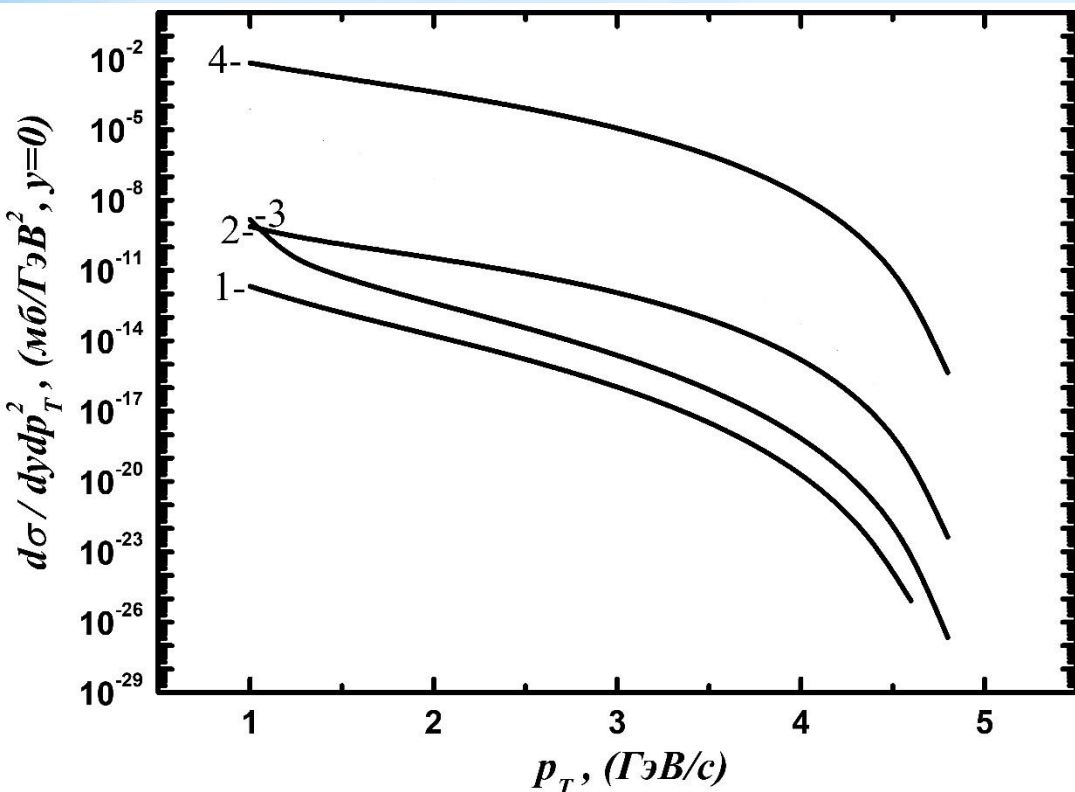


Fig.44 Comparing of the dependences of the differential cross section on the transverse momentum of photon  $p_T$  of subprocesses: 1.  $q\bar{q} \rightarrow gg\gamma$ , 2.  $q\bar{q} \rightarrow q\bar{q}\gamma$ , 3.  $q\bar{q} \rightarrow g\gamma\gamma$  and 4.  $q\bar{q} \rightarrow \gamma\gamma$ , respectively at  $\sqrt{s} = 10 \text{ GeV}$  and  $y = 0$

Fig.44 shows all corrections to the process of annihilation of a quark-antiquark pair. As can be seen from the figure, the correction of process 4 is larger, which indicates that it makes a large contribution. Process 1 gives the smallest value. In the process of annihilation of a quark-antiquark pair, the corrections, as well as in the Compton process, decrease with increasing  $p_T$  and the contributions are significant at small value of  $p_T$ .

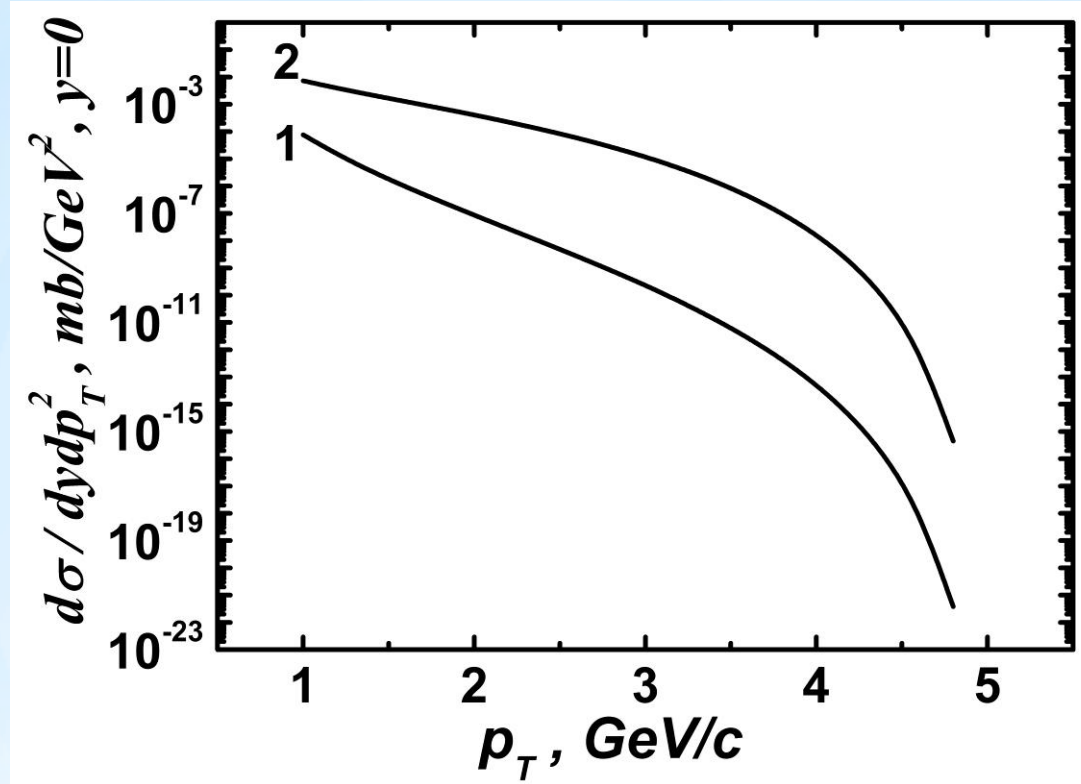


Fig.45 The dependence of differential cross sections of annihilation of quark-antiquark pair (curve 1) and sum of all corrections to annihilation quark-antiquark pair and annihilation (curve 2) on transverse momentum  $p_T$  at  $\sqrt{s} = 10 \text{ GeV}$  and  $y=0$ .

As seen fig.45 contributions of corrections to annihilation process is significant at  $p_T = 3.5 \text{ GeV}/c$ .

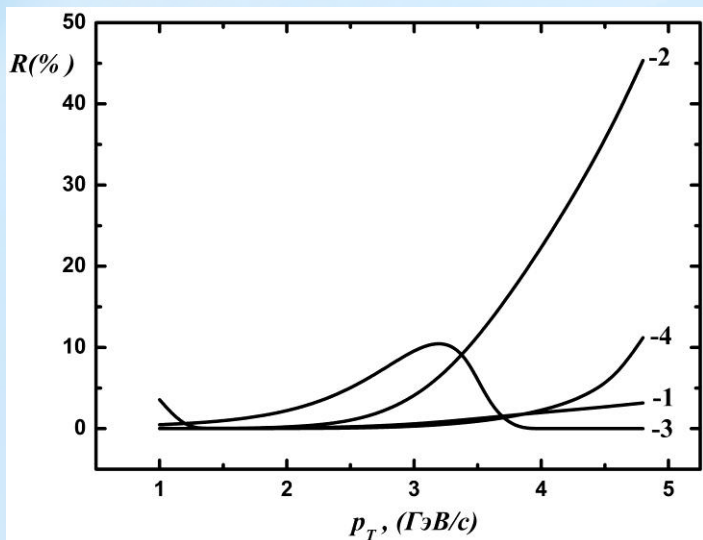


Fig.46 Dependence of the ratio of differential cross sections of the radiation corrections 1.  $qg \rightarrow qg\gamma$  , 2.  $qg \rightarrow g\gamma\gamma$  , 3.  $q\gamma \rightarrow qg\gamma$  and 4.  $g\gamma \rightarrow q\bar{q}\gamma$  to Compton scattering on the main process of prompt photon formation.

Fig.46 shows that process 2 has a large contribution at large  $p_T$ , and process 3 has a large contribution at small  $p_T$ .

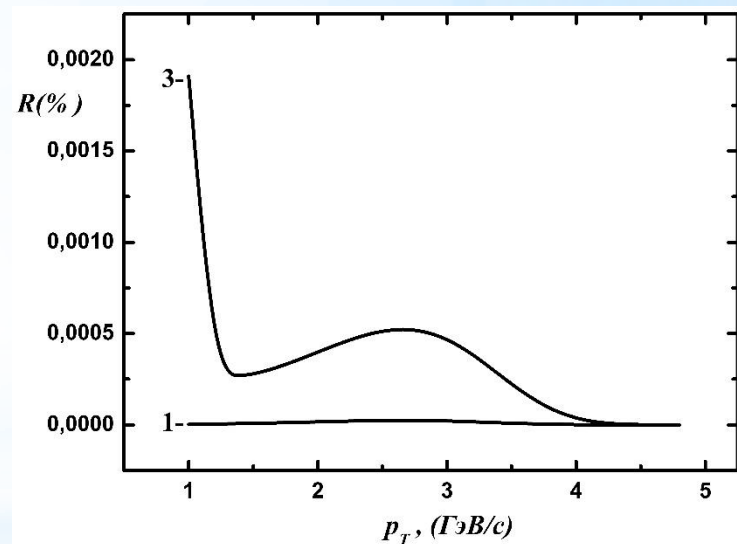
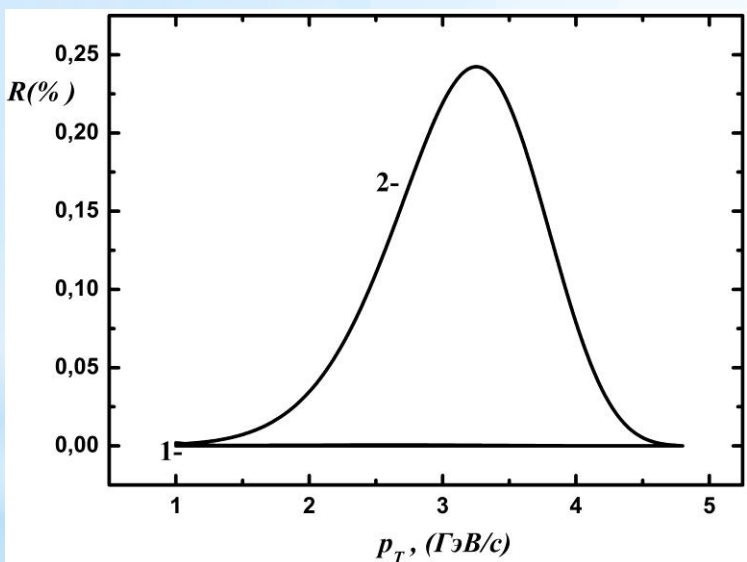


Fig.47 Dependence of the ratio of the differential cross sections of the radiation corrections 1.  $q\bar{q} \rightarrow gg\gamma$  , 2.  $q\bar{q} \rightarrow q\bar{q}\gamma$  and 3.  $q\bar{q} \rightarrow g\gamma\gamma$  to the annihilation of a quark-antiquark pair on the main process of prompt photon production.

As can be seen from Fig.47, process 2 has the largest contribution, and process 1 has the smallest. Comparing the contributions of processes 1 and 2, it can be seen that the contribution of process 2 is greater in the  $p_T$  interval equal to [1.5, 4.5]

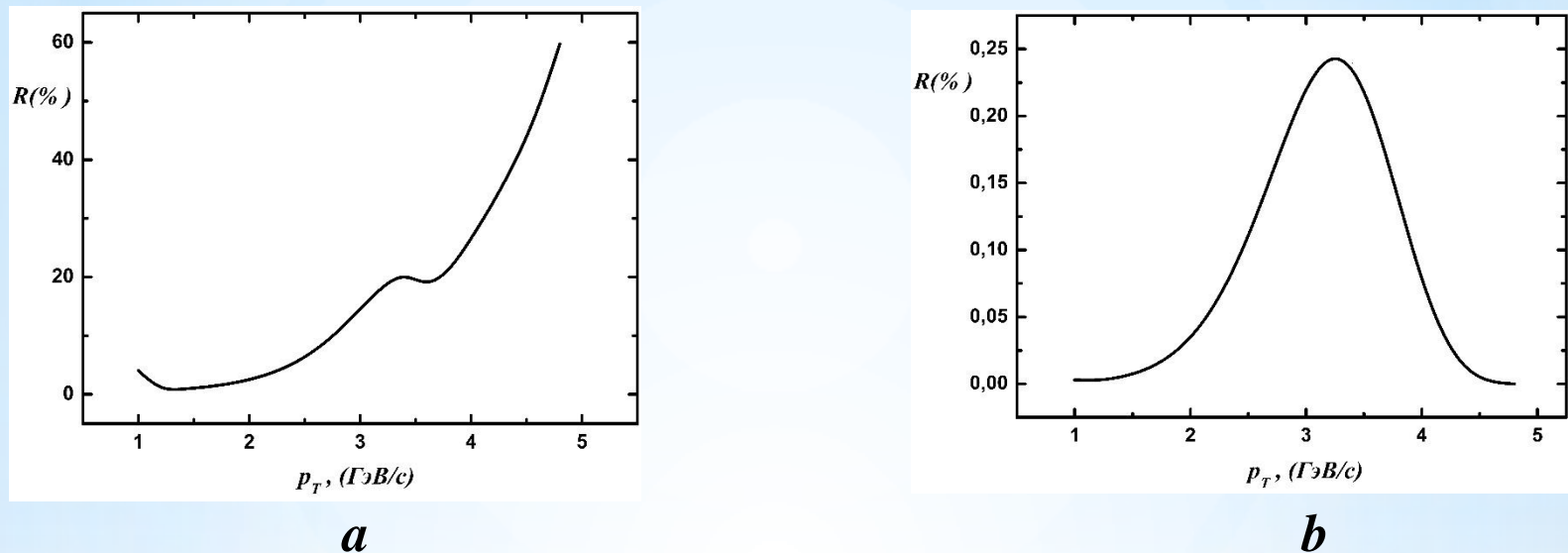


Fig.48 Dependences of the ratio of the sum of differential cross sections of a) radiation corrections to Compton scattering, b) radiation corrections to the annihilation of a quark-antiquark pair on the main process of prompt photon production

Fig.48 (a,b) shows the ratio of the sum of corrections to the process of Compton scattering (a), annihilation of a quark-antiquark pair (b) to the main process ( $pp \rightarrow \gamma X$ ). The dependence of the ratio of the sum of Compton corrections on the Leading Order (LO) increases with increasing  $p_T$ . The ratio of the differential cross section of contributions to annihilation increases with increasing  $p_T$  and reaches a maximum at  $p_T = 3.5$  GeV/c, and then it decreases.

Table 1 shows the dependences of the ratio of the contribution of all corrections to the main processes on the transverse momentum.

$P_T$	R(%)	$P_T$	R(%)
1	4	3	15
1.2	1	3.2	19
1.4	1	3.4	21
1.6	1	3.6	19
1.8	2	3.8	21
2	3	4	27
2.2	4	4.2	33
2.4	5	4.4	40
2.6	8	4.6	48
2.8	11	4.8	60

The value of the contribution of radiation corrections  $R$ :

$$R = \frac{\sigma_{rad}}{\sigma_{LO}} \times 100\%$$

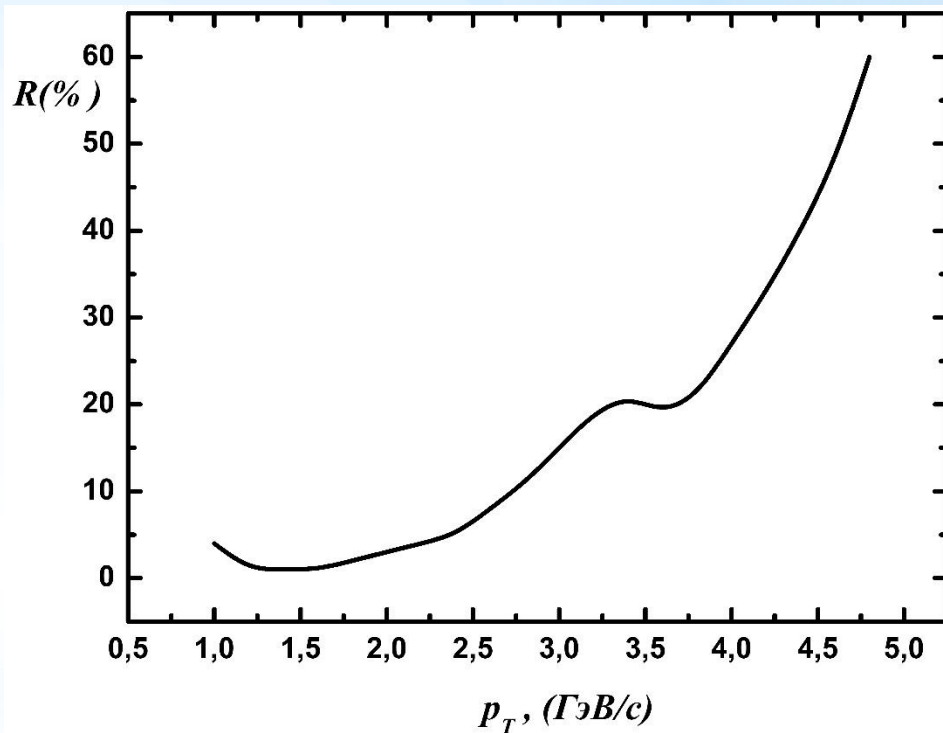


Fig.49 Dependence of the ratio of differential cross sections of radiation corrections to the main process on the transverse momentum of photon  $p_T$  at  $\sqrt{s} = 10 \text{ GeV}$  and  $y=0$ , taking into account the polarization of the initial particles

Fig.50 shows the dependence of the ratios of the differential cross sections, calculated with and without taking into account polarization, on the energy of colliding protons.

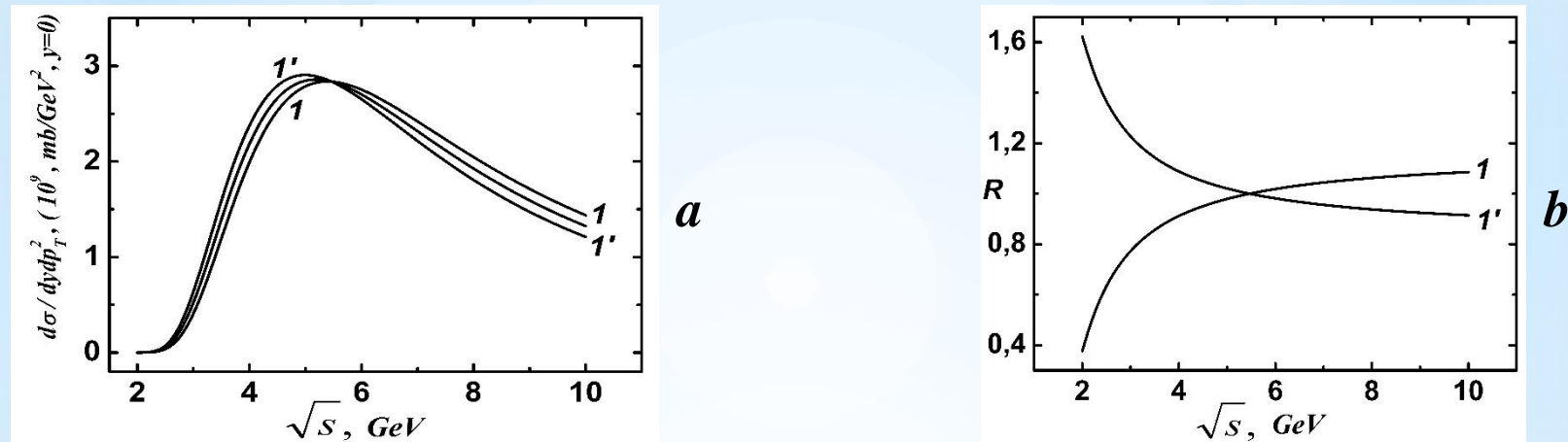


Fig.50 Curve 1.  $\lambda_1 \lambda_2 = +0.81$  and  $y = 0$ , Curve 1'.  $\lambda_1 \lambda_2 = -0.81$  and  $y = 0$

As can be seen from fig.50(b), the ratio of differential cross sections, calculated with polarization  $\lambda_1 \lambda_2 < 0$  ( $\lambda_1 \lambda_2 > 0$ ) and without polarization, decreases (increases) with increasing energy of colliding protons. Polarization has a great influence at low energies, at  $\sqrt{s} = 5.5 \text{ GeV}$  the differential cross sections calculated without polarization and with polarization taken into account coincide, and then with increasing transverse momentum, the differential cross section calculated taking into account polarization  $\lambda_1 \lambda_2 < 0$  ( $\lambda_1 \lambda_2 > 0$ ) becomes smaller (more) than the differential cross section calculated without taking into account polarization.

## VI. The doublespin asymmetry of subprocesses

The doublespin asymmetry of the subprocess  $q\bar{q} \rightarrow \gamma\gamma$ ,  $q\bar{q} \rightarrow gg\gamma$  and  $q\bar{q} \rightarrow g\gamma\gamma$   $A_{LL}$  does not depend on  $\sqrt{s}$ ,  $\cos(\theta)$  and  $p_T$ . The expression for the doublespin asymmetry for the subprocess  $q\bar{q} \rightarrow \gamma\gamma$ ,  $q\bar{q} \rightarrow gg\gamma$  and  $q\bar{q} \rightarrow g\gamma\gamma$  has the following form:

$$A_{LL} = -\lambda_1 \lambda_2$$

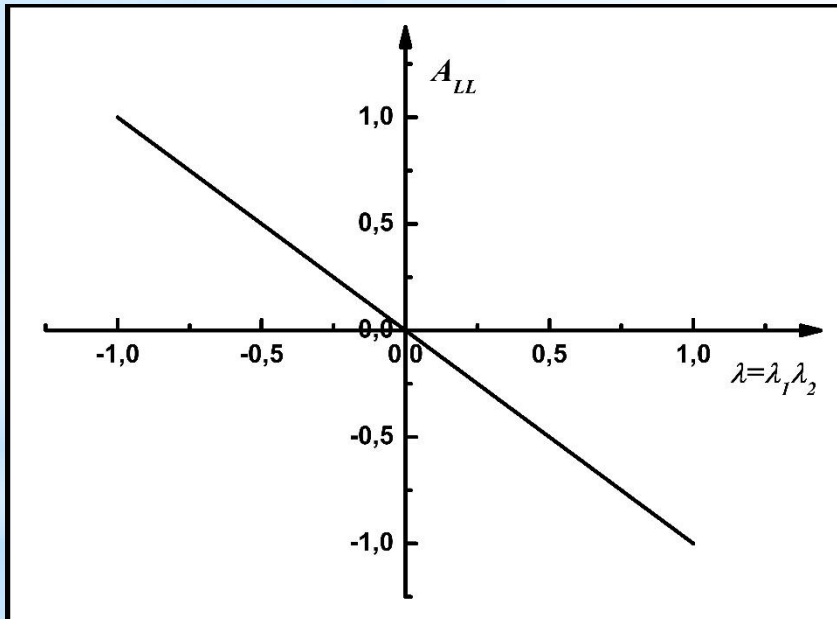


Fig.51 Dependence of the doublespin asymmetry  $A_{LL}$  on the helicity product  $\lambda_1 \lambda_2$

The study showed that  $A_{LL}$  for these processes do not depend on  $\sqrt{s}$ ,  $\cos(\theta)$  and  $p_T$ .

# The dependence of double spin asymmetry $A_{LL}$ of subprocess $q\bar{q} \rightarrow q\bar{q}\gamma$ on energy $\sqrt{s}$ , $p_T$ , $\text{Cos}(\theta)$ , $y$ and $x_T$

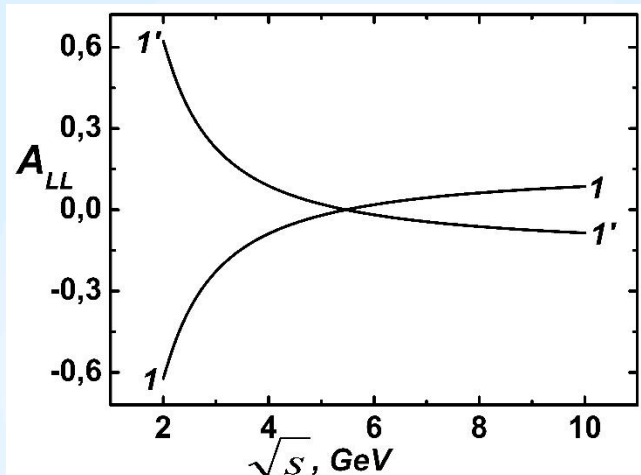


Fig.52 Dependence of the double spin asymmetry  $A_{LL}$  on the sum of the energy of colliding particles  $\sqrt{s}$  at  $p_T = 0.9 \text{ GeV}/c$ ,  $\lambda_1\lambda_2 = -0.81$  (curve 1');  $\lambda_1\lambda_2 = 0.81$  (curve 1) and  $y = 0$ ,

As can be seen from fig.52, the double spin asymmetry of differential cross sections, calculated with polarization  $\lambda_1\lambda_2 < 0$  ( $\lambda_1\lambda_2 > 0$ ) and without polarization, decreases (increases) with increasing energy of colliding protons. Polarization has a great influence at low energies, at  $\sqrt{s} = 5.5 \text{ GeV}$  the differential cross sections calculated without polarization and with polarization taken into account coincide, and then with increasing transverse momentum, the differential cross section calculated taking into account polarization  $\lambda_1\lambda_2 < 0$  ( $\lambda_1\lambda_2 > 0$ ) becomes smaller (more) than the differential cross section calculated without polarization.

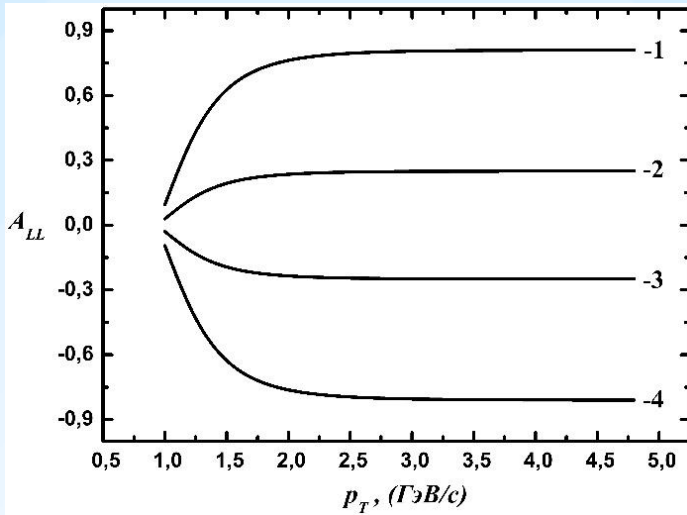
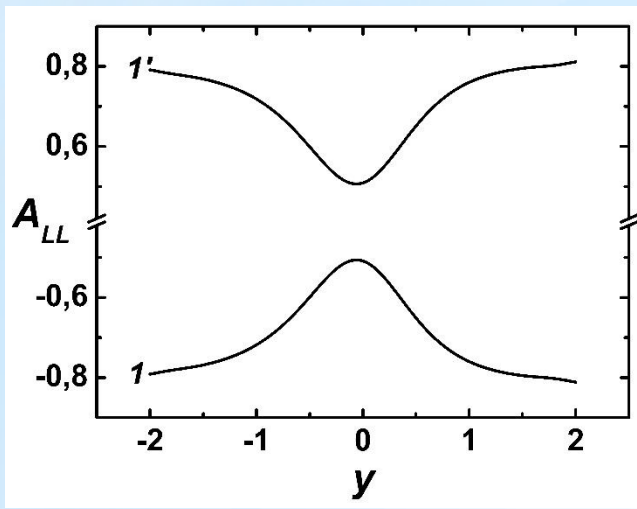
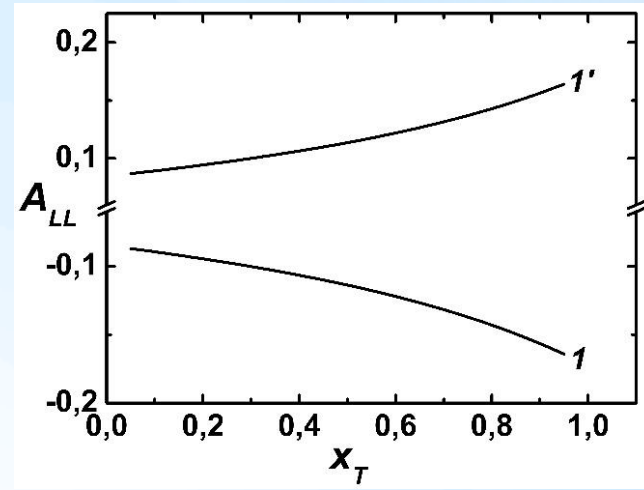


Fig.53 Dependence of the doublespin asymmetry  $A_{LL}$  on transverse momentum of photon  $p_T$  at 1.  $\lambda_1\lambda_2=-0.81$ ; 2.  $\lambda_1\lambda_2=-0.25$ ; 3.  $\lambda_1\lambda_2=0.25$ ; 4.  $\lambda_1\lambda_2=0.81$ .

As can be seen from fig.53, the doublespin asymmetry of the process increases (decreases) with an increase in the transverse momentum at  $\lambda_1\lambda_2<0$  ( $\lambda_1\lambda_2>0$ ) and reaches a plateau at certain  $p_T$ . The value of this  $p_T$  increases with the absolute value of  $\lambda_1\lambda_2$ .



*a*



*b*

Fig.54 Dependence of the doublespin asymmetry  $A_{LL}$  on  $y$  and  $x_T$  at  $\lambda_1\lambda_2=-0.81$  (curve 1');  $\lambda_1\lambda_2=0.81$  (curve 1).

In the fig.54(a) is presented the dependence of double spin asymmetry on  $y$  at  $\lambda_1\lambda_2=0.81$  and  $-0.81$  curve 1 and curve 1', correspondingly.

As see from fig.54(a) double spin asymmetry  $A_{LL}$  increases (curve 1), decreases (curve 1') in the interval  $y [-2, 0]$  and at  $y=0$  have maximum and future decreases (curve 1), increases (curve 1') with increasing  $y$ .

In the fig.54(b) is presented the dependence of double spin asymmetry on  $x_T$  at  $\lambda_1\lambda_2=0.81$  and  $-0.81$  curve 1 and curve 1', correspondingly. As see from fig.54(b) double spin asymmetry  $A_{LL}$  decreases (curve 1), increases (curve 1') with increasing  $x_T$ .

Table 2 shows the dependence of the doublespin asymmetry of  $q\bar{q} \rightarrow q\bar{q}\gamma$  on the product of order of helicity  $\text{Cos } (\theta)=[-1,1]$ . Throughout the  $\text{Cos } (\theta)$  change interval, the  $A_{LL}$  value is constant and equal to:

$\lambda_1\lambda_2$	$A_{LL}$
0	0
$\pm 0.01$	$\mp 0.001166$
$\pm 0.04$	$\mp 0.00466$
$\pm 0.16$	$\mp 0.018659$
$\pm 0.25$	$\mp 0.0291$
$\pm 0.36$	$\mp 0.04198$
$\pm 0.49$	$\mp 0.0571$
$\pm 0.64$	$\mp 0.0746$
$\pm 0.81$	$\mp 0.09446$
$\pm 1$	$\mp 0.1166$

$$A_{LL} = -0.117\lambda_1\lambda_2$$

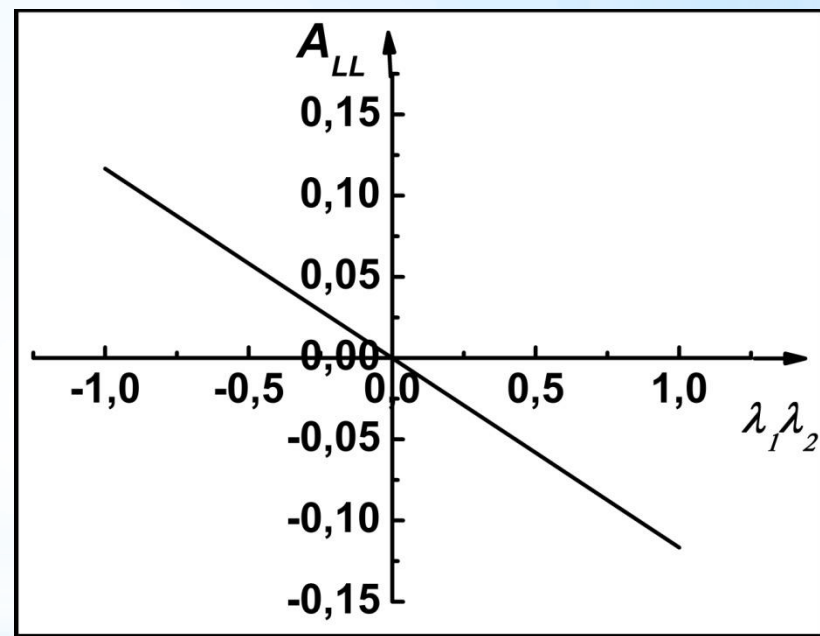


Fig.55 Dependence of doublespin asymmetry  $A_{LL}$  on the product of  $\lambda_1\lambda_2$  helicity at  $\text{Cos } (\theta) = [-1,1]$  for  $q\bar{q} \rightarrow q\bar{q}\gamma$  subprocess

# Conclusions

Radiation corrections to quark-gluon Compton scattering processes:

$$q\gamma \rightarrow q\gamma, q\gamma \rightarrow qg, g\gamma \rightarrow q\bar{q}, q\gamma \rightarrow qg\gamma, qg \rightarrow g\gamma\gamma, qg \rightarrow qg\gamma \text{ and } g\gamma \rightarrow q\bar{q}\gamma$$

$$\text{and annihilation of a quark-antiquark pair: } q\bar{q} \rightarrow \gamma\gamma, q\bar{q} \rightarrow g\gamma\gamma, q\bar{q} \rightarrow q\bar{q}\gamma$$

and  $q\bar{q} \rightarrow gg\gamma$  without and with taking into account the polarization of the quark are considered.

The dependences of the differential cross section of processes on the energy of colliding protons, the transverse momentum  $p_T$ , the cosine of the scattering angle,  $y$  photons, and  $x_T$  were studied.

The differential cross section of the processes under consideration decreases with increasing transverse momentum of photon.

The following results were obtained:

for Compton scattering process:  $\frac{d\sigma(q\gamma \rightarrow qg)}{dydp_T^2} > \frac{d\sigma(g\gamma \rightarrow q\bar{q})}{dydp_T^2} > \frac{d\sigma(q\gamma \rightarrow q\gamma)}{dydp_T^2}$  and

$$\frac{d\sigma(q\gamma \rightarrow qg\gamma)}{dydp_T^2} > \frac{d\sigma(qg \rightarrow g\gamma\gamma)}{dydp_T^2} > \frac{d\sigma(qg \rightarrow qg\gamma)}{dydp_T^2} > \frac{d\sigma(g\gamma \rightarrow q\bar{q}\gamma)}{dydp_T^2}$$

and for the process of annihilation of a quark-antiquark pair.

$$\frac{d\sigma(q\bar{q} \rightarrow g\gamma\gamma)}{dydp_T^2} > \frac{d\sigma(q\bar{q} \rightarrow q\bar{q}\gamma)}{dydp_T^2} > \frac{d\sigma(q\bar{q} \rightarrow gg\gamma)}{dydp_T^2}$$

It has been found that the contributions of the corrections to the differential cross section of quark-gluon Compton scattering are more significant than the contributions of the corrections to the differential cross section of the annihilation of a quark-antiquark pair.

At low values of  $p_T$ , the subprocess with sea quarks dominates, and at high values of  $p_T$ , the subprocess with valence quarks in the subprocess dominates  $q\gamma \rightarrow q\gamma$ .

Real Compton scattering  $q\gamma \rightarrow q\gamma$  has a smaller differential cross section than the process of virtual Compton scattering  $qg \rightarrow q\gamma$ . This is due to the fact that, at the initial moment of collision, the distribution of photons inside the quark gluon plasma is smaller than the distribution of gluons.

The process  $q\bar{q} \rightarrow q\bar{q}\gamma$  with propagator  $\gamma$  have much value of differential cross section than, this process with  $g$  propagator.

It was shown that the doublespin asymmetry  $A_{LL}$  subprocesses  $q\bar{q} \rightarrow gg\gamma$ ,  $q\bar{q} \rightarrow g\gamma\gamma$  and  $q\bar{q} \rightarrow \gamma\gamma$  do not depend on  $\sqrt{s}$ ,  $p_T$  and  $\text{Cos}(\theta)$ . The doublespin asymmetry expression for these subprocesses is as follows  $A_{LL} = -\lambda_1\lambda_2$

The doublespin asymmetry of the process  $q\bar{q} \rightarrow q\bar{q}\gamma$  increases (decreases) with an increase in the transverse momentum at  $\lambda_1\lambda_2 < 0$  ( $\lambda_1\lambda_2 > 0$ ) and reaches a plateau at certain  $p_T$ . The value of this  $p_T$  increases with the absolute value of  $\lambda_1\lambda_2$ . The doublespin asymmetry expression for these subprocesses is as follows  $A_{LL} = -0.117\lambda_1\lambda_2$

## LITERATURE

1. Germain M., on behalf of the ALICE Collaboration // **Nuclear Physics A** 2017. V. 967 V. 696.
2. Arbuzov A., Bacchetta A., Butenschoen M. et al. // **arXiv:2011.15005v4** [hep-ex] 2021.
3. Cerny V., Lichard P., Pisut J. // **Z. Phys. C** 1986. **V. 31** P. 163.
4. Duke W. and Owens JF Quantum-chromodynamic corrections to deep-inelastic Compton scattering // **Phys. Rev. D** V. 26, n0.7 1 october 1982 P.1600-1609
5. Owens JF Large-momentum-transfer production of direct photons, jets, and particles // **Reviews of Modern Physics**, v.59, N 2, 1987, P.465-503
6. Bagger JA, Gunion JF Higher-twist contributions, quantum chromodynamics, and inclusive meson photoproduction at high  $p_T$  // *Physical Review D*, V.25, N 9, 1982, 2287-2299
7. Qrishin V.Q. *Inklyuzivniye prochessi v adronnikh vzaimodeystviyakh pri visokikh enerqiyakh* , *Uspekhi Fizicheskikh Nauk (UFN)* , **127** ( 1979) 51-98, (in Russian).
8. Levintov II *Polyarizasiya bistrikh protonov i neytronov* , *Uspekhi Fizicheskikh Nauk ( UFN )*, **54** ( 1954) 285-314, (in Russian).

**THANK YOU FOR  
ATTENTION !**